Allowable Design Release Stresses for Pretensioned Concrete Beams

by

Alfredo Castro, B.S.C.E.

Thesis

Presented to the Faculty of the Graduate School of

The University of Texas at Austin

in Partial Fulfillment

of the Requirements

for the Degree of

Master of Science in Engineering

The University of Texas at Austin

August 2003

Allowable Design Release Stresses for Pretensioned Concrete Beams

Approved by
Supervising Committee:

_____

Michael E. Kreger, Supervisor

_____

Oguzhan Bayrak, Supervisor

Dedication

To my wife, my parents, and my brothers

Acknowledgements

Table of Contents

List of Tables

List of Figures

CHAPTER 1

Introduction

1.1 OVERVIEW

Premature deterioration of precast bridge girders has been detected at numerous locations throughout the State of Texas. Two chemical mechanisms known as alkali-silica reaction (ASR) and delayed ettringite formation (DEF) have been identified as the main causes. These mechanisms lead to expansion and cracking of concrete and, consequently, to loss of strength and durability. Controlling them involves reducing the overall alkali load in concrete and the heat of hydration.

Precast producers must meet one of several requirements listed in ACI Special Provisions 201 to limit ASR. Many have chosen to use low-alkali cement. However, this type of cement is more expensive and results in a lower rate of strength gain for concrete containing this cement than for concrete containing ASTM C150 Type III cement. Another option for reducing ASR as well as reducing heat of hydration involves reducing the amount of Type III cement. Although it is more economical, this option would lead to even lower rates of compressive strength gain, delaying the release of pretensioned members unless the allowable stress limits at prestress transfer specified by AASHTO and ACI are increased.

The required concrete compressive strength at prestress force release is determined by these limits. Therefore, increasing them would not only compensate for delays in prestress release resulting from lower rates of concrete strength gain, but could positively impact the economic advantages of

1

pretensioned concrete by enhancing the productivity in precast manufacturing plants.

1.2 ALLOWABLE STRESS LIMITS

Ensuring serviceability is the primary reason for establishing allowable stress limits in prestressed concrete members. Provisions included in current bridge design specifications and building codes are intended primarily to prevent cracking and excessive deflection or camber. Additionally, the extreme fiber compressive stress limit is an indirect way to prevent concrete crushing at transfer due to application of the prestress force. The current allowable stress limits at transfer are presented in Table 1-1.

Table 1-1: Allowable concrete stress limits at prestress transfer

American Association of State Highway and Transportation Officials (AASHTO, 1996) (Pretensioned Members)	
Compression	$0.60 f'_{ci}$
Tension (no bonded reinforcement)	200psi or $3\sqrt{f'_{ci}}$
Tension (with bonded reinforcement to resist the total tensile force in concrete)	$7.5\sqrt{f'_{ci}}$
American Concrete Institute (ACI 318-02) (Pretensioned and Post-tensioned Flexural Members)	
Extreme fiber stress in compression	$0.60 f'_{ci}$
Extreme fiber stress in tension except at locations other than the ends of simply supported members	$3\sqrt{f'_{ci}}$
Extreme fiber stress in tension at ends of simply supported members	$6\sqrt{f'_{ci}}$

1.3 OBJECTIVE OF RESEARCH

This thesis presents the results of a research project conducted at the Ferguson Structural Engineering Laboratory at The University of Texas at Austin, and funded by the Texas Department of Transportation. The main objective was to determine the impact of elevated concrete stresses in pretensioned concrete beams at prestress transfer.

1.4 SCOPE OF RESEARCH

This project included a thorough review of literature related to allowable stresses in prestressed concrete members, and the design, fabrication, monitoring, and evaluation of behavior of 30 reduced-scale beam specimens subjected to stresses at prestress release that exceeded current specified limits. These specimens were intended to represent standard shapes used in the precast concrete bridge industry. The influence of cross-section geometry, rate of concrete strength gain, and concrete mix used to cast specimens on the response of beams subjected to elevated concrete stresses at prestress release was analyzed.

1.5 CHAPTER OUTLINE

Chapter 2 presents a compilation of literature related to allowable stresses specified for prestressed concrete members and the properties of high-strength concrete. This literature review extends from the early development of reinforced concrete provisions to the latest research performed on these topics. Chapter 3 describes the methods used to design and analyze the test specimens. The nominal properties of the beam specimens are also presented. Chapter 4 describes the experimental program including assembly of the prestressing facility, fabrication and instrumentation of test specimens, and the data acquisition

systems. Chapter 5 presents the response of the specimens and evaluates their behavior in relation to current design provisions. Finally, Chapter 6 summarizes the results and findings of the research project and presents recommendations for future research.

CHAPTER 2

Literature Review

2.1 OVERVIEW

This research program was initiated with a detailed review of documents related to allowable stresses specified for prestressed concrete members. The objective was to identify research related to allowable stresses conducted by researchers in previous studies, and to uncover any background information related to the development of code requirements. Therefore, it was necessary to study literature dating back to the early development of reinforced concrete provisions. A summary of this material is presented in this chapter.

Allowable stress provisions developed by early code writers were influenced by a relative lack of control over the mechanical properties of concrete. Years of research and experience resulted in significant improvements in concrete quality and the development of high-performance materials used today for most precast applications. Significant research was conducted during the last two decades on the mechanical properties of high-strength concrete. The results of some of this research, as it relates to prestressed concrete applications, are presented here.

2.2 HISTORY OF THE ALLOWABLE STRESSES

The use of allowable stresses in design of concrete members began in the early twentieth century with the first report published by the National Association of Cement Users. Initially, allowable stress limits for plain and reinforced

concrete were set at fixed values. Experience and research lead to better methods for controlling the mechanical properties of concrete and supported the establishment of stress limits expressed as percentages of the concrete compressive strength.

Traditionally, prestressed concrete practice has preceded research and codes (Hawkins, 1981). The Walnut Lane Bridge in Philadelphia was constructed in 1949, three years before the first recommendations for prestressed concrete were published by the Federal Bureau of Public Roads. This continues to be the case as recent research has evaluated the validity of code requirements for concrete stresses at transfer and service while, in some prestressing plants, compressive stresses as high as $0.75f'_{ci}$ in double tee members are commonly allowed at release.

The history of provisions for plain, reinforced, and prestressed concrete is discussed further in the following sections of this chapter.

2.2.1 Plain and Reinforced Concrete (Kerekes, 1954)

In response to a lack of standard practice in concrete design and reliable information on concrete behavior, two organizations were formed in the early 1900's. First, representatives of the American Society for Testing Materials, American Society of Civil Engineers, American Railway Engineering and Maintenance of Way Association (later American Railway Engineering Association), and the Association of American Portland Cement Manufacturers (later Portland Cement Association) formed the Joint Committee on Reinforced Concrete in 1904. The main objective of the committee was to standardize reinforced concrete practice.

A few months later, an informal meeting in January of 1905 resulted in the formation of the National Association of Cement Users (NACU), currently known

as the American Concrete Institute. Distributing information and experience and promoting methods to improve the uses of cement became the objectives of this association. The original intent of the founders of the association was to discuss and solve problems related solely to concrete block construction. Consequently, various committees were organized to study the different cement applications and products (Maples, 1954).

A report published in 1907 by the Committee on Laws and Ordinances of NACU marked the first attempt to write a reinforced concrete code. This document dealt more with sidewalks, streets, floors, and cement products such as concrete blocks than with design procedures for structural reinforced concrete. Nevertheless, allowable concrete stresses for reinforced concrete elements were established to be 500 psi for direct compression, 800 psi for "cross bending", 300 psi for direct shear, and 30 psi for "secondary tension". Concrete compressive strengths of up to 2000 psi were recognized at this time.

A second report published by NACU in 1908 included recommendations for reinforced concrete construction by the National Board of Fire Underwriters. A design approach similar to today's strength design method and suggestions to improve fire resistance of structural concrete and steel frames were presented in the report but ultimately, were not adopted by NACU. The proposed design method required a factor of safety of four to be applied to the total working load. This amplified working load would have resulted in a "stress in the steel equal to the elastic limit and a stress in the concrete equal to 2000 psi" (Kerekes, 1954). Another interesting aspect of the proposed recommendations was that, regardless of end conditions, all beams and girders were considered to be simply supported.

In 1909, an increased interest in construction methods and costs resulted in revision of previous recommendations and proposal of new regulations by the First Joint Committee. The Committee on Reinforced Concrete of the NACU

also produced a report at this time. As mentioned, NACU did not adopt the Fire Underwriter's recommendations for a design method based on a factor of safety applied to the working loads. Instead, an allowable concrete fiber working stress of 650 psi was proposed. This value could be increased by 15 percent near the supports of continuous beams. Compared to other municipal codes in 1909, this regulation was liberal. The Joint Committee proposed essentially the same concrete stress limits as the NACU.

In February of 1910, following a limited number of revisions to the 1909 report, the *Standard Building Regulations for the Use of Reinforced Concrete* was adopted by the NACU. Provisions related to concrete fiber stress limits remained unchanged from the earlier report.

In 1913, the Board of Direction of the National Association of Cement Users changed the name of the society to the American Concrete Institute. This name was believed to be more descriptive of the actual interests and objectives of the association.

By 1916, the need for revision of the existing reinforced concrete regulations was clear after comparing the available design methods to results obtained from laboratory work and tests performed on actual buildings during previous years. In addition, reliable methods for controlling concrete strengths had also been developed. Consequently, ACI proposed revised regulations which presented important changes with regard to allowable stress limits. Instead of establishing fixed stress limits, these new regulations expressed the allowable stresses as a function of the 28-day concrete compressive strength. The recommended allowable concrete stresses were: $0.25f'_c$ for direct compression, $0.75f'_c$ for shear (reinforced concrete only), $0.50f'_c$ for bearing, and $0.375f'_c$ for the extreme fiber compressive stress. A fiber compressive stress of $0.475f'_c$ was

permitted adjacent to the supports of continuous beams. In 1916, 3000 to 3300 psi concrete strengths were readily available.

The final report by the First Joint Committee was published in 1917. Members of the ACI believed that this Joint Committee report did not consider important data and contained many arbitrary rules (Kerekes, 1954). Therefore, revised regulations published by ACI that same year did not adopt several recommendations made by the Joint Committee. For instance, while the Joint Committee kept the previously suggested allowable compressive fiber stress of $0.475f'_c$ adjacent to the supports of continuous members, ACI reduced it to $0.41f'_c$.

In 1925, working stresses allowed by the Second Joint Committee and ACI were very similar except for the allowable extreme fiber compressive stresses in continuous beams. While ACI permitted $0.41f'_c$ adjacent to the supports and $0.375f'_c$ elsewhere, the Second Joint Committee recommended $0.45f'_c$ and $0.40f'_c$.

No further changes occurred until the 1940-41 period. The final report of the Third Joint Committee in 1940 and the Building Code Requirements for Reinforced Concrete (ACI 318-41) in 1941 were very similar. The section of the ACI Code on allowable unit stresses presented a single value of $0.45f'_c$ for the fiber compressive stress at any location along a continuous member. This value is still the limit today for the maximum fiber stress in a pretensioned element under sustained loads.

A committee on prestressed concrete was formed by the ACI in 1942 to revise available information, propose design procedures and recommend needed research (Hawkins, 1981). Shortly after the creation of the ACI prestressed concrete committee, significant changes in reinforced concrete design were implemented by the ACI in the Building Code. The *Ultimate Strength Design*

Method (USD) was first introduced as an appendix in the 1956 ACI Building Code Requirements. By 1971, this approach had completely replaced the *Working Stress Design Method (WSD)* which had been incorporated in the appendices and renamed the *Alternate Design Method.* The USD is currently known as the *Strength Design Method.*

2.2.2 Prestressed Concrete (Hawkins, 1981)

The Walnut Lane Bridge in Philadelphia was the first prestressed concrete bridge built in the United States. Constructed in 1949, it had a 160-foot long center span made up of 13 precast and post-tensioned girders weighing approximately 150 tons each (Peterson, 1954). Motivated by the successful construction of this structure, reorganization in 1952 of the previous ACI Committee on Prestressed Concrete resulted in the formation of the ACI-ASCE Joint Committee 323 on Prestressed Concrete.

Joint Committee 323 played an important role in developing the *Criteria for Prestressed Concrete Bridges* published in 1952 and 1954 by the Federal Bureau of Public Roads, currently the Federal Highway Administration. This document marked the first attempt to create a set of recommendations for prestressed concrete and served as a guide in the early years of this industry. Significant differences in opinion among those who contributed to its preparation resulted in allowable stress limits that are similar to those in use today.

The main objective of Joint Committee 323 was to develop the *Tentative Recommendations for Prestressed Concrete,* document published in 1958. In general, permissible concrete stresses remained unchanged from those previously proposed by the Federal Bureau of Public Roads. Extreme fiber compressive stresses at transfer were limited to $0.6f'_{ci}$ for pretensioned members and $0.55f'_{ci}$ for post-tensioned members. Compressive stresses at service load after prestress

losses have occurred were limited to $0.45f'_c$ for building elements and $0.40f'_c$ for bridge elements (Joint Committee 323, 1958). Members of the Joint Committee believed that these limits were reasonable for preventing excessive creep deformation and failure due to repeated loads (Huo, 1995).

By 1958, substantial knowledge on the behavior and design of reinforced concrete had been accumulated. In contrast, much of what is known today about prestressed concrete was generated later. No significant research on the topic of allowable stresses in prestressed concrete was conducted before the Federal Bureau of Public Roads and Joint Committee 323 published their recommendations. In fact, Siess, in private communication with M. Kreger, recalled no supporting research or rationalization for the established limit of $0.6f'_{ci}$, value that he disapproved of at the time (Siess, 2000). Between the years 1950 and 1952, C. P. Siess lead the subcommittee of ACI-ASCE Committee 323 in charge of developing definitions and notation for prestressed concrete.

In a paper published in 1960 by Siess, he expressed that codes are almost entirely empirical and that experience and provisions previously developed for reinforced concrete could not be transferred directly to prestressed concrete but could serve as a guide for the creation of new provisions for this emerging industry. The fact that the report by Joint Committee 323 was recommended practice rather than code requirements was important during the following years for the development of prestressed concrete. As Siess expressed in his paper, a specification can only be based on knowledge and practice available at the time it is developed, therefore imposing obstacles in the way of new practices attempted by engineers (Siess, 1960).

In the discussion of the *Tentative Recommendations for Prestressed Concrete*, T. Y. Lin, another leading authority in the field of prestressed concrete, wrote: "While it is true that such simple sets of allowable stresses have been used

11

for some time and have apparently yielded safe results, it must be realized that this was more a matter of coincidence than of rational justification. Most of these values were empirically employed by pioneers of prestressed concrete, who at that time did not have as much knowledge and data as we now have, or as we will have...the strength and behavior of beams at transfer cannot be simply described by stresses but are dependent upon a number of factors, such as the shape of the section, the amount and the location of prestress, etc...At this stage of our knowledge regarding prestressed concrete, we are not in a position to fix definite allowable values for all the stresses under all conditions."

In spite of these dissenting opinions and the existing knowledge on prestressed concrete, building codes included allowable stress requirements soon after the publication of the report by Joint Committee 323. For instance, prestressed concrete provisions were first incorporated in the ACI Building Code in 1963 (ACI 318-63). Temporary concrete stresses immediately after transfer were limited to $0.6f'_{ci}$ in compression and $3\sqrt{f'_{ci}}$ in tension for members without auxiliary reinforcement. Allowable concrete stresses at the design load stage were $0.45f'_c$ for compression and $6\sqrt{f'_c}$ for tension in the precompressed zone. The tensile stress limit at service level was taken as zero for members subjected to adverse exposure conditions such as freezing temperatures or corrosive conditions.

While the permissible compressive stress at transfer has not changed since adopted in 1963, the limit stress at service level was revised and modified in ACI 318-95. Present ACI regulations for building members establish a maximum fiber compressive stress of $0.45f'_c$ for prestress plus sustained loads and $0.6f'_c$ for prestress plus total loads (ACI 318-02). These provisions do not differentiate between pretensioned and post-tensioned elements.

In contrast, the AASHTO (Standard Specification for Highway Bridges) limits the compressive stress at transfer to $0.60f'_{ci}$ for pretensioned members and $0.55f'_{ci}$ for post-tensioned members. At service level, compressive stress is limited to $0.40f'_c$ for prestress plus sustained loads and for live load plus one half the sum of the prestress and sustained loads. For other load combinations, the permissible stress at service load is $0.60f'_c$ (AASHTO, 1996).

Allowable tensile stresses also have not changed much since 1963. AASHTO (Standard Specification for Highway Bridges) permits 200 psi or $3\sqrt{f'_{ci}}$ at transfer. At service level, a tensile stress of $6\sqrt{f'c}$ is permitted except for members affected by severe corrosive conditions or without bonded reinforcement for which this value is reduced to $3\sqrt{f'_{ci}}$. The ACI provisions differ in that a stress value of $6\sqrt{f'_{ci}}$ is allowed at the ends of simply supported members at transfer. Also, the tensile stress requirements at service level are less rigorous due to the less sever exposure conditions expected for building members.

2.2.3 Recent Research

Design engineers often decide to debond or depress strands in prestressed concrete elements to control member end stresses and satisfy allowable stress requirements. These practices are believed to contribute to problems such as anchorage slip, reduction of shear capacity, and corrosion. Increasing or eliminating the allowable stresses prescribed by ACI and AASHTO would lead to efficient production processes and reduce the need for these practices.

Much research performed in the 1990's was focused on evaluating current allowable stress limits and proposing alternative design methods. Results and recommendations are discussed in this section.

2.2.3.1 Allowable Compressive Stresses for Prestressed Concrete (Pang and Russell)

In 1995, Pang and Russell studied the change in the compressive strength of concrete cylinders subjected to large sustained loads (Pang, 1996). Two different concrete mixes, both used in the prestressed concrete industry because of their high early strengths, were used to cast the specimens. These cylinders were then steam cured for 22 hours at 100°F; curing conditions typically used by prestressed concrete manufacturers to accelerate strength gain.

Following the accelerated curing process, specimens were subjected to high compressive stresses of $0.60f'_{ci}$, $0.70f'_{ci}$, and $0.80f'_{ci}$ for periods of time ranging from 7 to 180 days. It is important to emphasize that these stresses are all equal to or higher than the allowable compressive stress of $0.60f'_{ci}$ presently specified by ACI and AASHTO.

Compressive strength results obtained from tests performed after each loading period on control and loaded specimens showed no detrimental effects due to the application of high sustained loads. Creep of the specimens loaded to $0.70f'_{ci}$ and $0.80f'_{ci}$ was monitored and the behavior for all but two specimens was comparable to that for cylinders subjected to a lower sustained stress. Two of the specimens loaded to $0.80f'_{ci}$ failed under sustained load.

This experimental program was carried out using cylinders subjected to, what was intended to be, pure compression. It is possible that misalignment of the load applied to the specimens loaded to $0.80f'_{ci}$ was responsible for failure of the cylinders. This suggests that additional research to study the behavior of young concrete elements subjected large flexural compressive stresses is recommended.

2.2.3.2 Allowable Compressive Strength of Concrete at Prestress Release (Huo and Tadros)

In the Open Forum section of the first 1997 PCI Journal issue, Huo and Tadros analyzed the behavior of prestressed concrete members subjected to compressive stresses exceeding the specified limit of $0.60f'_{ci}$. They speculated that this extreme compressive fiber stress limit was intended to prevent concrete crushing at prestress transfer.

With respect to previous experimental studies like that conducted by Pang and Russell, the authors stated that because of the internal set of concrete and steel stresses induced by prestressing, behavior of prestressed concrete members is significantly different from that of elements subjected to externally applied compressive forces. The prestress force is a self-relieving mechanism affected by creep, shrinkage, relaxation, and elastic shortening.

Table 2-1: Cross-sectional properties of the 18"x18" member

Type of concrete	Normal weight
f'_{ci}	3500 psi
E_{ci}	3587 ksi
Ultimate Concrete Strain (ε_{cu})	0.003
Strain at peak stress (ε_0)	0.00225
Type of prestressing	½-in low-relaxation 270 ksi strands
E_{ps}	28,500 ksi
f_{pi}	189 ksi
A_{ps}	Variable

To investigate the performance of concrete at high stress levels, a concentrically prestressed 18 by 18-inch concrete element was selected. The assumed cross-sectional properties are shown in Table 2-1. The procedure followed by the authors consisted of gradually increasing the number of strands from 20 to 62 and computing the resulting concrete and steel stresses and strains. Calculations were performed utilizing a conventional linear analysis method as well as a nonlinear analysis method.

The linear method was based on the assumption that the relationship $f = \varepsilon \cdot E$ is valid. This simple assumption is normally preferred by engineers to compute stresses and strains in prestressed concrete members. In this case, the unknowns were estimated using the transformed section properties of the member as shown by the following equations.

$$f_c = \frac{\left(f_{pi} \cdot A_{ps}\right)}{\left[A_g + (n-1) \cdot A_{ps}\right]}$$

Equation 2-1

$$\varepsilon = \frac{f'_{ci}}{E_{ci}}$$

Equation 2-2

$$f_{po} = f_{pi} - n \cdot f_c$$

Equation 2-3

Although usually not attractive for design engineers, the authors emphasized that a nonlinear analysis is the only realistic way to estimate the internal stresses in prestressed concrete elements, especially considering the self-relieving nature of those. The nonlinear method they selected was based on the concrete stress-strain relationship proposed by Hognestad and represented by Equation 2-4. Compatibility and equilibrium conditions were satisfied in the

analysis by Equations 2-5 and 2-6 respectively. Calculations were performed using a spreadsheet program created by the authors.

$$f_c = f'_{ci} \cdot \left[2 \cdot \frac{\varepsilon}{\varepsilon_0} - \left(\frac{\varepsilon}{\varepsilon_0} \right)^2 \right] ; \ \varepsilon < \varepsilon_{cu} \qquad \textbf{\textit{Equation 2-4}}$$

$$f_{po} = f_{pi} - \varepsilon \cdot E_{ps} \qquad \textbf{\textit{Equation 2-5}}$$

$$f_{po} \cdot A_{ps} = f_c \cdot A_c \qquad \textbf{\textit{Equation 2-6}}$$

As indicated by Huo and Tadros, Equation 2-4 implies that concrete crushes when the strain reaches its ultimate value and not when the stress reaches f'_{ci} as would be assumed using the linear approach. This can be confirmed with a standard concrete cylinder test where load is applied through increments of strain. In this study, it was assumed that crushing occurs at a strain of 0.003, although higher strains can occur in concrete when it is confined by closely spaced ties or spirals.

Results from the analyses are shown in Figure 2-1. According to the nonlinear approach, in order to produce an f_c equal to $0.60f'_{ci}$, the number of strands would need to be increased from 20 to 26. As illustrated in the figure, the linear method predicted 25 strands to reach this same level of stress, thus indicating that the simplified method is sufficiently accurate up to the current stress limit. However, it was observed that as the stress and strain ratios increased, the difference in the amount of prestress required by each method to attain a higher level increased as well.

According to the linear analysis, using 45 strands tensioned to 189 ksi would induce a concrete stress equal to f'_{ci}. By performing the nonlinear analysis, the researchers concluded that the number of strands could be augmented to 58 to

reach the peak stress and to 62 to achieve the ultimate strain of 0.003. This method also showed that with 45 strands, the member would only be subjected to a stress of $0.90f'_{ci}$ and a strain of approximately 50 percent of its total deformation capacity. It was concluded that the linear approach did not correctly predict the concentrically applied prestressing force that would crush the concrete.
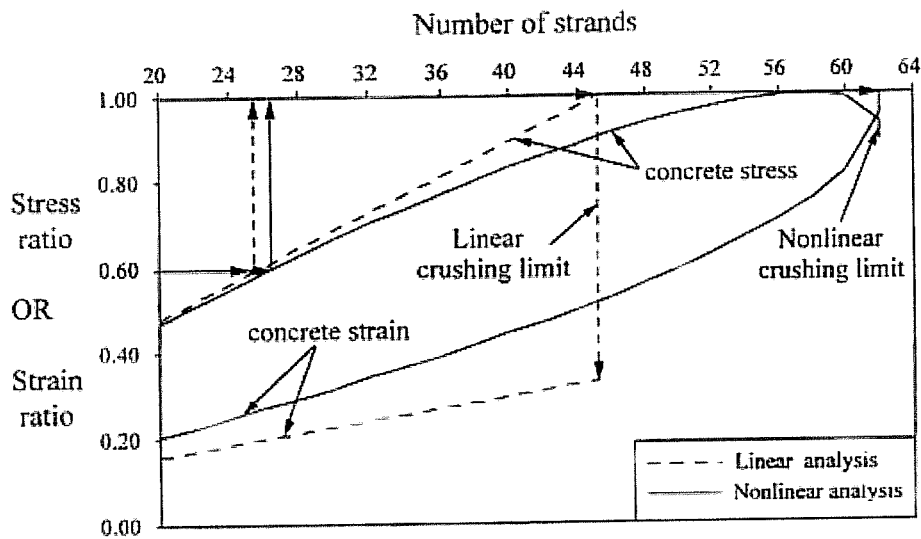
Figure 2-1: Results of linear and nonlinear analyses (Huo and Tadros, 1997)

With this example, Huo and Tadros showed the inherent conservativeness of linear analysis without making any definite recommendations regarding the implementation of higher allowable stresses for prestressed concrete at release. However, they presented a rational approach for more accurately computing stresses and strains in concrete, and emphasized that factors such as steel relaxation, creep, shrinkage, and accidental eccentricity should be carefully evaluated before any revisions in allowable release stresses are made.

Instead of performing any laboratory tests to support their discussion, the authors referenced a PCI Standard Design Practice report published in 1996 that states that initial compression in concrete is often allowed to exceed $0.60f'_{ci}$ in order to avoid debonding or depressing strands (PCI Technical Activities Council and PCI Committee on Building Code, 1996). The report also indicates that no problems have been observed by permitting compressive stresses as high as $0.75f'_{ci}$.

2.2.3.3 Strength Design of Pretensioned Flexural Concrete Members at Prestress Transfer (Noppakunwijai, Tadros, Ma, and Mast)

Noppakunwijai, Tadros, Ma, and Mast conducted a research program to develop a simplified strength design method for flexural pretensioned concrete members under the effects of prestress transfer. Results were published in the first issue of the 2001 PCI Journal.

The authors modeled prestressed concrete members as non-prestressed reinforced concrete columns subjected to flexure and axial compression equal to the force in the strands immediately before transfer. Hence, assumptions commonly made in reinforced concrete design were adopted. These assumptions include:

1. plane sections remain plane after bending,
2. concrete has no tensile strength,
3. the equivalent rectangular compressive stress block is applicable, and
4. the ultimate concrete compressive strain is 0.003.

Appropriate load factors and strength reduction factors were proposed by the authors after analyzing the uncertainties involved in the fabrication of

19

pretensioned concrete members. A strength reduction factor, ϕ, of 0.7 was proposed for both the nominal axial capacity, P_n, and the flexural capacity, M_n. This value was considered adequate until further research is available. However, the authors indicated that it may be too conservative for this application due to the temporary nature of the applied loads and the self-relieving nature of the internal induced stresses.

Table 2-2: Recommended load factors

Description	Load Factor
Prestress force just before release, P_i	1.2
Self-weight moment, M_g, acting in the same direction as the prestress moment	0.8
Self-weight moment, M_g, acting in the opposite direction as the prestress moment	1.2

Recommended load factors are shown in Table 2-2. As can be observed, two different load factors were suggested for the member self-weight moment due to the uncertainty of lifting locations. With regard to the load factor for the axial compression force, P_i, the same value used in design of post-tensioned anchorage zones, according to ACI 318-99, was suggested.
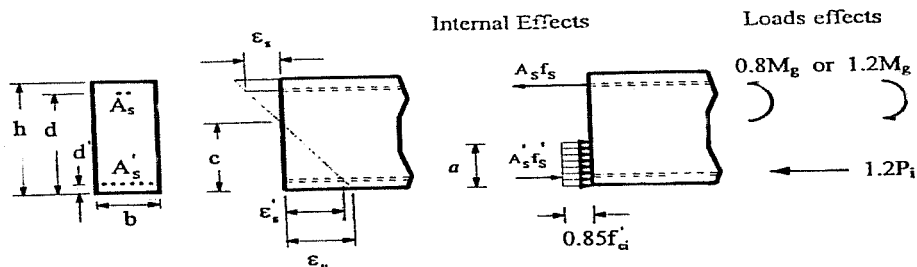
Figure 2-2: Force diagram for strength design method
(Noppakunwijai et al, 2001)

Based on the assumptions listed earlier (also shown in Figure 2-2), a set of equations satisfying equilibrium and compatibility were developed to estimate the flexural strength of pretensioned members. The resulting equations (2-7 through 2-10) listed below can be used to compute a desired unknown by specifying known cross-sectional properties. For example, the unknown quantity can be the concrete compressive strength at release, f'_{ci}, or the area of top reinforcement, A_s.

$$\varepsilon'_s = \left(\frac{c-d'}{c}\right) \cdot 0.003; \qquad f'_s = \varepsilon'_s \cdot E_{ps} \qquad\qquad \textbf{\textit{Equation 2-7}}$$

$$\varepsilon_s = \left(\frac{d-c}{c}\right) \cdot 0.003; \qquad f_s = \varepsilon_s \cdot E_s \qquad\qquad \textbf{\textit{Equation 2-8}}$$

$$0.85 \cdot f'_{ci} \cdot b \cdot a + A'_s \cdot f'_c - A_s \cdot f_s = \frac{1.2 \cdot P_i}{\phi} \qquad\qquad \textbf{\textit{Equation 2-9}}$$

$$0.85 \cdot f'_{ci} \cdot b \cdot a \cdot \left(\frac{a}{2}-d'\right) - A_s \cdot f_s \cdot (d-d') = \frac{(0.8 \ or \ -1.2) \cdot M_g}{\phi} \qquad \textbf{\textit{Equation 2-10}}$$

As part of this research project, the strength design method was then employed to analyze various standard double-tee, rectangular, and inverted-tee cross sections. It was concluded that geometry of the cross section is an important factor for controlling the required concrete compressive strength at transfer of pretensioned concrete members. While the resulting stress limits for PCI double-tee sections varied from $0.73f'_{ci}$ to $0.76f'_{ci}$, values for the NU inverted-tee sections were between $0.66f'_{ci}$ and $0.67f'_{ci}$. Rectangular sections were an intermediate case with allowable stresses between $0.69f'_{ci}$ and $0.70f'_{ci}$. Although appropriate assumptions were made to ensure a conservative design approach, maximum compressive fiber stresses higher than those currently

21

permitted were calculated for the three types of sections. In fact, the authors stated that this method will generally lead to stresses exceeding the limit specified by ACI and AASHTO.

The researchers recommended substituting an empirical formula (Equation 2-11) that reflects the importance of the cross-section geometry for the allowable compressive stress of $0.6f'_{ci}$. In Equation 2-11, y_b is the location of the centroid measured from the bottom of the cross section, and h is the total section height. This formula was presented as a transitional measure, should the working stress approach be replaced by the strength design method.

$$\left(0.60 + \frac{y_b}{5 \cdot h}\right) \cdot f'_{ci} \leq 0.75 \cdot f'_{ci} \qquad \textbf{\textit{Equation 2-11}}$$

To support their theoretical work and investigate the impact of creep of concrete subjected to high stresses, the researchers fabricated and monitored the behavior of two 32-foot long inverted-tee beams. This type of cross section had resulted in the lowest allowable stress limits according to their analysis. Release concrete compressive stresses at the ends of these specimens reached $0.79f'_{ci}$ and $0.84f'_{ci}$, which are considerably higher than that currently permitted in the codes or that calculated by the proposed strength design method. No adverse effects due to the elevated concrete stresses were observed after monitoring camber and concrete strains for approximately four months.

As a result, the authors concluded that the compressive stress limit requirement at prestress transfer should be eliminated. They recommended using the strength design approach to replace working stress design. They stated that this alternative method would provide a more uniform factor of safety against concrete crushing because factors such as concrete strength, area of top reinforcement, and cross-section geometry are considered.

Despite the fact that the theoretical analyses presented by the authors support the suggested strength design method, experimental work was limited to two inverted-tee specimens. In addition, the method used to determine the corresponding concrete compressive stresses at transfer of $0.79f'_{ci}$ and $0.84f'_{ci}$ was not described. Further research including members with different cross sections and compressive stresses at release, as well as appropriate instrumentation to accurately estimate prestress forces is needed.

2.3 PROPERTIES OF HIGH-STRENGTH CONCRETE

Based on 28-day compressive strengths, concretes are usually classified as low, normal, and high-strength. High–strength concrete has historically been considered to have a compressive strength of at least 6000 psi. This type of concrete is commonly used in the United States to reduce column dimensions of high-rise buildings and to fabricate prestressed concrete elements.

For economical and structural reasons, concretes used for prestressed applications typically possess 28-day strengths ranging from 4500 to 10,000 psi. High early strengths are also typically required to facilitate rapid fabrication of elements. Among a variety of factors, the use of high quantities of ASTM C150 type III high-early strength cement, low water/cement ratios, and higher curing temperatures, characterize these concretes.

The three phases composing hardened concrete are the coarse aggregate, hydrated cement paste, and transition zone. The key to achieving a desired strength without impairing workability and placeability of the concrete resides in the inverse relationship between strength and porosity of these three phases. The porosity of the cement paste and the transition zone depends primarily on the water/cement ratio. Other influencing factors include the properties of the

individual materials and the mixing procedure. Therefore, to attain high strengths in concrete, it is necessary to exert strict quality control measures.

Mixing proportions of normal or conventional and high-strength concretes differ in many ways. While a water/cement ratio between 0.40 and 0.70 produces conventional concretes with compressive strengths ranging between 3000 and 6000 psi, for high-strength concrete this ratio is usually around 0.30. Such a low water/cement ratio would negatively affect the workability of fresh concrete if appropriate measures, such as using a high-range water reducer, are not employed. Replacement of cement with supplementary cementitious materials such as fly ash or silica fume is often done mainly to reduce the amount of heat produced during hydration and to improve concrete durability to resist problems such as alkali-silica reaction (ASR).

Numerous experimental studies have analyzed the differences between the internal microstructures of high-strength and conventional concretes, and how these affect the existing theory on which concrete design practice is based. Mechanical properties of concrete such as modulus of elasticity and modulus of rupture can be as important as the compressive strength for design purposes. Having a good estimate of the value of these parameters is necessary to correctly predict deformations and deflections of reinforced and prestressed concrete elements and structures. The following discussion summarizes results and conclusions obtained from several of these research projects.

2.3.1 Modulus of Elasticity

The standard test method for determining the static modulus of elasticity using 6 by 12-inch cylinders is described in ASTM C469. Direct determination using this procedure is time-consuming and often impractical. Consequently, structural engineers typically use simple empirical equations to relate modulus of

elasticity to compressive strength. Table 2-3 presents three of the most commonly used formulas which can be found in building codes.

Table 2-3: Empirical equations for predicting the elastic modulus of concrete

	Equation for E_c (psi)	Observations
ACI 318-02 (Pauw)	$$E_c = 33 \cdot w_c^{1.5} \cdot \sqrt{f_c'}$$	• $90 lbs/ft^3 \le w_c \le 155 lb/ft^3$ • $f_c' \le 6,000 psi$
ACI 363R-92 (Carrasquillo, Nilson, and Slate)	$$E_c = \left(40,000 \cdot \sqrt{f_c'} + 10^6\right) \cdot \left(\frac{w_c}{145}\right)^{1.5}$$	• $3,000 psi \le f_c' \le 12,000 psi$
CEB-FIP 1990	$$E_c = 593,4000 \cdot \alpha_\beta \cdot \left[(f_{cm})/10\right]^{1/3}$$	• $f_c' \le 11,600 psi$
Where: f_c' = Compressive strength of a 6 x 12 in standard cylinder f_{cm} = Average 28-day compressive strength Should be replaced by $f_{ck} + 1160$ if the compressive strength is not known f_{ck} = Characteristic compressive strength of a 6 x 12 in cylinder w_c = unit weight of concrete in lb/ft^3 α_β = Correction factor for type of aggregate taken as 1.2 for basalt/dense limestone, 1.0 for quartizitic, 0.9 for limestone, and 0.7 for sandstone			

Baalbaki and other researchers investigated the influence of coarse aggregate on the elastic properties of high-strength concrete (Baalbaki et al, 1991). For this purpose, three different types of crushed aggregates were used with the same matrix characterized by having a water/cement ratio of 0.27, Canadian type 30 cement, and silica fume. Comparison of the stress-strain hysteresis curves for 4 by 8-inch cylinders at 28 and 91 days of age with the

observed curves for cores obtained from the parent rock showed the intrinsic relationship between the properties of the coarse aggregate and the hardened concrete.

Among their findings, researchers observed that concrete with the highest compressive strength was obtained using sandstone as the aggregate. This concrete also showed the lowest elastic modulus, which was in agreement with the properties of the aggregate itself. The inverse happened when a quartizitic aggregate was used. These phenomena were explained as being the result of two factors:

1) Better bond was developed between the sandstone and the mortar because this aggregate is more porous.

2) Relative incompressibility of the quartizitic aggregates generated stress concentrations in the transition zone while the sandstone allowed a more uniform distribution of stresses.

The general conclusion drawn from their experimental study indicated that empirical formulas relating modulus of elasticity to compressive strength are not suitable for high-strength concrete. Researchers indicated that it is possible to correlate elastic modulus and compressive strength of normal-strength concrete by using simple empirical equations because both are determined primarily by the weakness of the hydrated cement paste and transition zone. This is not the case for high-strength concrete because the low water/cement ratio produces a hydrated cement paste that can be as strong as or even stronger than the coarse aggregate.

A year later, Baalbaki was part of another research team that confirmed these conclusions by evaluating seven different types of coarse aggregate (Baalbaki et al, 1992). Measured values of the elastic modulus for four of the

seven aggregates showed good agreement with the predictions made using the ACI 363R-92 formula. Differences ranging from 11 to 67 percent were found between predicted and measured values for the other three types of aggregate which included a quartzite and two limestones.

Mokhtarzadeh and French studied the mechanical properties of high-strength concrete focusing mainly on precast applications (Mokhtarzadeh and French, 2000). More than 6000 specimens made with 142 different concrete mixes where analyzed. A water/cement ratio of 0.30, ASTM C150 type I and III cements with and without supplementary cementitious materials, different cement contents, coarse aggregates, superplasticizers, and curing conditions were some of the variables investigated. They concluded that current equations must be used with caution and that it is difficult to generalize the effect of coarse aggregate on concrete stiffness by using correction factors for each type as is done for the CEB-FIP equation. It was also observed that elastic moduli measured with 4 by 8-inch cylinders were, on average, 620 ksi higher than those obtained from 6 by 12-inch specimens. In addition, the 1-day elastic modulus values were observed to be approximately 98% of the 28-day values.

Early-age elastic properties of high-strength concrete are extremely important in prestressed applications. Compressive strength determines when the prestress can be transferred to the concrete, while initial deflections and prestress losses are largely related to the modulus of elasticity. Significant changes in the stress-strain relationships for concrete have been observed by various researchers during the first few hours after casting.

Khan, Cook, and Mitchell performed a detailed study on the stress-strain properties of high-strength concrete during the first 72 hours after casting (Khan et al, 1995). Three concrete mixes with 28-day compressive strengths between 4300 and 14,500 psi were made using Type 10 Canadian cement, silica fume,

limestone, and water/cement ratios of 0.25, 0.30, and 0.50. 4 by 8-inch cylinders were subjected to air-dried, sealed and matched temperature curing conditions in order to represent the curing processes at different locations within the cross-section of a precast element.

Tests showed that during these first hours, strength and modulus are low while the peak strain is high. The shape of the stress-strain response at this age is very different from the curve exhibited by concrete at 28 days of age. The response begins to resemble 28-day response 24 hours after casting. Researchers also indicated that, at early ages, the rate at which the elastic modulus increases is higher than the rate at which strength increases. The general conclusion obtained from this experimental study is that stiffness of very early age concrete can be overestimated if the current ACI 318 modulus equation is used.

Finally, Mesbah, Lachemi and Aïtcin evaluated the early-age elastic modulus of concrete through a series of tests performed using 4 by 8-inch cylinders (Mesbah et al, 2002). Concretes with 28-day compressive strengths of 5600, 8000, and 11,000 psi were made using crushed limestone, type 10 Canadian cement, silica fume, and water/cement ratios between 0.30 and 0.45. Both, the static elastic modulus (ASTM C469) and the dynamic elastic modulus (ASTM C567) were measured. The latter is a nondestructive test that allowed them to observe the change in stiffness since the initiation of the hardening process.

In general, conclusions obtained from this study are similar to what Khan expressed in 1995. There is a clear difference between the stress-strain behaviors of concrete at early ages and mature concrete. Stiffness is very dependent on the concrete age, especially during the first hours after casting. Nevertheless, Mesbah observed good agreement between measured and predicted values of the early-age elastic modulus when the ACI 318 formula was used. The ACI 363R-92 equation was inappropriate for predicting the modulus at early ages.

2.3.2 Tensile strength

Some experimental studies have examined the existing equations that relate tensile and compressive strengths. Two commonly recognized ways to determine the tensile strength of concrete are the splitting tensile strength (ASTM C496) and modulus of rupture (ASTM C78). This discussion centers on the modulus of rupture or flexural tensile strength because this parameter is necessary to analyze the flexural behavior of pretensioned concrete members constructed and evaluated in this study. Table 2-4 shows recommended equations based on compressive strength to predict the modulus of rupture.

Table 2-4: Equations for predicting the modulus of rupture of concrete

	Equation for f_r (psi)
ACI 318-02	$f_r = 7.5 \cdot \sqrt{f_c'}$
ACI 363R-92	$f_r = 11.7 \cdot \sqrt{f_c'}$

Iravani investigated the applicability of current code equations for estimating the elastic properties of high-performance concrete (Iravani, 1996). ASTM C150 type I and III cements were used to formulate four different concrete mixes having water/cement ratios ranging between 0.21 and 0.40. Subsequently, 6 by 6 by 22-inch beams were cast and cured for 24 hours in a laboratory environment and then for 55 days at 100% relative humidity. Test results showed that the ACI 363 equation for flexural tensile strength is applicable to high-performance concrete.

Khan, Cook, and Mitchell also evaluated these equations in their experimental study completed in 1996 (Khan et al, 1996). The same materials, proportions, and procedures of their 1995 elastic modulus study characterized this

investigation. Curing conditions were observed to affect the tensile strength of concrete. Specimens subjected to matched-temperature curing typically demonstrated higher strengths. In general, the equation proposed by ACI 363 overestimated the modulus of rupture for all concretes except for some matched-cured specimens. Results also indicated that the ACI 318 expression overestimated the flexural tensile strength at very early ages of concretes with compressive strengths under 2175 psi and underestimated tensile strength when this value was exceeded.

As part of their investigation completed in 2000, Mokhtarzadeh and French also studied the tensile strength of concrete. Modulus of rupture of moist-cured specimens was correctly predicted by the ACI 363 expression. The expression $fr = 9.3 \cdot \sqrt{f_c'}$ was proposed for heat-cured specimens.

2.4 SUMMARY

As occurred in reinforced concrete practice during the early part of the last century, prestressed concrete design based on working stress criteria appears to be moving toward a strength design approach. In fact, present provisions by ACI and AASHTO require that prestressed flexural members be designed to satisfy both allowable stress and strength requirements.

Except for minor modifications, permissible stress provisions for prestressed concrete have remained unchanged since they were first introduced by the Federal Bureau of Public Roads nearly fifty years ago. At that time, methods for controlling concrete quality and lack of supporting research resulted in conservative stress limits based mainly on experience being used in design practice. Years of research and practice have lead to significant improvements

and today, high performance materials and reliable construction techniques are employed.

In 1996, the PCI Technical Activities Council and the PCI Committee on Building Code presented a report indicating that no problems had been observed when concrete compressive stresses as high as *0.75f'ci* were allowed at release of prestress force. This report illustrates recent interest of researchers and professional societies in revising existing allowable stress requirements.

Research on this topic performed in the last two decades indicates that it may be possible to increase allowable extreme fiber compressive stress limits at transfer. Requirements based on strength design criteria have also been examined. Most of these investigations lack the necessary experimental data to support changes. Therefore, an extensive experimental study has been conducted at The University of Texas at Austin with the objective of evaluating the effect of cross-sectional geometry, stress level, and concrete used to fabricate pretensioned flexural members.

The response of prestressed elements depends significantly on the modulus of elasticity, modulus of rupture, and compressive strength of the concrete utilized. Various building codes propose empirical formulas for predicting elastic modulus and tensile strength as a function of the compressive strength. The validity of these formulas for high-strength concrete is a subject of discussion. Most researchers have agreed that direct determination of these properties is the only way to guarantee accurate results. However, these formulas are commonly used by engineers in design and analysis of prestressed concrete members.

CHAPTER 3

Analysis and Design Procedures

3.1 OVERVIEW

This chapter describes the methods used to design and analyze the test specimens investigated in this project. A linear analysis approach commonly used by engineers is presented first. This approximate method for calculating stresses provides reasonable results for prestressed concrete members subjected to flexural stresses within the current allowable limits. In order to better predict the behavior of highly stressed elements, such as those tested in this research program, an analysis approach that accounts for nonlinear behavior of the concrete is also presented.

Factors that affect prestressed concrete behavior are also described in this chapter. These and other aspects considered in the design of the beam specimens are discussed. Finally, preliminary section dimensions of the specimens and strand patterns are presented. Calculation examples will be provided in Chapter 5.

3.2 FACTORS AFFECTING THE BEHAVIOR OF PRETENSIONED BEAMS

As indicated in the commentary of the ACI 318-02 Building Code, ensuring serviceability is the main reason for establishing allowable stress limits in prestressed concrete members. Provisions included in present ACI and AASHTO codes are primarily intended to prevent problems such as cracking and excessive deflection or camber. In addition, the extreme fiber compressive stress

32

limit is intended to prevent concrete crushing during transfer of the prestress force (Noppakunwijai et al, 2001).

The permissible stress provisions have not changed significantly since proposed in 1958 by Joint Committee 323 in the *Tentative Recommendations for Prestressed Concrete*. Following publication of this document, T. Y. Lin commented that behavior of prestressed concrete elements is not exclusively affected by stresses at transfer. He remarked that factors such as the cross-section shape and magnitude and location of the prestressing force must also be taken into consideration.

As discussed in Section 2.2.3.3, Noppakunwijai et al observed a relationship between the cross-section properties of the member and its behavior. They developed and used a strength design method to analyze several standard double tee, inverted tee, and rectangular cross sections. They concluded that, in order to provide a uniform factor of safety, the allowable compressive stress at release should be increased as the ratio of distance to the extreme compressive fiber and total depth of the member increases. They also observed that the compressive stress limit of $0.60f'_{ci}$ was very conservative for all the cross sections studied.

An additional factor that can affect the response of prestressed concrete members is the stress gradient that results from the location and magnitude of the prestress force (Figure 3-1). A beam with a high stress gradient and high extreme fiber stresses could behave well because stresses decrease rapidly over the height of the cross section. However, beams with low gradients and high compressive stresses could experience an abnormal amount of creep resulting in undesirable serviceability and performance.

HIGH GRADIENT   LOW GRADIENT

σ top / tension   σ top / compression

c.g.   c.g.

e   e

Po   Po

σ bottom / compression   σ bottom / compression
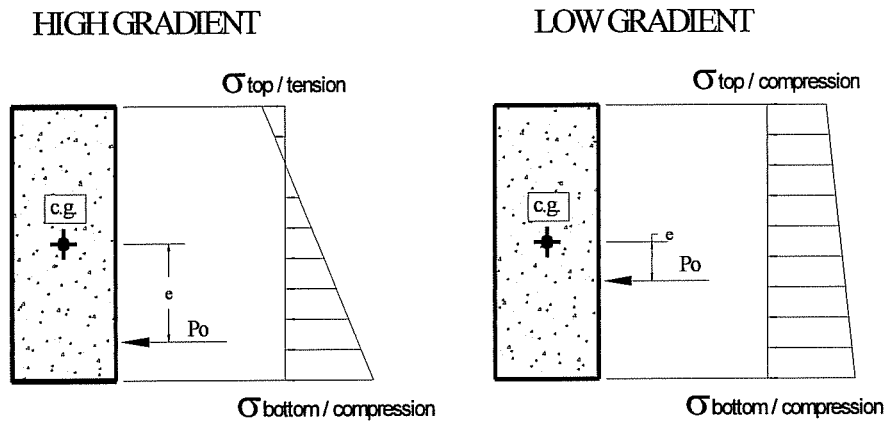
Figure 3-1: Stress gradients in prestressed concrete

Besides compressive strength, other concrete mechanical properties influence the behavior of prestressed elements. Initial deflections and prestress losses due to elastic shortening are primarily influenced by the elastic modulus at transfer. Time-dependent deflections are affected by the creep and shrinkage properties of concrete. Due to its internal microstructure, there is a profound relationship between the properties of high-strength concrete and coarse aggregate. Therefore, a change in aggregate could result in considerably different time-dependent behavior of prestressed members. As will be discussed in the next chapter, two types of aggregates were used in this program to evaluate the effect on member behavior following release of the prestress force. River rock (hard rock) was used to formulate a high-elastic-modulus concrete, while concrete with a lower modulus was batched using crushed limestone (soft rock). Creep of concrete made with soft aggregate was expected to be higher than that of concrete made with hard aggregate for the same mixing proportions (Mokhtarzadeh and French No.2, 2000).

34

The rate of strength gain at the time of release is another factor that may affect the behavior of prestressed concrete members after transfer. The strength gain rate is high in the early stages of the hydration process and gradually decreases with time. The time-dependent response of concrete members depends largely on the modulus of elasticity, which has traditionally been considered to be a function of compressive strength. Assuming this relationship is valid for early-age concrete, the elastic modulus also increases rapidly at early stages of the hydration process. Based on this reasoning, a member subjected to extreme fiber stresses above $0.60f'_{ci}$ when concrete is experiencing a high rate of strength gain will exhibit lower deflections than a member with a lower rate of strength gain subjected to the same stresses. As a point of reference, release of the prestress force typically occurs in precast plants within 24 hours of casting. At this stage, compressive strengths usually range from 55 to 60 percent of the 28-day strength (Burson Patton, 2002).

For precast applications, concrete made with ASTM C150 Type III cement is typically used in order to attain the concrete compressive strength required for prestress release at the desired time. As discussed in Section 2.3, the relationship between compressive strength and elastic modulus for this type of concrete has been investigated in recent years by researchers such as Khan, Cook, and Mitchell (Khan et al, 1995). In general, research has indicated that, unlike for normal-strength concrete, there is no clear correlation between strength and modulus for early-age concrete. Moreover, it has been observed that during the first 24 hours, stiffness increases more rapidly than strength. Elastic moduli as high as 98 percent of the 28-day values have been measured one day after casting (Mokhtarzadeh and French, 2000). In conclusion, the rate of strength gain cannot be easily correlated with the rate of stiffness gain, and therefore, it is difficult to generalize the effect of prestress release at different stages of concrete hydration.

3.3 ANALYSIS METHODS

3.3.1 Linear analysis and design

3.3.1.1 Allowable Stress Design

This approach is based on the assumptions that plane sections remain plane, and that the stress-strain behavior of concrete and steel are linear. Due to its simplicity, this procedure is typically used by designers to compute stresses in prestressed concrete members. It is reasonably accurate for extreme fiber compressive stresses as large as the current permissible limit of $0.6f'_{ci}$ (Huo and Tadros, 1997).

As shown in Equations 3-1 and 3-2, the simplicity of this approach lies in the fact that it only requires knowing the gross cross-section properties and the prestress force. The designer does not need to input material properties, and can use this approach to compute the required concrete strength at release by comparing the resulting stresses with allowable limits. It should be added that, according to current design provisions, prestressed concrete members must satisfy both allowable stress and strength requirements.

$$\sigma_{compression} = -\frac{P_0}{A_g} - \frac{P_0 \cdot e \cdot y_b}{I_g} \leq 0.60 f'_{ci} \qquad \qquad \textit{Equation 3-1}$$

$$\sigma_{tension} = -\frac{P_0}{A_g} + \frac{P_0 \cdot e \cdot y_t}{I_g} \leq 6\sqrt{f'_{ci}} \qquad \qquad \textit{Equation 3-2}$$

As a result of the location and magnitude of the prestress force, pretensioned concrete beams typically experience compressive stresses at the bottom extreme fiber and tensile stresses at the top fiber. The equations shown

36

above assume this condition, and as a result, the distance from the bottom extreme fiber to the centroid, y_b, is used to compute the maximum compressive stress, and the distance to the top fiber, y_t, is employed to calculate the maximum tensile stress.

As indicated, linear elastic material behavior is assumed. Hence, once the extreme fiber stresses are computed, the corresponding strains can be easily estimated, and so can the resulting curvatures. The resulting rotations and deflections along a beam can be determined by numerical integration of the curvatures.

Finally, in order to estimate the effective prestress force, a 10% reduction in prestress between jacking and transfer is normally assumed for stress-relieved strands, and 7.5% for low-relaxation strands. A more accurate procedure for estimating these losses can be found in the PCI Design Handbook (Precast/Prestressed Concrete Institute, 1999).

3.3.1.2 Strain Compatibility Approach

As indicated by Equations 3-3 through 3-6, this method assumes that the material stress-strain relationships are linear elastic and that concrete is not cracked. The terms used in these equations are defined in the Glossary. In this approach, Equations 3-7 and 3-8 are used to compute the curvature and strain at the centroid of the cross section due to prestress force and externally applied loads and moments (Collins and Mitchell, 1997). As a result, it is useful for estimating concrete stresses, member camber, and deflections.

$$f_c = E_c \varepsilon_{cf} = E_c \left(\varepsilon_c - \varepsilon_{sh} \right) \qquad\qquad \textbf{\textit{Equation 3-3}}$$

$$f_s = E_s \varepsilon_{sf} = E_s \varepsilon_s \qquad\qquad \textbf{\textit{Equation 3-4}}$$

$$f_p = E_p \varepsilon_{pf} = E_p \varepsilon_p \qquad\qquad\qquad \textbf{\textit{Equation 3-5}}$$

$$\Delta \varepsilon_p = \varepsilon_p - \varepsilon_c \qquad\qquad\qquad \textbf{\textit{Equation 3-6}}$$

$$\varepsilon_{cen} = \frac{N - N_o}{E_c \cdot A_{trans}} \qquad\qquad\qquad \textbf{\textit{Equation 3-7}}$$

$$\phi = \frac{M - M_o}{E_c \cdot I_{trans}} \qquad\qquad\qquad \textbf{\textit{Equation 3-8}}$$

where:

$$N_o = \int E_p \Delta \varepsilon_p dA_p - \int E_c \varepsilon_{co} dA_s - \int E_s \varepsilon_{so} dA_s - \int E_p \varepsilon_{po} dA_p \qquad \textbf{\textit{Equation 3-9}}$$

$$M_o = -\int E_p \Delta \varepsilon_{py} dA_p + \int E_c \varepsilon_{co} y dA_s + \int E_s \varepsilon_{so} y dA_s + \int E_p \varepsilon_{po} y dA_p \quad \textbf{\textit{Equation 3-10}}$$

For this study, Equations 3-9 and 3-10 were simplified to:

$$N_o = E_p \Delta \varepsilon_p A_{ps} - E_c \varepsilon_{co} A_c \qquad\qquad\qquad \textbf{\textit{Equation 3-11}}$$

$$M_o = E_p \Delta \varepsilon_p A_{ps} \left(y_{bt} - y_{b-ps} \right) - E_c \varepsilon_{co} A_c \left(y_{bt} - y_{b-c} \right) \qquad \textbf{\textit{Equation 3-12}}$$

3.3.2 Nonlinear Analysis

As stated by Huo and Tadros, nonlinear analysis is the most appropriate approach for calculating stresses in concrete members subjected to high prestress levels. Their actual response can be considerably different from that predicted based on a linear analysis, especially for cracked elements. Hence, an approach that takes into account the nonlinear stress-strain behavior of the materials is more suitable for analyzing the performance of most of the pretensioned beams

fabricated at Ferguson Laboratory during this study. For this purpose, a software package named RESPONSE and the stress-strain models shown in Table 3-1 were used during the research program (Collins and Mitchell, 1990).

Table 3-1: Stress-strain behavior for nonlinear analysis

Description	Expression
Concrete in compression	$\dfrac{\sigma_c}{f'_c} = \dfrac{n \cdot \left(\varepsilon_{cf} / \varepsilon'_c\right)}{n - 1 + \left(\varepsilon_{cf} / \varepsilon'_c\right)^{n \cdot k}}$
	$n = 0.8 + \dfrac{f'_c}{2500}$
	$k = 0.67 + \dfrac{f'_c}{9000} \geq 1$
	$\varepsilon'_c = \dfrac{f'_c}{Ec} \cdot \dfrac{n}{n-1}$
Concrete in tension	$\sigma_c = E_c \cdot \varepsilon_{cf}$ $f_r = 7.5 \cdot \sqrt{f'_c}$
Prestressing steel in tension (Ramberg-Osgood Model)	$f_p = 29000 \cdot \varepsilon_{pf} \cdot \left\{ 0.025 + \dfrac{0.975}{\left[1 + \left(118 \cdot \varepsilon_{pf}\right)^{10}\right]^{0.10}} \right\} \leq 270$

3.3.3 Prediction of camber

After prestress transfer, pretensioned concrete beams typically deform upward due to application of the prestress force. This upward deflection, also known as camber, can easily be calculated based on known cross-sectional properties and the prestress force. Essentially, curvatures along a beam can be computed using either of the aforementioned methods and then can be used to determine rotations and deflections by numerical integration. In addition, the Precast/Prestressed Concrete Institute (PCI) provides deflection equations and

suggests multipliers for estimating initial and long-term deflections, respectively (PCI, 1999). The applicable equations for typical conditions in Ferguson Laboratory are presented in Table 3-2.

Table 3-2: PCI expressions for camber estimation

Initial Camber	
Downward deflection due to self-weight of the member	$\Delta = \dfrac{5wl^4}{384EI}$
Upward deflection due to prestressing	$\Delta = \dfrac{P_o el^2}{8EI}$
Resulting camber	$\Delta = \dfrac{P_o el^2}{8EI} - \dfrac{5wl^4}{384EI}$
Long Term Camber	
Downward deflection due to self-weight of the member	$\Delta = 2.70 \cdot \dfrac{5wl^4}{384EI}$
Upward deflection due to prestressing	$\Delta = 2.45 \cdot \dfrac{P_o el^2}{8EI}$
Resulting camber	$\Delta = \dfrac{4.9 P_o el^2}{16EI} - \dfrac{27wl^4}{768EI}$

PCI provides these multipliers as a guide for calculating long-term cambers and deflections. Results obtained through this method must be considered as mere estimates. Therefore, a more rigorous analysis based on the method described in 3.3.1.2 was conducted to evaluate the time-dependent variations in camber for the test specimens.

It is not necessary to consider creep, shrinkage, relaxation and temperature effects in the calculation of initial camber. However, these effects generally result in a gradual reduction of the prestress force with time. Consequently, they must

be taken into account when evaluating the time-dependent response of pretensioned beams.

ACI Committee 209 has published a unified method for predicting volumetric changes of concrete with time (ACI Committee 209, 1992). The Precast/Prestressed Concrete Institute (PCI, 1999) and AASHTO (AASHTO, 1996) have also proposed simplified procedures for estimating these effects. Accurate results can only be expected with these methods if the predictions are made based on creep and shrinkage data obtained by testing the actual materials. Such tests were not performed for the materials used in this project. Thus, it was necessary to rely on previously suggested expressions like those shown in Table 3-3. These expressions were used in combination with the procedure described in 3.3.1.2 to estimate concrete strains at different times after release. Table 3-3 indicates that creep and relaxation effects were accounted for through the use of a reduced elastic modulus, and shrinkage was included by introducing a shrinkage strain that is a function of time and an ultimate shrinkage strain.

Concrete volumetric changes due to temperature were not considered in the analysis. The specimens were kept indoors where the ambient temperature never changed more than 25°F while the beams were being monitored. If considered in the analysis, this variation in temperature would result in very small variations of the predicted cambers. For instance, a change of just ±2.4% of the predicted 30-day camber for specimen R3-76-5 (Table 3-7) would result from a variation of ±25°F if the coefficient of thermal expansion for hardened concrete and steel is assumed to be $6 \cdot 10^{-6}$.

Table 3-3: Expressions for time-dependent material behavior

Description	Expression	Reference
Concrete Creep	$$E_{c,eff} = \frac{E_c}{1+v(t,t_i)}$$ $$v(t,t_i) = 1.2 \cdot 3.5 \cdot k_c k_f \left(1.58 - \frac{H}{120}\right) t_i^{-0.118} \frac{(t-t_i)^{0.6}}{10+(t-t_i)^{0.6}}$$	AASHTO, 1996
Shrinkage	$$\varepsilon_{sh} = -k_s k_h \left(\frac{t}{35+t}\right) 0.51 \times 10^{-3}$$	AASHTO, 1996
Prestressing steel Relaxation	$$E_{p,eff} = \frac{f_p}{f_{pi}} E_p$$ $$\frac{f_p}{f_{pi}} = 1 - C_T \frac{\log t}{45}\left(\frac{f_{pi}}{f_{py}} - 0.55\right)$$	Ontario Highway Bridge Design Code (OHBDC), 1983
Where	k_c, k_s, k_f, k_h = factors that account for member size and shape, creep properties of high-strength concrete, and relative humidity. H = relative humidity t_i = concrete age at initial loading f_{py}, f_{pi} = yield strength and initial prestress	
Notes	• As recommended by Collins and Mitchell (Collins and Mitchell, 1997), the predicted strand relaxation was increased by a factor C_T for temperatures other than T=70°F. Where: $$C_T = 1 + \left(\frac{T-70}{30}\right)$$ • As suggested by Collins and Mitchell, predicted concrete shrinkage was increased by 20 percent since moist-cured concrete elements were exposed to drying before t=5 days.	

42

3.4   DESIGN OF BEAM SPECIMENS

A series of test specimens were designed at Ferguson Laboratory to study the influence of cross-sectional geometry, rate of strength gain, coarse aggregate type, and stress gradient on the response of pretensioned concrete beams subjected to high release stresses. It was the intent to design, fabricate, and monitor the behavior of specimens representative of shapes used in the precast concrete industry; especially those used by the Texas Department of Transportation (Figures 3-2, 3-3, and 3-4).

As discussed in Section 3.2, a relationship between the behavior of a member and its cross-section geometry, expressed as the ratio y_b/h, was suggested by Noppakunwijai et al. Consequently, the centroid location was used as a guide for developing appropriate small-scale beam cross sections for this study. Cross-sectional properties of standard TxDOT girders are presented in Tables 3-4, 3-5, and 3-6. As observed, the average y_b/h ratios for U and double-tee shapes are 0.41 and 0.68, respectively. The ratio for an AASHTO Type IV I-girder is 0.46.

Inverted tee, tee, and rectangular beams, having these approximate y_b/h ratios, were designed to represent each of the three standard shapes mentioned (U-beam, double tee, and I-beam, respectively). Their dimensions were determined following the allowable stress design procedure described in Section 3.3.1. The resulting cross sections and release stresses and strengths are shown in Figure 3-5 and Table 3-7.

The specimen designations shown in Table 3-7 include the type of cross section (Figure 3-5), the target extreme fiber compressive stress at transfer expressed as a percentage of the concrete strength at release, and finally, the number corresponding with the cast. As will be discussed in Chapter 4, five different concrete castings were performed in this study, and three different concrete mixes were used. The length of each test specimen was fifteen feet, so a

total of six specimens, or two per bay, could be cast at the same time in the prestressing bed.
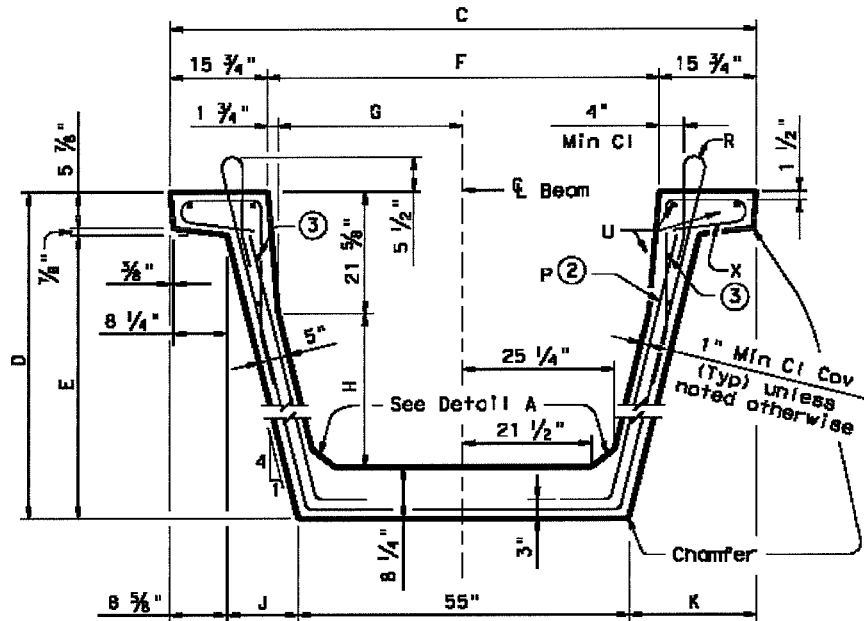
Figure 3-2: Cross section of TxDOT U girders

Table 3-4: Properties of standard TxDOT U girders

Beam Type	C (in)	D (in)	y_t (in)	y_b (in)	A (in^2)	I (in^4)	y_b/h
U40	89	40	23.66	16.30	979.9	183108	0.41
U54	96	54	31.58	22.36	1120.0	403020	0.41
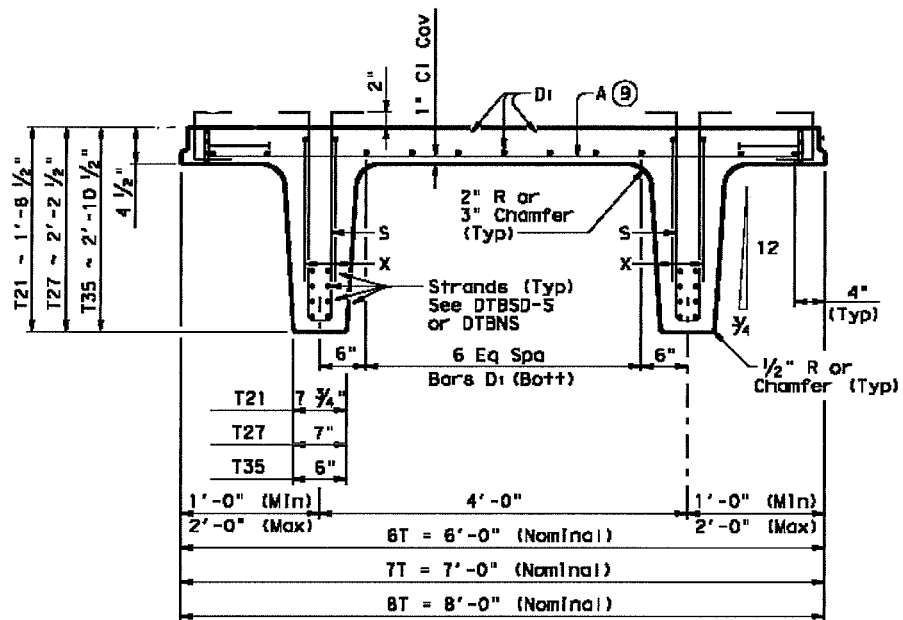
Figure 3-3: Cross section of TxDOT double tee girders

Table 3-5: Properties of standard TXDOT double tee girders

Beam Type	Width (ft)	Depth (in)	y_t (in)	y_b (in)	A (in^2)	I (in^4)	y_b/h
6T21	6.00	20.50	6.88	13.62	603	21140	0.66
7T21	7.00	20.50	6.50	14.00	657	22292	0.68
8T21	8.00	20.50	6.17	14.33	711	23283	0.70
6T27	6.00	26.50	8.99	17.51	691	42511	0.66
7T27	7.00	26.50	8.51	17.99	745	44881	0.68
8T27	8.00	26.50	8.08	18.42	799	46942	0.70
6T35	6.00	34.50	11.79	22.71	795	84325	0.66
7T35	7.00	34.50	11.18	23.32	849	89017	0.68
8T35	8.00	34.50	10.65	23.85	903	93159	0.69

45

a) Type IV Beam   b) 8in x 18in Specimen
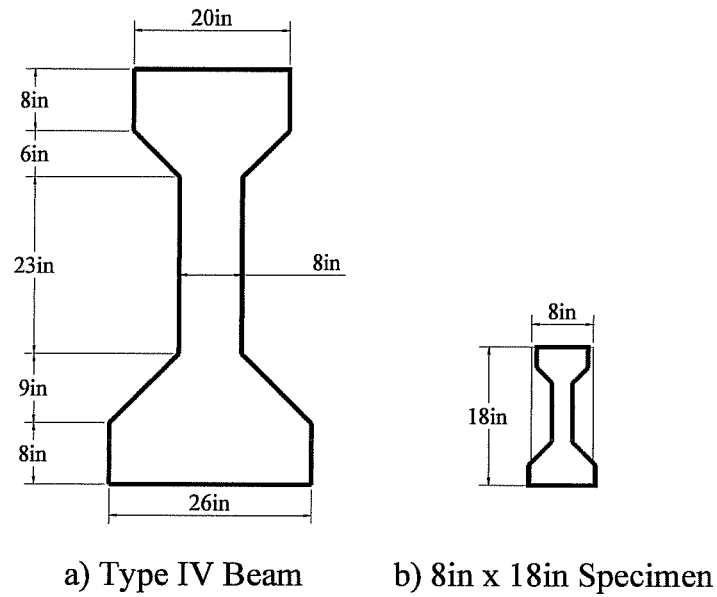
Figure 3-4: a) AASHTO Type IV beam; b) 1:3 Scaled Type IV beam and 8 by 18-in test specimen

Table 3-6: Properties of TXDOT (AASHTO Type IV) I-girder

Beam Type	Width (in)	Depth (in)	y_t (in)	y_b (in)	A (in^2)	I (in^4)	y_b/h
AASHTO TYPE IV	26	54	29.27	24.73	789	260,730	0.46

Beam type: **R1**
A_{ps}: 0.92 in²
A_s': 0 in²
y_b: 9.00 in
y_b / h : 0.50

Beam type: **IT1**
A_{ps}: 1.22 in²
A_s': 0 in²
y_b: 7.50 in
y_b / h : 0.42

Beam type: **R2**
A_{ps}: 1.53 in²
A_s': 0 in²
y_b: 9.00 in
y_b / h : 0.50

Beam type: **IT2**
A_{ps}: 1.53 in²
A_s': 0 in²
y_b: 7.88 in
y_b / h : 0.41

Beam type: **R3**
A_{ps}: 1.22 in²
A_s': 0 in²
y_b: 9.00 in
y_b / h : 0.50

Beam type: **IT3**
A_{ps}: 1.53 in²
A_s': 0.22 in²
y_b: 7.88 in
y_b / h : 0.41

Beam type: **T1**
A_{ps}: 0.46 in²
A_s': 0 in²
y_b: 10.27 in
y_b / h : 0.66

Beam type: **T2**
A_{ps}: 0.61 in²
A_s': 0 in²
y_b: 10.27 in
y_b / h : 0.66

Figure 3-5: Test specimen cross sections

47

Table 3-7: Details of beam specimens

Designation	No. of specimens	Mix Type	e (in)	P_0 (kips)	f'_{ci} (psi)	Target Stresses σ_{BOTTOM}	Target Stresses σ_{TOP}
R1-60-1	2	1	3.25	172	5500	$-0.60\ f'_{ci}$	$1.8\sqrt{f'_{ci}}$
R1-70-1	2	1	3.25	172	4700	$-0.70\ f'_{ci}$	$1.9\sqrt{f'_{ci}}$
R1-75-1	2	1	3.25	172	4400	$-0.75\ f'_{ci}$	$2.0\sqrt{f'_{ci}}$
R2-75-2	1	1	1.10	286	4800	$-0.75\ f'_{ci}$	$-0.35\ f'_{ci}$
R2-85-2	1	1	1.60	286	4800	$-0.85\ f'_{ci}$	$-0.26\ f'_{ci}$
T1-74-2	1	1	5.47	86	4000	$-0.74\ f'_{ci}$	$4.2\sqrt{f'_{ci}}$
T1-82-2	1	1	6.22	86	4000	$-0.82\ f'_{ci}$	$6.4\sqrt{f'_{ci}}$
IT1-76-2	1	1	3.00	229	3800	$-0.76\ f'_{ci}$	$3.5\sqrt{f'_{ci}}$
IT1-84-2	1	1	3.75	229	3800	$-0.84\ f'_{ci}$	$10.8\sqrt{f'_{ci}}$
R3-76-3	1	1	3.50	193	3800	$-0.76\ f'_{ci}$	$3.6\sqrt{f'_{ci}}$
R3-82-3	1	1	4.00	193	3800	$-0.82\ f'_{ci}$	$7.2\sqrt{f'_{ci}}$
T2-76-3	1	1	4.50	96	3800	$-0.79\ f'_{ci}$	$1.3\sqrt{f'_{ci}}$
T2-85-3	1	1	5.25	96	3800	$-0.85\ f'_{ci}$	$4.0\sqrt{f'_{ci}}$
IT2-85-3	1	1	3.66	258	3800	$-0.85\ f'_{ci}$	$9.3\sqrt{f'_{ci}}$
IT3-85-3	1	1	3.66	258	3800	$-0.85\ f'_{ci}$	$9.3\sqrt{f'_{ci}}$
R3-76-4	1	2	3.50	193	3800	$-0.76\ f'_{ci}$	$3.6\sqrt{f'_{ci}}$
R3-82-4	1	2	4.00	193	3800	$-0.82\ f'_{ci}$	$7.2\sqrt{f'_{ci}}$
T2-76-4	1	2	4.50	96	3800	$-0.79\ f'_{ci}$	$1.3\sqrt{f'_{ci}}$
T2-85-4	1	2	5.25	96	3800	$-0.85\ f'_{ci}$	$4.0\sqrt{f'_{ci}}$
IT2-85-4	1	2	3.66	258	3800	$-0.85\ f'_{ci}$	$9.3\sqrt{f'_{ci}}$
IT3-85-4	1	2	3.66	258	3800	$-0.85\ f'_{ci}$	$9.3\sqrt{f'_{ci}}$
R3-76-5	1	3	3.50	193	3800	$-0.76\ f'_{ci}$	$3.6\sqrt{f'_{ci}}$
R3-82-5	1	3	4.00	193	3800	$-0.82\ f'_{ci}$	$7.2\sqrt{f'_{ci}}$
T2-76-5	1	3	4.50	96	3800	$-0.79\ f'_{ci}$	$1.3\sqrt{f'_{ci}}$
T2-85-5	1	3	5.25	86	3800	$-0.85\ f'_{ci}$	$4.0\sqrt{f'_{ci}}$
IT2-85-5	1	3	3.66	258	3800	$-0.85\ f'_{ci}$	$9.3\sqrt{f'_{ci}}$
IT3-85-5	1	3	3.66	258	3800	$-0.85\ f'_{ci}$	$9.3\sqrt{f'_{ci}}$

The first six specimens were designed by Steven Rogers to be released at different concrete compressive strengths (Rogers, 2002). While the target bottom fiber stresses ranged from $0.60f'_{ci}$ to $0.75f'_{ci}$, the top tensile stresses did not exceed the current allowable limits. The six beams in the second casting were designed to target maximum compressive stresses at release ranging from $0.74f'_{ci}$ to $0.85f'_{ci}$ by varying the eccentricities and concrete strengths at release. Specimens R2-75-2 and R2-85-2 were designed to study the effect of a low stress gradient on the time-dependent behavior of this type of specimen. Note in Table 3-7 that the top fiber stresses for these beams were also in compression. The current allowable tensile stress limit of $6\sqrt{f'_{ci}}$ was exceeded in specimens T1-82-2 and IT1-84-2. However, no top reinforcement, as required by ACI and AASHTO, was used in the top of these beams to resist the tensile force.

The specimen design used for the third casting was also used for the fourth and fifth casting. As indicated in the table, the only difference between the three different casts of specimens was the concrete mix. Using these three sets of specimens, the researchers intended to investigate the effects of cross-sectional properties and mechanical properties of concrete on the time-dependent behavior of the specimens. At prestress force transfer, the extreme fiber compressive stresses in these beams ranged from $0.76f'_{ci}$ to $0.85f'_{ci}$ and the tensile stresses from $1.3\sqrt{f'_{ci}}$ to $9.3\sqrt{f'_{ci}}$. These concrete stresses resulted from providing different prestress force eccentricities while releasing all the beams at a concrete strength of 3800 psi. A top fiber tensile stress of $9.3\sqrt{f'_{ci}}$ was computed for the IT2 and IT3 specimens based on the aforementioned linear approach. However, nonprestressed top reinforcement was placed in only the IT3 beams. Steel reinforcement to resist bursting stresses produced during release was also designed according to the AASHTO provisions and was placed in the ends of

specimens fabricated for the third through fifth casting (AASHTO, 1998). Reinforcement details can be found in Appendix C.

3.5 SUMMARY

The objective of this study is to examine the influence of cross-sectional geometry, rate of concrete strength gain, coarse aggregate type, and stress gradient on the time-dependent response of pretensioned concrete beams subjected to elevated stresses at release (application of the pretensioning force). Based on recommendations made by previous researchers, the ratio between the distance from the centroid of the section to the extreme compressive fiber, and the total depth, was calculated for various TxDOT bridge girder types and was used as a guide in selecting representative small-scale beam sections. Actual dimensions of the specimens were determined using the allowable stress design method taking into consideration the capacity of the prestressing facility in Ferguson Laboratory.

The design of the test specimens and actual beams utilizes the assumption of linear elastic stress-strain behavior of the materials. The response of cracked and highly stressed elements can be significantly different from that predicted based on this assumption. Consequently, an approach that takes into account the nonlinear stress-strain behavior of the materials was also used to analyze the behavior of the pretensioned beams fabricated in Ferguson Laboratory. Because it requires more computational effort, a software package called RESPONSE was employed.

The behavior of the test specimens is affected by factors such as creep, shrinkage, and relaxation. Hence, these factors must be considered in the prediction of long-term camber. In the absence of tests performed specifically to

characterize the time-dependent behavior of materials used in this project, it was necessary to utilize empirical expressions suggested by AASHTO and the Ontario Ministry of Transportation and Communications to predict the time-dependent behavior of the specimens. These expressions were used in combination with the strain compatibility analysis procedure to compute the variation in concrete strains and member deflections with time.

CHAPTER 4

Experimental Program

4.1 OVERVIEW

This chapter provides a description of the experimental program carried out in Ferguson Structural Engineering Laboratory to investigate the time-dependent behavior of pretensioned concrete beams subjected to stresses at prestress release that exceed currently allowable stresses. The design and fabrication of the pretensioning bed, fabrication of beam specimens, instrumentation and data acquisition equipment, and materials used in the experimental program, are described here. The five sets of specimens fabricated and monitored in this study were cast on the dates listed in Table 4-1. Groups of specimens will be referred to at various points in the chapter by the set numbers listed in this table.

Table 4-1: Casting dates for groups of beam specimens

Set No.	Specimens	Date of cast
1	6 rectangular	June 26, 2002
2	2 rectangular / 2 tee / 2 inverted tee	August 13, 2002
3	2 rectangular / 2 tee / 2 inverted tee	September 24, 2002
4	2 rectangular / 2 tee / 2 inverted tee	December 5, 2002
5	2 rectangular / 2 tee / 2 inverted tee	March 4, 2003

Prior to fabrication and monitoring of the five sets of specimens listed in Table 4-1, a preliminary set of beams were fabricated and monitored by Rogers (Rogers, 2002) to test fabrication procedures and instrumentation. Modifications

in the experimental program, especially with respect to instrumentation and monitoring, were made in response to observations made during the pilot study by Rogers.

4.2 PRESTRESSING FACILITY

A prestressing facility capable of accommodating three bays of beam specimens, with two beams per bay, was constructed in Ferguson Laboratory. As shown in Figure 4-1, it was composed of a reaction frame and three plywood platforms. Steel buttresses and bulkheads used previously by Bruce Russell (Russell, 1992) were repaired, painted, and incorporated in this prestressing bed. Four 35-foot long, 12 x 12 in. structural steel tubes with a 1/2-in. wall thickness completed the reaction frame.
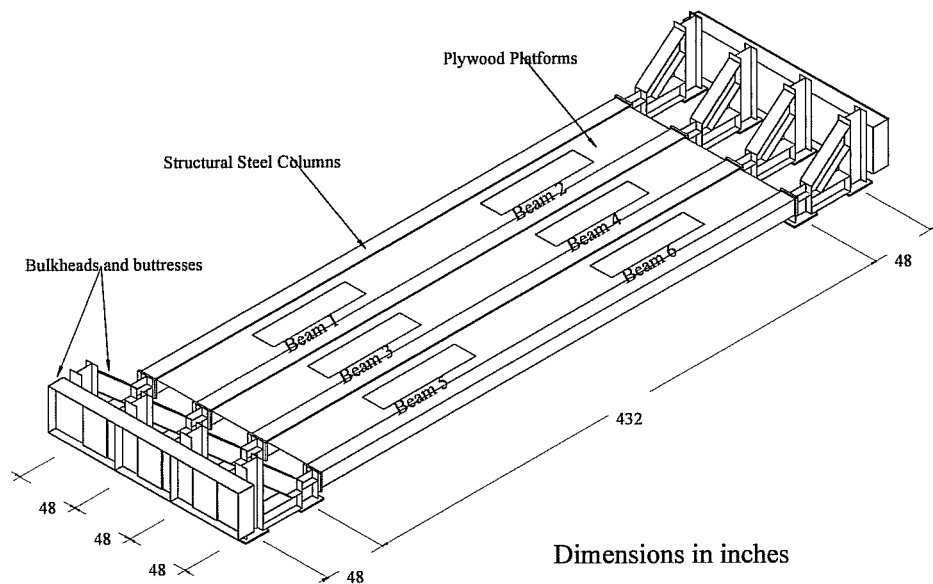
Figure 4-1: Prestressing Facility at Ferguson Laboratory

The capacity of the reaction frame at each end of the prestressing bed (Figure 4-1) was initially computed based on assumptions about the maximum amount of prestressing required and the eccentricity of that prestress force. Once all beams had been designed, and the number of strands and eccentricity of the strands was known, it was possible to refine earlier calculations for the capacity of the prestressing bed. Figure 4-2 shows a free body diagram of one of the buttresses used to transfer the prestress forces applied to the bulkheads to the laboratory floor.

The bulkheads are made of 35.5-inch deep steel plate girders modified with 0.75-in thick plates that bear against the buttresses. Half inch prestressing strands can be passed through holes drilled at a 2-inch spacing and then be anchored on the outside of these elements. The bulkheads serve to distribute the force in the strands to the buttresses. In the free body diagram, $W_{BULKHEAD}$ represents the approximate self-weight of the bulkhead supported by a buttress.

The buttresses are frames made up of standard W14x61 steel shapes. These elements are connected to the reinforced concrete laboratory floor using eight 1-inch diameter threaded steel rods. The four rods located at the outer tie-down connection were post-tensioned to 30 kips each, for a total of 120 kips. This force and the self-weight of the buttress are represented in Figure 4-2 by F_{FLOOR} and $W_{BUTTRESS}$, respectively.

The load-carrying capacity for this study required of the buttresses could not be provided by the buttresses alone, even after the tie-down rods were post-tensioned. The friction force developed at the floor-buttress interface, F_F, and the tension in the rods were not sufficient to resist the overturning moment and lateral load exerted by the prestress force, P_i, located at a height, h_p, of 26 inches. Therefore, the 35-foot long steel tubes were placed between opposing buttresses

at a height, h_c, of 13 inches to provide the necessary capacity. The axial strength of these elements is 490 kips according to the LRFD specifications by the American Institute of Steel Construction (AISC, 2001).

F_{FLOOR} = 120kip
$W_{BULKHEAD}$ = 0.83kip
$W_{BUTTRESS}$ = 0.77kip
W_{COLUMN} = 1.40kip
$F_F = 0.2(R_a + R_b)$
$R_a = (P_i (h_p - h_c) - 24.6h_c + 5826)/48$
$R_b = 123 - R_a$
$R_c = P_i - F_F$

Dimensions in inches
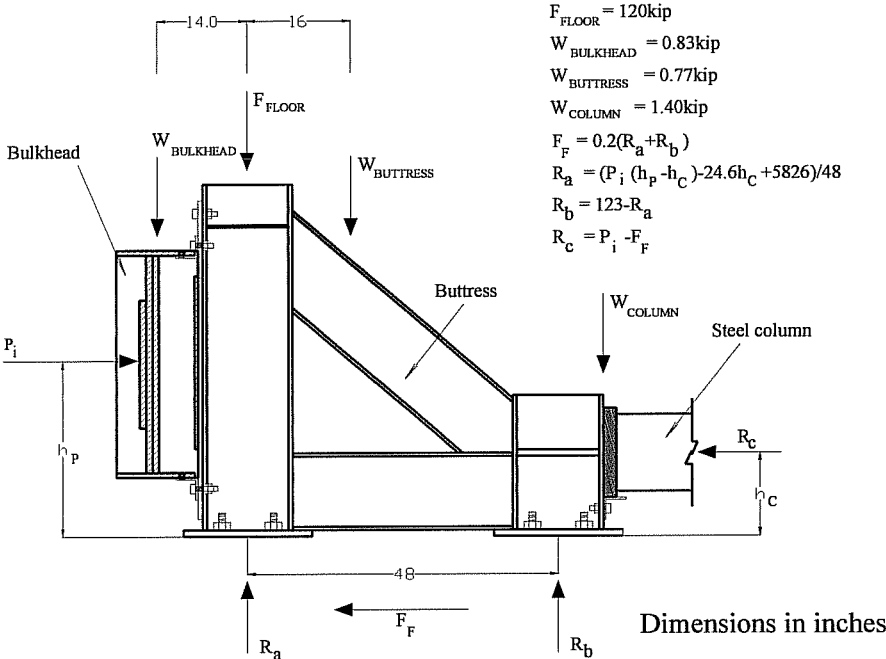
Figure 4-2: Free body diagram for one buttress

The equations shown in Figure 4-2 were obtained by applying force and moment equilibrium principles to the two-dimensional model. The equations were then used to compute the load-carrying capacity of the frame by specifying known dimensions and loads. One of the parameters used in the equations was the location of the prestress force, h_p. A critical height of 27.5 inches was used after analyzing the position of the strands for all test specimens.

55

Because the precise friction coefficient needed to calculate the force generated at the floor-buttress interface was not known, a value of 0.20 was initially assumed. Later, the analysis was performed considering no friction force ($\mu = 0$.). This range of friction coefficients lead to the results presented in Table 4-2.

Table 4-2: 2D analysis results for one buttress

h_p (in)	h_c (in)	μ	P_i (kips)	F_F (kips)	R_a (kips)	R_b (kips)	R_c (kips)
27.5	13.0	0.2	375	24.6	1.4 Adequate > 0	121.6	350.4 Adequate < 500
27.5	13.0	0	375	0	8.1 Adequate > 0	114.9	375 Adequate < 500

It was concluded that the capacity of the reaction frame is governed by the working load limit of the steel rods used to provide the tie-down force at the outer end of each buttress and not the axial strength of the compression members. For this reaction frame configuration, a prestress force above 375 kips would produce an uplift force at the outer tie-down location exceeding the post-tensioning in the rods.

The buttress system was also analyzed using SAP2000 to refine estimates of member stresses and deformations (CSI, 1998). According to this analysis, an applied prestress force of 375 kips results in inward displacement of the buttresses of approximately 0.15in and stresses satisfying the ASD specifications by the American Institute of Steel Construction (AISC, 1989).

In order to impose a margin of safety against uplift of the buttresses at the outer tie-down location, the capacity of the buttresses was reduced by a factor of safety of 1.5, resulting in a load carrying capacity for each reaction frame of 250

kips. It must be emphasized that the central buttresses resist a higher load since they contribute to the resistance of forces applied at both the central and outside bays. Therefore, the specimens with the least number of strands were placed in the central bay. The maximum load applied on any buttress during this study was approximately 220 kips.

Construction details for the plywood platforms located between the steel tubes were fairly simple. Essentially, they consisted of timber frames topped by 0.75-inch plywood decks. Adequate vertical and lateral support was provided to prevent significant deflection due to the self-weight of the specimens and during prestress force release. The platforms were originally constructed to provide the strand eccentricity needed for the first set of specimens (Rogers, 2002). Smaller removable wood platforms with predefined heights where later assembled and placed on top of the original platforms to accommodate eccentricities required for subsequent specimens.

4.3 DETAILS OF LABORATORY WORK

4.3.1 General

The research program began during the summer of 2000. As it progressed, testing procedures evolved in order to improve the accuracy and reliability of measurements that were being made. Modifications to the testing program are highlighted in the following subsections.

Concrete ready-mix plants in Central Texas do not typically keep Type III cement in stock. Because this cement was needed to produce concrete mixes that would behave like those used in a typical Texas precast manufacturing plant, it was decided, after considering numerous options, to batch the concrete with Type III cement in Ferguson Laboratory. A mixing truck was rented on an hourly

basis, and aggregates were purchased from a local concrete supplier. Water, admixtures, and cementitious materials were added in the laboratory. Trial batches were carried out in advance in order to anticipate the characteristics of fresh and hardened concrete. Additional details related to the concrete mixes used in this study will be presented in later subsections.

The following experimental procedure was generally used for the five castings that were conducted. Additional detail is provided in the subsections that follow.

1) Adjust the overall platform height to generate the prestress force eccentricity required for each specimen.

2) Instrument the prestressing strands and place them and the non-prestressed reinforcement at the appropriate locations.

3) Install the formwork panels making sure that the desired cross sections are obtained.

4) Tension strands to the required prestress level.

5) Install thermocouples at critical beam locations to measure the reference temperature used by the Sure Cure equipment to cure concrete cylinders.

6) Cast the pretensioned concrete beams, being careful to avoid damage to thermocouples and strain gauges.

7) Cover the exposed concrete surfaces with wet burlap and plastic to provide a moist curing environment and enhance concrete strength gain rate.

8) Remove the burlap and plastic shortly before release and install linear potentiometers to monitor deflection of the specimens. At this point, the formwork should be loosened to allow the beams to deflect freely during prestress transfer.

9) Release the prestress force when, according to standard compression tests performed on match-cured cylinders, concrete has reached the desired compressive strength.

10) Monitor the behavior of specimens over an extended period of time.

The quality of the results obtained from the testing program depended on careful execution of this procedure. Knowing, within reasonable accuracy, the actual cross-section properties and applied prestress forces was crucial for determining extreme concrete fiber stresses in the pretensioned flexural members at transfer. In addition, accurate prediction of the response of these elements to the imposed stresses could be made only if the material properties and support conditions were well known.

4.3.2   Material Properties

4.3.2.1   Prestressed Steel Reinforcement

Half-inch, 270ksi, low relaxation steel strands were used to fabricate all concrete specimens monitored in this study. Methods for estimating prestress force losses and stress-strain models for this type of steel strand are available in the literature. For instance, the Ramberg-Osgood model presented in Table 3-1 was found in reference 12 (Collins and Mitchell, 1997). The existing theoretical methods for calculating prestress losses due to wedge seating, relaxation, and elastic shortening can provide acceptable results for design. However, these methods may not be sufficient to predict accurately the prestress force losses that occur in beams fabricated in this laboratory investigation. As a result, researchers relied on strain gauges during the study to determine prestress forces. Because of durability concerns pointed out by Russell (Russell, 1992), appropriate strain

gauges and installation techniques were identified to ensure the accuracy of strain measurements.

A stress-strain calibration curve was developed by testing strand samples instrumented with strain gauges mounted on each of the outer wires. Four tension tests were performed according to the ASTM A370 procedure. V-gripping devices were employed in these four tests. The use of barrel-and-chuck devices for gripping the strand samples during the tension test is not allowed by ASTM A370. However, two additional tests were performed using the same barrel-and-chuck devices that would later be used to pretension the strands in the prestressing bed. Stress was calculated by dividing the force measured with a load cell in the testing machine by a nominal cross-sectional area of 0.153 in^2. Rogers presented a detailed explanation of these tension tests and concluded that Equation 4-1 was a reasonable way to relate measured strains to strand stresses (Rogers, 2002).

$$f_{ps} = -1.80E8 \cdot \varepsilon_{ps-sg}{}^3 + 1.65E6 \cdot \varepsilon_{ps-sg}{}^2 + 2.67E4 \cdot \varepsilon_{ps-sg} + 2.81 \qquad \textbf{\textit{Equation 4-1}}$$

In Equation 4-1, ε_{ps-sg} is the strain measured by strain gauges oriented along the axes of individual wires and not the axis of the strand (Figure 4-3). Therefore, this equation represents a calibration curve and not the actual stress-strain behavior of the strand. A curve representing the actual stress-strain behavior was not specifically required for the laboratory study. However, a Ramberg-Osgood model was used later to perform nonlinear analyses of the prestressed concrete specimens. This model was presented in Table 3-1.
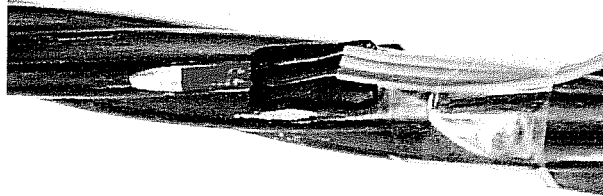
Figure 4-3: Strain gauge mounted parallel to individual wire

The length of strand samples tested to develop Equation 4-1 ranged from 24 to 36 inches, depending on the gripping device used. However, the length of strands used to fabricate the pretensioned beams was approximately 47 feet. To study the applicability of the calibration curve developed by Rogers to the actual conditions in the prestressing bed, two full-length strands were tested prior to fabrication of the first set of beams. Two strain gauges were installed on each strand following the same procedure used in the previous tension tests. The anchorage devices and ram used to apply tension were the same as those employed during the prestressing operation before casting. Although it was not precisely measured, the loading rate was similar to that used during prestressing.

A load cell with a maximum capacity of 50 kips was utilized to determine the tension force. As before, stresses were calculated by dividing this force by the nominal strand area. Strains were taken as the average of readings from the two strain gauges installed on each strand. Because strand stresses before casting concrete were expected to be as high as *80% f_{pu}*, both full-length specimens were tensioned above this value. It is important to note that both strain and force readings were acquired while loading and unloading the second specimen. Readings were taken only during loading for the first specimen.
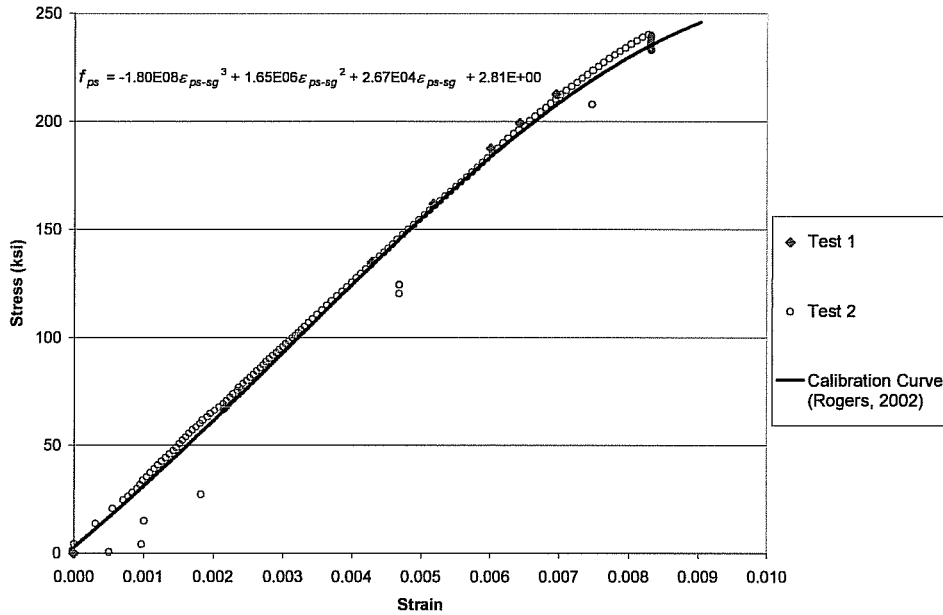
Figure 4-4: Results of tension tests on full-length strand samples

Figure 4-4 shows the stress-strain calibration curve accompanied by the results obtained from tension tests performed on two full-length strand specimens. This figure corroborates the applicability of the equation suggested by Rogers. However, calculated and measured stresses for strains between 0.001 and 0.002 differ by as much as 8%. Equation 4-2 was developed to improve the agreement between measured stresses and strains and the calibration curve.

$$f_{ps} = -1.61E10 \cdot \varepsilon_{ps-sg}^{4} + 1.67E8 \cdot \varepsilon_{ps-sg}^{3} - 7.95E5 \cdot \varepsilon_{ps-sg}^{2} + 3.24E4 \cdot \varepsilon_{ps-sg} \qquad \textit{Equation 4-2}$$

$$f_{ps} = 30,215 \cdot \left(\varepsilon_{ps-max} - \varepsilon_{ps-sg} \right) \qquad \textit{Equation 4-3}$$

The readings taken while unloading the second strand specimen lead to Equation 4-3. In this equation, ε_{ps-max} is the strain corresponding with the highest stress achieved, while ε_{ps-sg} is the strain measured as the strand unloads. As can

be observed in Figure 4-5, the unloading behavior is modeled by a linear relationship with a slope of 30,215 ksi. This value cannot be taken as the actual elastic modulus of the strands because it relates the axial stress to strain oriented along the axis of an individual wire. However, for the purpose of this thesis, it will be referred to as the apparent elastic modulus of the strands.

The final stress-strain calibration model used throughout this experimental program is presented in Figure 4-5. As shown, Equation 4-2 was used to determine strand stress during loading, while Equation 4-3 served to compute prestress losses due to wedge seating and elastic shortening. The model could not be used to estimate relaxation losses because they do not result in measurable changes in strain. However, relaxation losses at transfer as low as 1% of the jacking stress were calculated based on theoretical models (Collins and Mitchell, 1997).
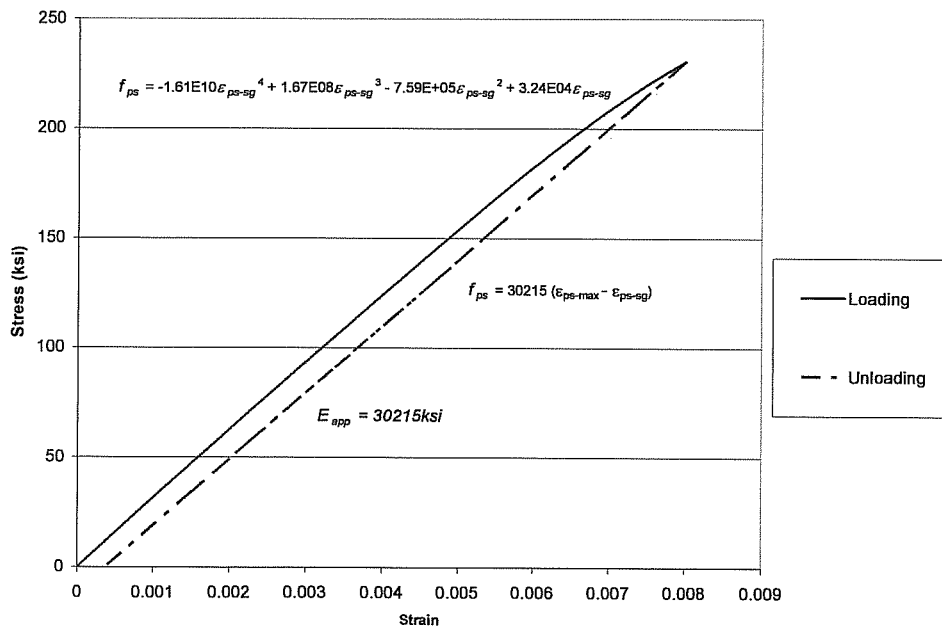
Figure 4-5: Final stress-strain calibration model

At the time this calibration model was developed, tensile stresses expected in the strands of the beam specimens ranged from *80%f_{pu}* at jacking to *60%f_{pu}* after all losses. For this stress range, the tension test results indicated a model accuracy of $\pm 2\%$.

4.3.2.2 Non-prestressed Steel Reinforcement

The end regions of the pretensioned concrete members fabricated in this study were reinforced to resist bursting stresses generated during prestress transfer. Deformed steel reinforcement was also used to control cracking at the top of four inverted tee specimens. Conventional deformed bars made of Grade 60 ASTM A615 steel were used for these purposes. Reinforcement details are provided in Appendix C.

4.3.2.3 Concrete

One of the objectives of this research project was to evaluate the effect of concrete composition on the behavior of pretensioned members after transfer. The initial deflections experienced by these members are directly related to the elastic properties of the materials contained in them. In addition, long-term response of the members is affected by time-dependent effects, such as creep and shrinkage of concrete, and relaxation of the prestressing strands.

Creep is related primarily to the microstructure of the hydrated cement paste and aggregate-paste interface. Previous researchers have concluded that higher curing temperatures adversely affect creep. Additionally, a direct relationship between the coarse aggregate and creep behavior exhibited by concrete has been noted (Mokhtarzadeh and French No.2, 2000).

Physical and mechanical properties of the aggregate as well as its concentration in the mix determine how it influences creep. Even if the coarse

aggregate itself does not experience creep, its grading, size, and shape can affect the time-dependent behavior of concrete. In general, soft aggregates and smooth aggregates typically lead to more creep.

Three different concrete mixes were used to cast the pretensioned specimens tested during this program. They were all similar to standard mixes used in a prestressing plant in Victoria, Texas. The same cementitious materials and admixtures used in this plant were used in this study.

Mixes 1 and 2 were developed to study the influence of different types of coarse aggregate on the initial and long-term performance of pretensioned beams released at high stress levels. Crushed limestone and river gravel were used because they are commonly found in concrete applications throughout Texas. These two aggregates are some times referred to as "soft rock" and "hard rock," respectively. As observed in Tables 4-3 and 4-4, their concentration was kept constant and sizes were similar. However, they differed in stiffness and shape, which are characteristics known for affecting the mechanical properties and creep behavior of high-strength concrete. These 6.5-sack mixes (6.5 sacks of cement per cubic yard of concrete) are typically used in prestressed applications because high concrete strengths are achieved within a few hours of concrete casting. The high cement content also results in a significant amount of heat produced during the hydration process.

Premature deterioration of concrete due to alkali-silica reaction and delayed ettringite formation can be controlled by reducing the overall alkali load in the concrete and the heat developed during hydration. One approach to achieve this is to reduce the cement content in the mix. This was done for the third mix in which the cementitious materials content was reduced by 10.7%. In addition, Class C fly ash represented 31.3% by weight of the total cementitious materials.

Table 4-3: Aggregate properties

	River Rock	Crushed Limestone	River Sand
Gradation	ASTM C33 Grade 56	ASTM C33 Grade 56	ASTM C33
Size	1 inch	1 inch	-
Fineness Modulus	-	-	2.74
Specific Gravity	2.62	2.52	2.62
Particle Shape	Rounded	Angular	-

Table 4-4: Concrete composition (per cu. yd.) and characteristics

	Mix 1	Mix 2	Mix 3
Water / Cementitious Materials Ratio	0.33	0.33	0.34
Water (lbs)	204	203	182
Alamo Type III Cement (lbs)	608	608	373
W.A. Parish Class C Fly Ash (lbs)	-	-	170
Natural River Sand (lbs)	1183	1177	1322
1-inch River Rock (lbs)	2044	-	-
1-inch Crushed Limestone (lbs)	-	2042	2006
High-range water-reducing admixture (oz) -Rheobuild 1000 by Master Builders-	158	158	109
Retarding admixture (oz) -Pozzolith 300R by Master Builders-	21	21	16
Unit weight (lbs/ft^3)	154	158	150
7-day Compressive Strength (psi)	8330	8670	6375
28-day Compressive Strength (psi)	10030	10000	7390
28-day Modulus of elasticity (ksi)	5885	4850	5007
Slump (in)	7	8.5	9

4.3.3 Instrumentation and Data Acquisition

The research team originally intended to monitor the time-dependent behavior of the pretensioned beams using surface-mounted strain gauges and mechanical strain gauges (DEMEC targets), but concluded during the pilot series of tests that it was not possible to remove the formwork sufficiently early to allow the necessary time for surface preparation and curing of adhesives used to affix the gauges to the concrete surface. Consequently, the research team decided to monitor time-dependent behavior of the pretensioned concrete beams by accurately measuring camber. Other critical quantities that required precise determination were the prestress force in strands and the concrete compressive strength. The instrumentation used to measure these quantities included:

1) Electrical strain gauges mounted on prestressing strands
2) Two thermocouples per beam located at midspan
3) Linear potentiometers
4) Dial gauges

Two data acquisition systems that were quite stable throughout the duration of the study were used to acquire strain, displacement, and temperature data from the pretensioned beam specimens. These systems included Campbell Scientific dataloggers and compatible multiplexers that increased the number of sensors that could be scanned. As shown in Figure 4-6, strain gauges were connected to a CR23X datalogger while the linear potentiometers and backup thermocouples were attached to a CR21X(L) datalogger. The data acquisition systems were powered by 12V rechargeable batteries that were frequently checked to prevent voltage irregularities.

The dataloggers collected data from the sensors and stored them in memory until the data were downloaded using a personal computer containing the software called PC208W. Once downloaded, the voltage readings were converted into engineering units using formulas that will be presented later. Measurements were taken every five seconds during the pretensioning operation, and then every five minutes until the prestress force was released. Later, this sampling rate was further expanded to thirty minutes in order to avoid saturating the system memory.

Alongside the dataloggers, a Sure Cure system was utilized to match-cure 4 by 8-in cylinders made of the same concrete used to cast the beams. One thermocouple per beam was installed to measure reference temperatures. A detailed description of the device will be provided in a later subsection.
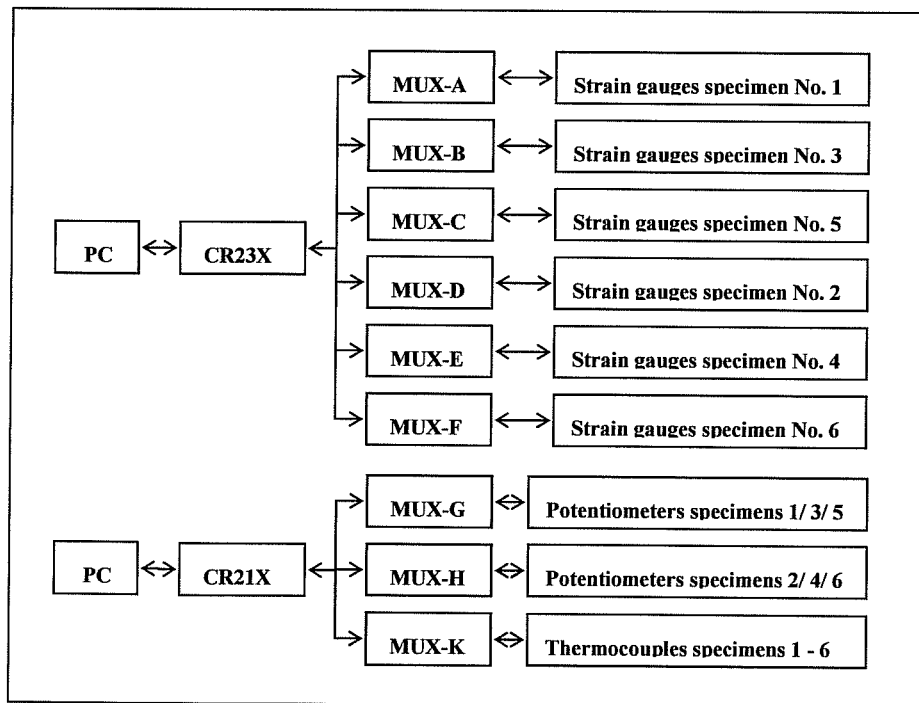
Figure 4-6: CR21X(L) and CR23X diagrams

4.3.3.1 Instrumentation of the prestressing strands

Figure 4-1 indicated that two pretensioned beams were cast in each bay of the prestressing bed. Thus, each pair of specimens shared the strands used in that bay. Each strand was instrumented with one strain gauge at midspan of each beam to determine the tension force before and after transfer by relating measured strain to stress using the calibration model discussed in Section 4.3.2.1. The properties of these gauges are shown in Table 4-5.

Table 4-5: Properties of strain gauges

Type	FLA-5-11-3LT
Manufacturer	Tokyo Sokki Kenkyujo Co.
Gauge Factor	2.13
Resistance	$119.5 \pm 0.5\Omega$
Dimensions	1.5 x 5 mm
Compatible Adhesive	TML – CN

Voltage readings taken by the CR23X system were converted to strains using Equation 4-4. In this equation, V_{DAQ} is the voltage read by the system, and GF is the gauge factor. Although the manufacturer recommends a value of 2.13, the gauge factor was adjusted following a procedure known as shunt calibration. This is a widely used method for verifying the accuracy of measurements and scaling those affected by voltage drops related to factors such as long cable lengths.

$$\Delta\varepsilon = \frac{4}{GF} \cdot \left(\frac{V_{DAQ}}{1000}\right) \cdot \left[\frac{1}{1 - 2 \cdot \left(\frac{V_{DAQ}}{1000}\right)}\right]$$

Equation 4-4

69

The strain gauges were installed following the manufacturer's recommendations, which included lightly polishing the steel surface and applying the appropriate adhesive and waterproof coating. Strain gauges were further protected by covering them with a small piece of rubber held in place by metallic tape. This practice resulted in durable strain gauges. Only a small percentage of gauges failed, in most cases during concrete casting.

4.3.3.2 Camber measurement

Precise measurement of camber was critical for assessing the behavior of the pretensioned concrete beams after transfer. Timber frames used by Rogers during the pilot study were replaced with steel frames that spanned over the prestressing bed and supported three linear potentiometers located at each end and at midspan of each beam (Figure 4-7). Deflection of each beam (camber) was calculated by subtracting the average of the end measurements from the midspan measurement. This configuration proved to be unsatisfactory because measurements appeared to be affected by the horizontal displacement of the beams at release. A 1 by 2-inch steel tube simply supported at the ends of each specimen was used for the third through fifth groups of beams to support a potentiometer at midspan (Figure 4-8). For this support system, deflection at midspan was measured relative to the beam ends, and horizontal translation of the beams at release did not affect accuracy of the results. Figure 4-9 illustrates these two deflection-measuring systems and shows the location of the linear potentiometers.
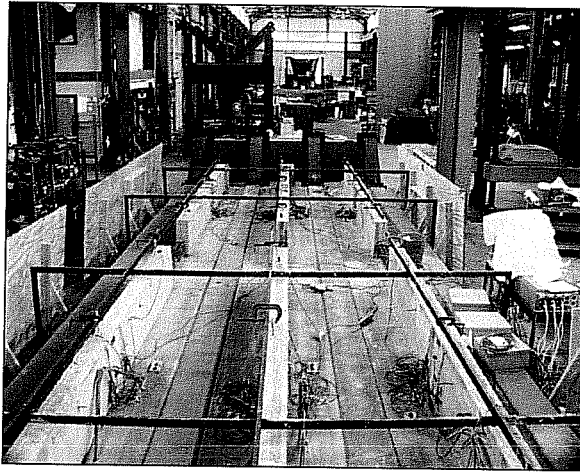
Figure 4-7: Original steel frames with three potentiometers per beam
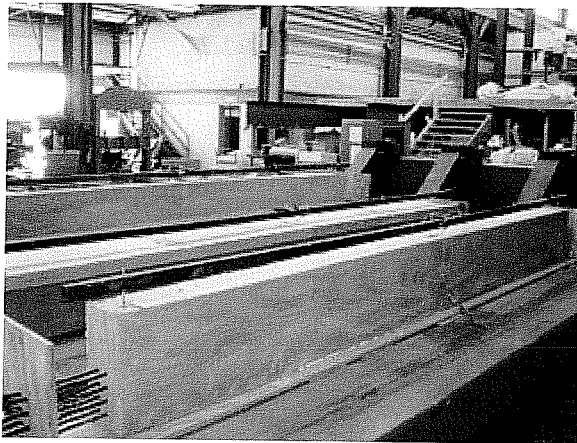
Figure 4-8: Optimized configuration with one potentiometer per beam
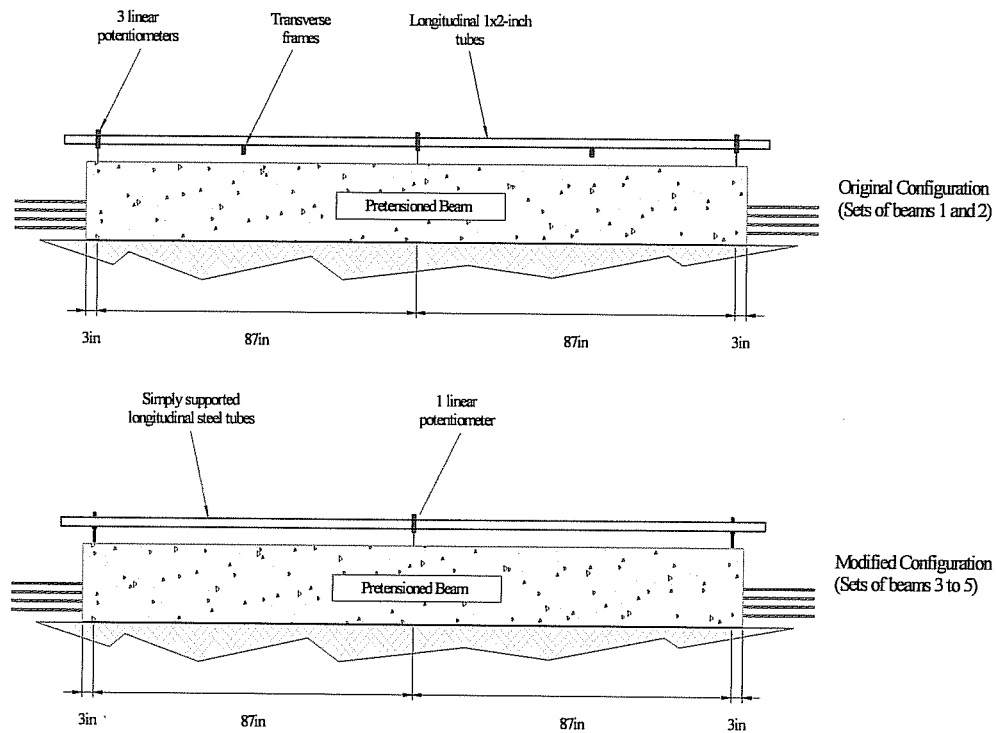
Figure 4-9: Experimental setups for camber measurement

Two-inch linear potentiometers were used to digitally monitor camber while specimens were still on the prestressing bed. These devices were calibrated prior to each cast by applying known displacement quantities and recording the corresponding voltage readings taken by the CR21X(L) system. This procedure served to examine the performance of the instruments and generate linear equations that were later used during testing to convert recorded voltages to displacement units.

The simple support conditions for the final system used to measure camber were achieved by inserting 3/8-inch threaded rods in the fresh concrete at 3 inches from the beam ends (Figure 4-10). Oversized holes matching the location of the rods were drilled through the tubes to allow free rotation at the

supports. Two nuts were tightened together on the 3/8-inch threaded rods to hold the tubes at the required distance from the top of the specimens.
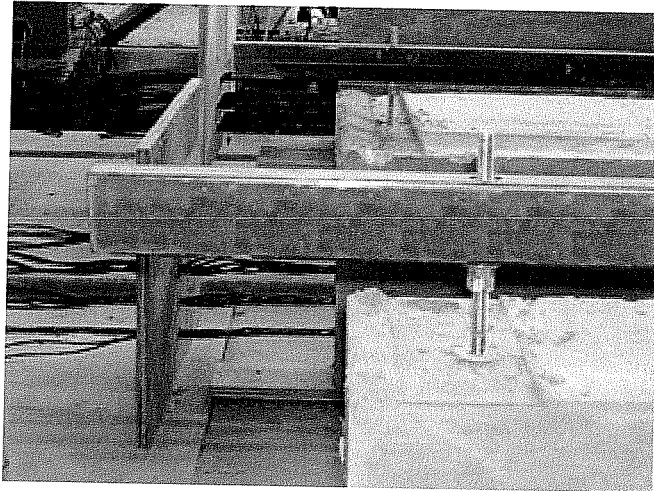
Figure 4-10: Support of frame for camber measurement
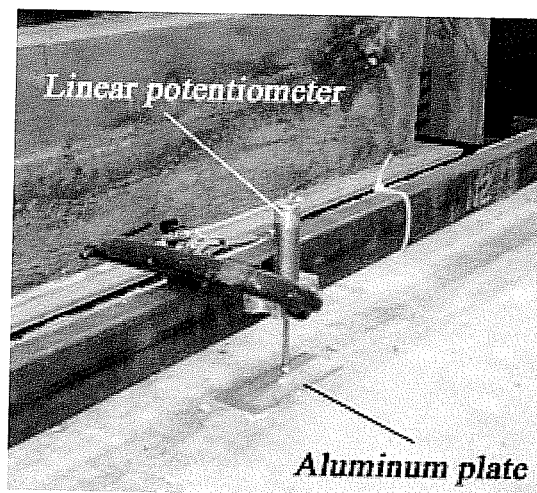
Figure 4-11: Linear potentiometer

As shown in Figure 4-11, the linear potentiometers were firmly clamped to the steel tubes. Also, small aluminum plates were glued to the specimens at the point of contact with the linear potentiometer to avoid erroneous displacement measurements related to imperfections on the concrete surface.

The total amount of time a set of specimens was monitored in the prestressing bed depended primarily on the timeline for the start of fabrication of the next group of beams. However, all beams were kept in the prestressing bed for a minimum of one week. After this time, beams were moved to the laboratory floor and positioned on top of steel plates placed 3 inches from member ends, resulting in span lengths of approximately 174 inches. A steel frame was then assembled to support dial gauges used to continue monitoring camber (Figure 4-12). These dial gauges had an accuracy of ±0.0005 in.
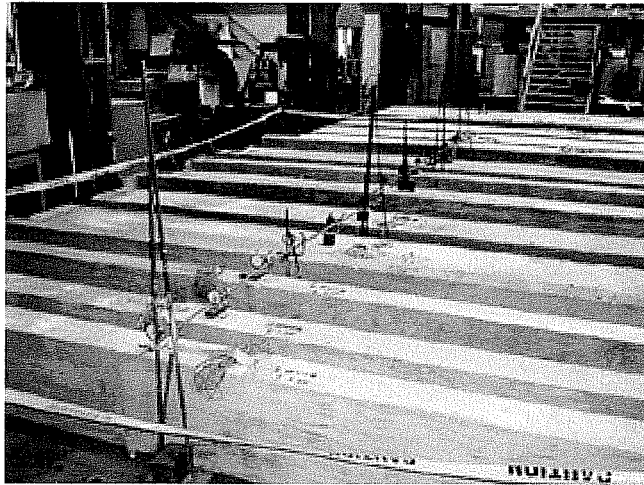
Figure 4-12: Specimens being monitored on laboratory floor

4.3.3.3 Sure Cure

A concrete curing system called Sure Cure was used to cure 4 by 8-inch cylinders at the same temperature developed inside test specimens. This procedure is known as match-curing and is used in several precast plants because it provides a better representation of the compressive strength of concrete in the precast members. During hydration, the temperature generated in standard 4 by 8-inch and 6 by 12-inch cylinders is typically lower than that in larger elements made up of the same concrete. Hence, the compressive strength measured based on these cylinders can be significantly lower than the actual strength of concrete in the member.

A complete explanation of how to operate the Sure Cure software and hardware was provided by Rogers (Rogers, 2002). In order to utilize the Sure Cure system, it is necessary to instrument the precast members with thermocouples to measure the reference temperatures for the system. Temperature can vary considerably within a concrete member, and so can strength. Therefore, the thermocouples used in this study were placed at locations where high temperatures were expected in order to obtain upper-bound estimates of the compressive strength reached in each beam. Strengths obtained from the 4 by 8-in. Sure Cure cylinders were then used to conservatively compare the stresses imposed at transfer to the allowable limits specified by ACI and AASHTO.

Two thermocouples per beam were installed at midspan, with one connected to the Sure Cure system and the other to the CR21X(L). The thermocouples attached to the CR21X(L) were used to verify the measurements taken by the match-curing system. The red dots in Figure 4-13 represent the approximate height and location at which sensors were positioned in each type of cross section.
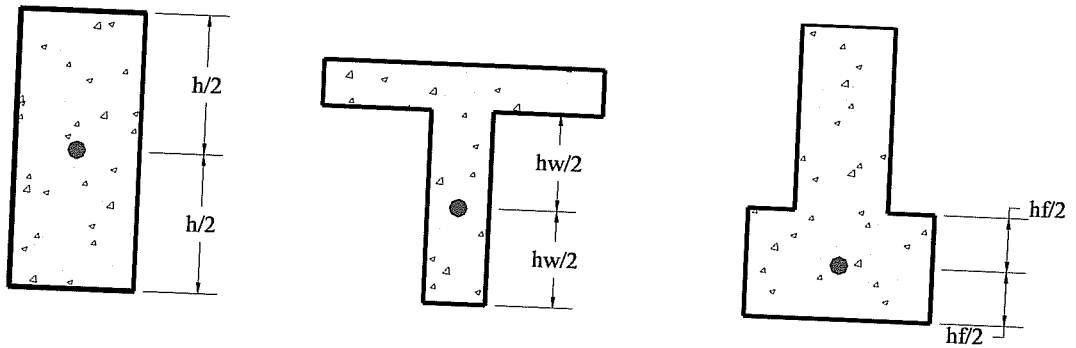
Figure 4-13: Position of the thermocouples

Twelve 4 by 8-inch Sure Cure cylinders, two per beam, were made during each cast. Because the cross sections of members cast in each bay were the same, their temperature histories were very similar. Therefore, four cylinders were available to determine the concrete compressive strength of each pair of pretensioned beams that were released simultaneously.

4.3.4 Pretensioning Operation

Depending on the test specimen, the target stress in the strands was *75%f_{pu}* or *70%f_{pu}*. The pretensioning operation was performed with great care using a single-strand ram and hydraulic pump equipped with a pressure transducer. Two methods were used to stress prestressing strands to the desired level:

- Relating the ram pressure to strand stress using a simple calculation incorporating the ram area.
- Relating a strain gauge reading to stress using the calibration model described in 4.3.2.1.

76

Comparison of results from both methods permitted verification of the stresses and estimation of the seating losses. As mentioned in 4.3.3, strain readings were taken every five seconds during the pretensioning operation. The stressing operation was as follows:

1) Record strain readings just before applying force.

2) Tension each strand until a pressure reading of 500 psi is reached to verify that the strain gauges are working properly. The change in strain readings should correspond with a stress of $10\%f_{pu}$.

3) Tension strands to $80\%f_{pu}$ (4150 psi on the pressure transducer) to target a stress of $75\%f_{pu}$ after seating losses. If the target stress is $70\%f_{pu}$, tension strands to $75\%f_{pu}$ (3900psi) and release the pressure.

4) Record the change in strain readings after seating losses and verify the target stresses. If any strand requires more tension, repeat steps 2 and 3 and check the stresses again.

5) Measure the resulting strand elongations after anchorage seating, calculate the corresponding stresses, and compare with stresses inferred from strain gauge readings for further verification.

It is important to note that the reaction frame deforms due to the applied forces. Therefore, as one strand is tensioned, stress in others decreases. This required strands to be tensioned several times in order to achieve the desired stresses.

4.3.5 Casting Operation

The concrete mixes used to cast the pretensioned beams were described previously in Section 4.3.2.3. Due to unavailability in Central Texas of ready-mix concrete made with Type III cement, the concrete had to be batched in the laboratory. A truck mixer was loaded with the aggregates at the ready-mix plant, then the other components, including water, cement, fly ash, and admixtures, were carefully measured and loaded into the truck at the laboratory.

The casting operation did not differ much from what is typically done in a construction or precast plant. Concrete was placed in the forms using an overhead bucket supported by the traveling crane in Ferguson Laboratory and consolidated using mechanical vibrators. The top surface was finished with steel trowels to reduce the irregularities that could affect the cross-sectional dimensions of the specimens.

To emulate the curing conditions provided in precast plants, the exposed surfaces were covered with wet burlap and plastic. They were uncovered a few minutes prior to prestress release to affix the aluminum plates to the top surface of the beam using five-minute epoxy and to install the linear potentiometers.

4.3.6 Compressive Strength Determination

The compressive strength of concrete was determined according to the ASTM C39 procedure. Sure-Cure and conventional cylinders were tested frequently until the required release strength was achieved for tested Sure-Cure cylinders. Then, air cured conventional 4 by 8-inch and 6 by 12-inch cylinders were used to determine the 7, 14, and 28-day strengths. These cylinders were placed beside the beams until they were tested.

4.3.7 Prestress Force Release

Once the desired concrete compressive strength was reached, the tensioned strands were cut between the beams using an acetylene torch. This process was done gradually, wire-by-wire, to reduce the amount of energy transferred to the specimens at release. The order in which strands were cut was such that the prestress force was kept as symmetric as possible, both vertically and horizontally.

4.4 SUMMARY

A prestressing facility was constructed in Ferguson Structural Engineering Laboratory to fabricate pretensioned concrete beams to be used in the evaluation of the effect of elevated release stresses on the behavior of pretensioned concrete members. A reaction frame consisting of steel bulkheads, buttresses, and compression members was designed to carry a maximum prestress force of 250 kips per buttress with a factor of safety of 1.5.

The main objective of this research program was to delve into the possibility of increasing the extreme fiber concrete stresses allowed by current ACI and AASHTO provisions. Accurate and reliable measurement of prestress forces, concrete strengths, and member deflections was essential to meet this objective. The instrumentation employed in the study included strain gauges attached to the steel strands, thermocouples, linear potentiometers, and dial gauges. A stress-strain calibration model was developed to relate strain readings from strands to stresses. This model was derived from a series of tension tests performed using strands with lengths ranging from 24 inches to 47 feet.

To obtain a representative estimation of the compressive strength of concrete in the test specimens, a match-curing system called Sure Cure was used.

This system served to cure 4 by 8-inch cylinders at the same temperatures developed at select locations in the beams during hydration.

The specimen fabrication procedures described in this chapter were not too different from those typically employed in precast plants. These procedures included tensioning and releasing strands, and casting and curing of specimens.

CHAPTER 5

Presentation and Analysis of Results

5.1 OVERVIEW

This chapter presents the results from five sets of pretensioned beams cast and monitored in Ferguson Structural Engineering Laboratory at The University of Texas at Austin. The time-dependent response of five sets of six beam specimens was observed in an attempt to determine whether existing allowable stress limits at prestress release can be increased beyond current limits. The methods employed to compute extreme fiber concrete stresses and to predict the behavior of the beam specimens are also described.

5.2 PRESTRESS FORCE

It was necessary to have an accurate estimate of the prestress force in each beam in order to calculate concrete stresses at extreme flexural fibers at release. Results obtained during the conduct of this study demonstrated that reasonably reliable estimates of the prestressing force were obtained from strain gauges applied to prestressing strands. As explained in Section 4.3.2.1, a calibration model was used to relate readings from strain gauges to tensile stresses in strands. The stress history was obtained for each strand except for strands with defective or damaged strain gauges. Stress versus time curves are presented in Appendix A for all strands.

Figure 5-1 will be used to explain how strain data was collected for use in determination of the effective prestress force. It shows the stress history for two of eight strands used in Specimen R3-76-5. The target stress for these strands was

$0.70f_{pu}$. A single-strand ram and hydraulic pump were used during the tensioning operation. Figure 5-1 indicates that these strands were initially stressed to between 199ksi and 206ksi, or $0.74f_{pu}$ and $0.76f_{pu}$. After reaching this peak, a reduction of approximately 16 ksi or $0.06f_{pu}$ was observed. Considering the length of strands used in the prestressing facility, a loss of 16 ksi represents a shortening of 0.28 inches. This reduction represents the anchorage seating loss that occurred after the pressure in the ram was released. In fact, the average of the seating losses observed for all strands stressed during this study was $0.06f_{pu}$.

As a result, strands were tensioned to $0.80f_{pu}$ and $0.76f_{pu}$ to target stresses of $0.75f_{pu}$ and $0.70f_{pu}$. These values satisfy current provisions limiting the tensile stress in prestressing steel due to the jacking force to $0.80f_{pu}$ (ACI318-02) and the stress immediately before transfer to $0.75f_{pu}$ (AASHTO, 1996).
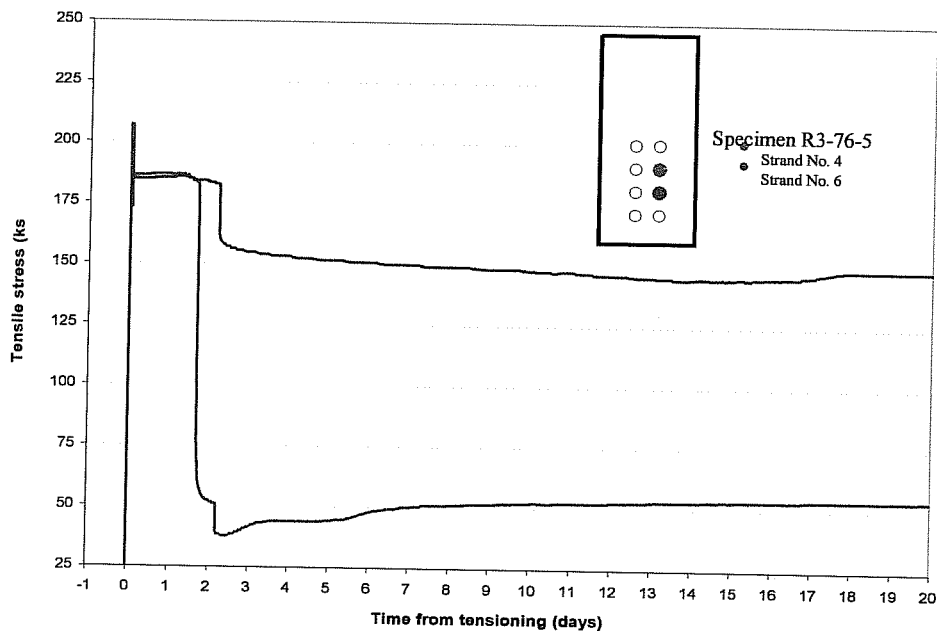

Figure 5-1: Example of tensile stress in strands

After seating losses, prestress in the strands (illustrated in Figure 5-1) ranged from $0.68f_{pu}$ to $0.70f_{pu}$. Readings from the strain gauge mounted on strand 6 indicated that the stress remained almost constant until the strand was cut and force was transferred to the beams. Strand 4 illustrates a case in which the strain gauge was damaged during casting. Although not shown in this figure, a strain gauge installed on the same strand but at midspan of Specimen R3-82-5 indicated that tension did not decrease dramatically as indicated by the gauge on strand 4 of Specimen R3-76-5. Only fifteen percent of all strain gauges failed at this stage. Data from faulty strain gauges were not used in the estimation of effective prestress forces.

According to Figure 5-1, the prestress force was transferred to the beam specimens approximately two days after tensioning the strands. Elastic shortening losses occurred instantaneously. The magnitude of these losses is a function of the properties of the concrete, the cross section, and the location of the strand. Based on strain gauge data, the elastic shortening loss in Specimen R3-76-5 for strand 6 was 19ksi. Considering data from all working strain gauges, the average elastic shortening loss for this beam was 17ksi or $0.06f_{pu}$. An elastic shortening loss of 16ksi was calculated following the approximate method recommended by PCI (PCI, 1999).

If taken directly from the stress history curve, the effective prestress in strand 6 would be 162 ksi. However, relaxation of the strands is not represented in the stress history because it does not result in measurable changes in strain. Based on the expression presented in Table 3-3, relaxation losses at transfer were estimated to be $0.01f_{pu}$. After subtracting this loss from the aforementioned value, the effective prestress used to compute concrete stresses was 159 ksi. Considering data from all working strain gauges, the average prestress in the strands of Specimen R3-76-5 was 165 ksi at transfer. Hence, the estimated

effective prestress force for this beam was 201 kips. This procedure was used to determine the effective prestress force for each specimen.

After release, readings from strain gauges generally indicated a gradual decrease in stress associated primarily with concrete creep and shrinkage. Inconsistencies were observed in measurements made with some strain gauges a few days after casting. However, strain measurements after transfer were not absolutely crucial because time-dependent behavior of specimens was evaluated using camber measurements.

5.3 CALCULATION EXAMPLE

Results from the testing program are presented and discussed in the following sections of this chapter. A calculation example for Specimen R3-76-5 is included in this section in order to facilitate the understanding of tables and figures presented in later sections. Gross cross-sectional properties of this beam and average strand tensile stresses are presented in Table 5-1.

Table 5-1: R3-76-5 data for concrete stress calculation

Cross section		Prestressing Steel	
A_g (in^2) =	144	A_{ps} (in^2) =	1.22
I_g (in^4) =	3888	E_p (ksi) =	29000
y_b (in) =	9	Stress immediately before transfer (ksi) =	182
y_t (in) =	9	Stress immediately after transfer (ksi) =	165
e (in) =	3.48	Concrete	
M_{sw} (k-in) =	50.63	f'_{ci} (psi) =	4045
		E'_{ci} (ksi) = $57\sqrt{f'_{ci}}$ =	3625

1. Elastic shortening prestress loss:

   a) Inferred elastic shortening losses

   $$ES = 182 - 165 = 17.0\,ksi$$

   b) Elastic shortening losses by PCI method

   $$K_{cir} = 0.9$$
   $$K_{ES} = 1.0$$
   $$P_i = 182 \cdot 1.22 = 222\,kips$$
   $$f_{cir} = K_{cir} \cdot \left(\frac{P_i}{A_g} + \frac{P_i \cdot e^2}{I_g} \right) - \frac{M_{sw} \cdot e}{I_g} = 1.96$$
   $$ES = \frac{K_{ES} \cdot f_{cir} \cdot E_p}{E_{ci}} = 15.7\,ksi$$

2. Effective prestress force

   $$P_o = 165\,ksi \cdot 1.22\,in^2 = 201\,kips$$

3. Extreme fiber concrete stresses at transfer

   $$\sigma_{TOP} = -\frac{P_o}{A_g} + \frac{P_o \cdot e \cdot y_t}{I_g} = -\frac{201}{144} + \frac{201 \cdot 3.48 \cdot 9.00}{3888}$$
   $$\Rightarrow \sigma_{TOP} = 223\,psi = 3.5\sqrt{f'_{ci}}$$

   $$\sigma_{BOTTOM} = -\frac{P_o}{A_g} - \frac{P_o \cdot e \cdot y_b}{I_g} = -\frac{201}{144} - \frac{201 \cdot 3.48 \cdot 9.00}{3888}$$
   $$\Rightarrow \sigma_{BOTTOM} = -3020\,psi = 0.75\,f'_{ci}$$

4. Revised estimate of extreme fiber stresses using strain compatibility approach

$$A_{trans} = A_g + \left(\frac{E_p}{E_{ci}} - 1\right) \cdot A_{ps} = 152.6\, in^2$$

$$y_{bt} = \frac{A_g \cdot y_b + A_{ps} \cdot \left(\frac{E_p}{E_{ci}} - 1\right) \cdot (y_b - e)}{A_{trans}} = 8.80\, in$$

$$y_{tt} = 18 - y_{bt} = 9.20\, in$$

$$I_{trans} = I_g + A_g \cdot (y_b - y_{bt})^2 + A_{ps} \cdot \left(\frac{E_p}{E_{ci}} - 1\right) \cdot (y_b - e - y_{bt})^2 = 3986\, in^4$$

$$e_{pt} = y_{bt} - (y_b - e) = 3.29\, in$$

$$\Delta\varepsilon_p \approx \frac{182}{29000} = 6.28 \cdot 10^{-3}$$

$$N_o = E_p \cdot \Delta\varepsilon_p \cdot A_{ps} = 222\, kips.$$

$$M_0 = E_p \cdot \Delta\varepsilon_p \cdot A_{ps} \cdot e_{pt} = 731\, k-in$$

$$\varepsilon_{cen} = \frac{-N_0}{E_{ci} \cdot A_{trans}} = -4.01 \cdot 10^{-4}$$

$$\phi = \frac{M_{sw} - M_o}{E_{ci} \cdot I_{trans}} = -5.08 \cdot 10^{-5}\, rad/in$$

$$\varepsilon_{top} = \varepsilon_{cen} - \phi \cdot y_{tt} = -4.01 \cdot 10^{-4} + 5.08 \cdot 10^{-5} \cdot 9.20 = 6.64 \cdot 10^{-5}$$

$$\sigma_{TOP} = E_{ci} \cdot \varepsilon_{top} = 3625 \cdot 6.63 \cdot 10^{-5} = 240\, psi = 3.8\sqrt{f'_{ci}}$$

$$\varepsilon_{bottom} = \varepsilon_{cen} - \phi \cdot y_{bt} = -4.01 \cdot 10^{-4} + 5.08 \cdot 10^{-5} \cdot -8.80 = -8.48 \cdot 10^{-4}$$

$$\sigma_{TOP} = E_{ci} \cdot \varepsilon_{top} = 3625 \cdot -8.48 \cdot 10^{-4} = -3070\, psi = 0.76 f'_{ci}$$

$$\varepsilon_p = \Delta\varepsilon_p + \varepsilon_{cen} - \phi \cdot e_{pt} = 6.28 \cdot 10^{-3} - 4.01 \cdot 10^{-4} + 5.08 \cdot 10^{-5} \cdot -3.29 = 5.71 \cdot 10^{-3}$$

$$f_p = E_p \cdot \varepsilon_p = 29000 \cdot 5.71 \cdot 10^{-3} = 166\, ksi$$

5. Revised estimate of extreme fiber stresses using nonlinear approach (RESPONSE)

$$\phi = -5.56 \cdot 10^{-5} \, rad/in$$

$$\varepsilon_{top} = 8.20 \cdot 10^{-5}$$

$$\sigma_{TOP} = E_{ci} \cdot \varepsilon_{top} = 3625 \cdot 8.20 \cdot 10^{-5} = 297 psi = 4.7 \sqrt{f'_{ci}}$$

$$\varepsilon_{bottom} = -9.19 \cdot 10^{-4}$$

$$\sigma_{BOTTOM} = \frac{f'_{ci} \cdot n \cdot \left(\varepsilon_{bottom}/\varepsilon'_{ci}\right)}{n - 1 + \left(\varepsilon_{bottom}/\varepsilon'_{ci}\right)^{n \cdot k}} = -2970 psi = 0.73 f'_{ci}$$

$$\varepsilon_p = 5.69 \cdot 10^{-3}$$

$$f_p = 29000 \cdot \varepsilon_p \left\{ 0.025 + \frac{0.975}{\left[1 + \left(118 \cdot \varepsilon_p\right)^{10}\right]^{0.10}} \right\} = 164 ksi$$

6. Camber estimation (PCI)

a) Initial camber

$$\Delta = \frac{P_o \cdot e \cdot l^2}{8 \cdot E \cdot I} - \frac{5 \cdot w \cdot l^4}{384 \cdot E \cdot I} = \frac{201 \cdot 3.48 \cdot 180^2}{8 \cdot 3625 \cdot 3888} - \frac{5 \cdot 0.013 \cdot 180^4}{384 \cdot 3625 \cdot 3888}$$

$$\Rightarrow \Delta_{initial} = 0.201 - 0.013 = 0.19 \, in$$

b) Long-term camber

$$\Delta = \frac{4.9 \cdot P_o \cdot e \cdot l^2}{16 \cdot E \cdot I} - \frac{27 \cdot w \cdot l^4}{768 \cdot E \cdot I} = \frac{4.9 \cdot 201 \cdot 3.48 \cdot 180^2}{16 \cdot 3625 \cdot 3888} - \frac{27 \cdot 0.013 \cdot 180^4}{768 \cdot 3625 \cdot 3888}$$

$$\Rightarrow \Delta_{initial} = 0.492 - 0.034 = 0.46 in$$

7. Camber estimation (using strain compatibility).

According to Figure 5-2, and based on the second moment-area theorem, camber can be calculated using Equation 5-1.

w=0.013kips/in

P_o → ← P_o

|—90—|—90—|

M

M=50.63k-in

6.92E-8

$\dfrac{M}{E_c \, I_{TRANS}}$
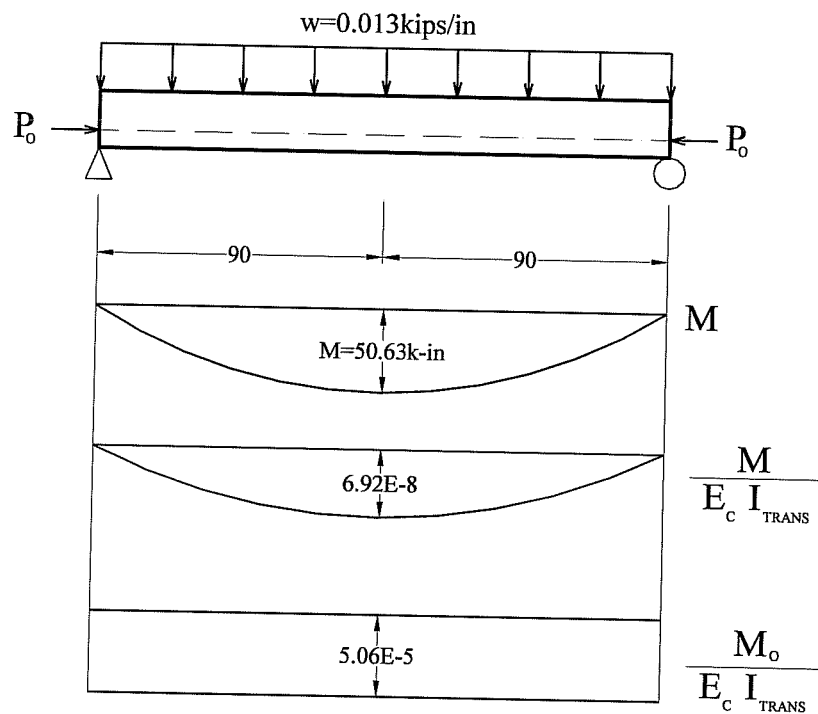
5.06E-5

$\dfrac{M_o}{E_c \, I_{TRANS}}$

Figure 5-2: Camber calculation

$$\Delta = 0.5 \cdot \left(\frac{L}{2}\right)^2 \cdot \frac{M_o}{E_c \cdot I_{TRANS}} - \frac{5}{12} \cdot \left(\frac{L}{2}\right)^2 \cdot \frac{M_{sw}}{E_c \cdot I_{TRANS}}$$ **Equation 5-1**

a) Initial camber

$$\Delta = 0.5 \cdot \left(\frac{180}{2}\right)^2 \cdot \frac{731}{3625 \cdot 3986} - \frac{5}{12} \cdot \left(\frac{180}{2}\right)^2 \cdot \frac{50.63}{3625 \cdot 3986} = 0.19\,in$$

b) Camber 30 days after transfer

- Creep

$$k_c = 0.53; k_f = 0.67; H = 70\%; t_i = 1\,day; t = 31$$

$$v(t, t_i) = 3.5 k_c k_f \left(1.58 - \frac{H}{120}\right) t_i^{-0.118} \frac{(t - t_i)^{0.6}}{10 + (t - t_i)^{0.6}} = 0.54$$

$$E_{c-eff} = \frac{E_{ci}}{1 + \phi(t, t_i)} = \frac{3625}{1 + 0.54} = 2360\,ksi$$

- Shrinkage

$$k_s = 0.54; k_h = 1.00; t = 31$$

$$\varepsilon_{sh} = -1.2 \cdot k_s k_h \left(\frac{t}{35 + t}\right) 0.51 \times 10^{-3} = -1.5 \cdot 10^{-4}$$

- Relaxation (T=75°F)

$$f_{pi} = 182\,ksi; f_{py} = 243\,ksi; t = 768\,hours$$

$$\frac{f_p}{f_{pi}} = 1 - \left(1 + \frac{T - 70}{30}\right) \cdot \frac{\log t}{45} \left(\frac{f_{pi}}{f_{py}} - 0.55\right) = 0.98$$

$$E_{p,eff} = \frac{f_p}{f_{pi}} E_p = 0.98 \cdot 29000 = 28420\,ksi$$

89

- Then

$$A_{trans} = A_g + \left(\frac{E_{p'eff}}{E_{c,eff}} - 1 \right) \cdot A_{ps} = 157.5\, in^2$$

$$y_{bt} = \frac{A_g \cdot y_b + A_{ps} \cdot \left(\frac{E_{p'eff}}{E_{c,eff}} - 1 \right) \cdot (y_b - e)}{A_{trans}} = 8.70\, in$$

$$y_{tt} = 18 - y_{bt} = 9.30\, in$$

$$I_{trans} = I_g + A_g \cdot (y_b - y_{bt})^2 + A_{ps} \cdot \left(\frac{E_p}{E_{ci}} - 1 \right) \cdot (y_b - e - y_{bt})^2 = 4038\, in^4$$

$$e_{pt} = y_{bt} - (y_b - e) = 3.19\, in$$

$$\Delta \varepsilon_p \approx \frac{182}{28420} = 6.40 \cdot 10^{-3}$$

$$N_o = E_{p,eff} \cdot \Delta \varepsilon_p \cdot A_{ps} - E_{c,eff} \cdot \varepsilon_{sh} \cdot A_c = 273\, kips.$$

$$M_o = E_{p'eff} \cdot \Delta \varepsilon_p \cdot A_{ps} \cdot e_{pt} - E_{c,eff} \cdot \varepsilon_{sh} \cdot A_c \cdot (y_{bt} - 9) = 693\, k - in$$
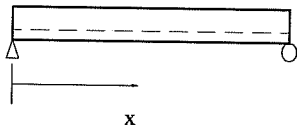
$$\Delta = 0.5 \cdot \left(\frac{180}{2} \right)^2 \cdot \frac{693}{2360 \cdot 4038} - \frac{5}{12} \cdot \left(\frac{180}{2} \right)^2 \cdot \frac{50.63}{2360 \cdot 4038} = 0.28\, in$$

To account for the cracked cross section of those specimens with tensile stresses exceeding $f_r = 7.5 \sqrt{f'_{ci}}$, the moment of inertia for the transformed section, I_{trans}, was replaced by I_e (Equation 5-2) which is a modified version of Equation 9-8 in the ACI 318-02 code.

$$I_e = \left(\frac{M_{cr}}{M_a} \right)^3 \cdot I_{trans} + \left[1 - \left(\frac{M_{cr}}{M_a} \right)^3 \right] \cdot I_{cr-trans} \qquad \textbf{\textit{Equation 5-2}}$$

2) Camber estimation (nonlinear approach)

Table 5-2: Initial camber calculation by nonlinear approach

X (in)	M (k-in)	ϕ (rad/in)	$\theta = \int \phi \cdot dx$ (rad)	$\Delta = \int \theta \cdot dx$ (in)	Commentary
0	0	$-54.9 \cdot 10^{-6}$	$4.7 \cdot 10^{-3}$	0.00	• X = distance from support
10	10.6	$-54.2 \cdot 10^{-6}$	$4.2 \cdot 10^{-3}$	0.04	
20	20.0	$-53.4 \cdot 10^{-6}$	$3.6 \cdot 10^{-3}$	0.08	
30	28.1	$-52.7 \cdot 10^{-6}$	$3.1 \cdot 10^{-3}$	0.12	
40	35.0	$-52.2 \cdot 10^{-6}$	$2.6 \cdot 10^{-3}$	0.15	• Simple support conditions assumed at both ends of the beam.
50	40.6	$-51.7 \cdot 10^{-6}$	$2.1 \cdot 10^{-3}$	0.17	
60	45.0	$-51.4 \cdot 10^{-6}$	$1.5 \cdot 10^{-3}$	0.19	
70	48.1	$-51.2 \cdot 10^{-6}$	$1.0 \cdot 10^{-3}$	0.20	
80	50.0	$-51.0 \cdot 10^{-6}$	$0.5 \cdot 10^{-3}$	0.21	• ϕ obtained from nonlinear analysis (RESPONSE)
90	**50.6**	$-50.9 \cdot 10^{-6}$	**0**	**0.21**	
100	50.0	$-51.0 \cdot 10^{-6}$	$-0.5 \cdot 10^{-3}$	0.21	
110	48.1	$-51.2 \cdot 10^{-6}$	$-1.0 \cdot 10^{-3}$	0.20	• **The estimated initial camber is 0.21 inches.**
120	45.0	$-51.4 \cdot 10^{-6}$	$-1.5 \cdot 10^{-3}$	0.19	
130	40.6	$-51.7 \cdot 10^{-6}$	$-2.1 \cdot 10^{-3}$	0.17	
140	35.0	$-52.2 \cdot 10^{-6}$	$-2.6 \cdot 10^{-3}$	0.15	
150	28.1	$-52.7 \cdot 10^{-6}$	$-3.1 \cdot 10^{-3}$	0.12	
160	20.0	$-53.4 \cdot 10^{-6}$	$-3.6 \cdot 10^{-3}$	0.08	
170	10.6	$-54.2 \cdot 10^{-6}$	$-4.2 \cdot 10^{-3}$	0.04	
180	0	$-54.9 \cdot 10^{-6}$	$-4.7 \cdot 10^{-3}$	0.00	

5.4 PRESENTATION OF RESULTS FOR SET NUMBER 1

5.4.1 General

This set of beams, fabricated on June 26, 2002, included Specimens R1-60-1 (a) and (b), R1-70-1 (a) and (b), and R1-75-1 (a) and (b). Concrete mix 1 in Table 4-4 was used to cast these 15-foot long rectangular beams designed to target compressive stresses of $0.6f'_{ci}$, $0.7f'_{ci}$, and $0.75f'_{ci}$ at one extreme flexural fiber, and tensile stresses of approximately $2\sqrt{f'_{ci}}$ at the other extreme flexural fiber. No mild longitudinal reinforcement or transverse reinforcement was used in these beams.

The concrete compressive strengths required to achieve these stress levels at transfer were 4400psi, 4700psi, and 5500psi. The plan was to simultaneously release two specimens located in the same bay immediately after determining that concrete had reached the desired strength.

Steel frames spanning over the beams were used to support three linear potentiometers per beam specimen (Figure 4-7) to measure deflections while specimens were still on the prestressing bed. Additional instrumentation included strain gauges on the prestressing strands and surface-mounted strain gauges to measure concrete strains. Two strain gauges per beam were installed on each strand for a total of 72.

A control specimen without any reinforcement and having the same dimensions as the pretensioned beams was also cast. Concrete surface strain gauges were installed to monitor thermal and shrinkage strains, with the intent of later subtracting these from strains measured in the six prestressed specimens. As explained in an earlier chapter, formwork was not removed immediately from the beams, and consequently, surface gauges were installed 24 hours after release of the prestress force. As a result, the surface strain measurements did not include

deformations associated with release. The research team determined that little useful information was collected with these gauges, so future sets of beams were not instrumented with surface-mounted concrete strain gauges.

For reasons that will be discussed further in the following section, the prestress force was not released at the proper time to achieve the desired extreme fiber concrete stresses. In addition, only the linear potentiometers used to measure camber of beams R1-60-1 (a) and (b) were installed before transfer. In the case of Specimens R1-70-1 and R1-75-1, the potentiometers were installed 2.5 hours and 1 hour after their respective release times.

The beams were kept in the prestressing bed for approximately 12 days where strains and deflections were automatically measured and recorded by the data acquisition systems described in Section 4.3.3. The specimens were then moved to the laboratory floor where camber was monitored an additional 85 days using mechanical dial gauges.

5.4.2 Concrete Compressive Strength

Figure 5-3 illustrates the temperature history measured in the first set of beams using thermocouples. It is important to clarify that the first peak of approximately 105°F corresponds with the time at which concrete was initially placed in the forms. According to the figure, temperatures generated in all the beams were very similar. This is consistent with the fact that all beams in the set had the same cross section, and thermocouples were located at similar locations in each beam. As a result, all of the Sure Cure cylinders were cured at comparable conditions. The maximum temperature measured during concrete hydration was 145°F. It can be added that the average temperature inside Ferguson Laboratory was approximately 84°F on June 26, 2002.

A trial batch of concrete was cast in October 2001 to test the Sure Cure concrete curing system. A concrete element with the same dimensions as the pretensioned beams was cast and instrumented with thermocouples to measure the reference temperature for the Sure Cure system. Results of this trial batch indicated that required strengths of 4400 psi, 4700 psi, and 5500 psi would be reached approximately 15, 17, and 20 hours after mixing. However, these strengths were achieved significantly faster on June 26, 2002; a compressive strength of 5700 psi was measured after only 9.5 hours. Consequently, the prestress force was not released at the proper times to produce the desired concrete stress levels. Times at which the prestress forces were transferred to each one of the three pairs of beam specimens in set 1 are shown in Figure 5-3 with dashed lines. It can be observed that forces were not released simultaneously. The exact times are presented in Table 5-3.
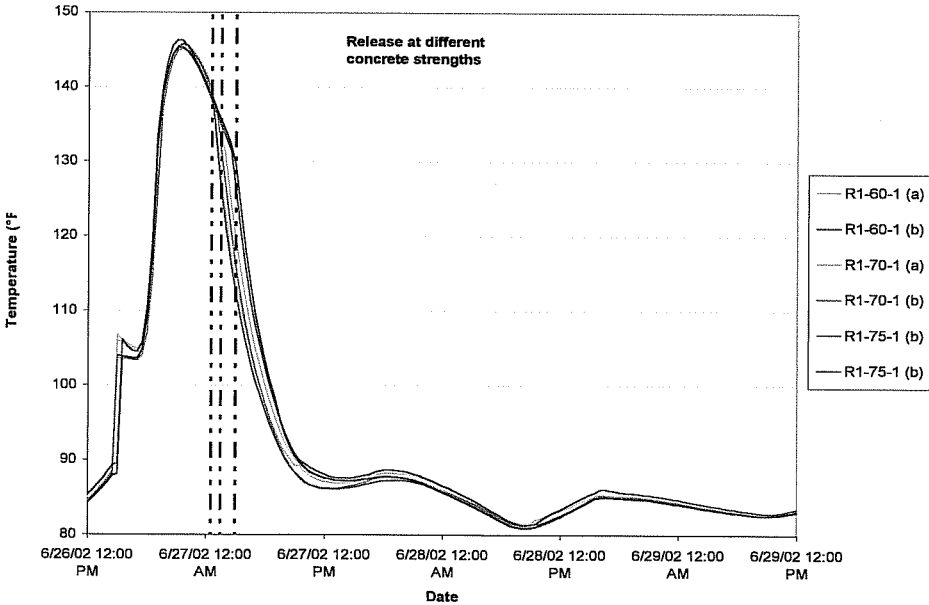

Figure 5-3: Measured temperatures (Set 1)

The increase in rate of strength gain was related, in part, to a difference of approximately 10°F between the ambient temperatures in June and October. However, after careful examination, it was determined that the actual mix proportions were different from those previously specified for mix 1. A reduction in the amount of water per cubic yard, from 204 lbs to 195 lbs, and an increase in the amount of Type III cement, from 608 lbs to 623 lbs, resulted in a water/cement ratio of 0.31 instead of 0.34. This was likely the most important factor affecting the rate of strength gain.
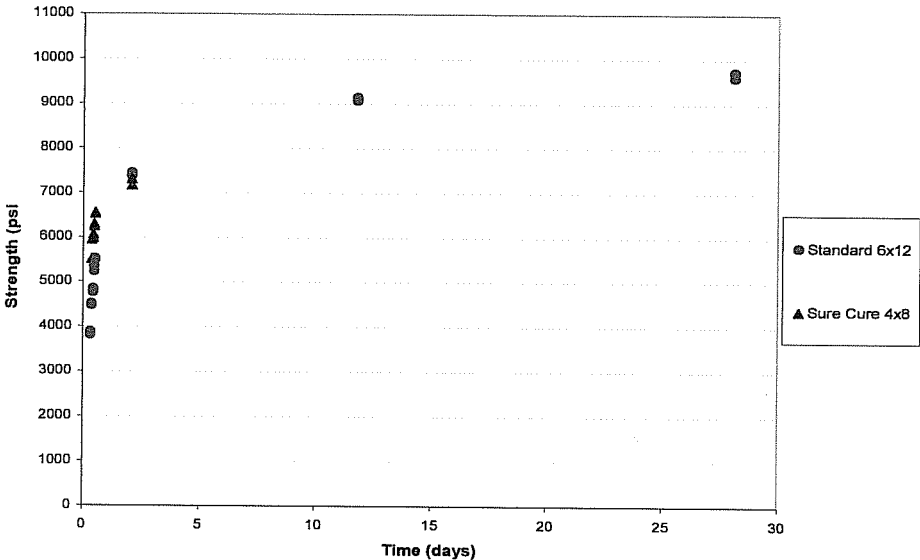

Figure 5-4: Concrete compressive strength vs. time (Set 1)

Figure 5-4 presents the development of strength with time for the concrete used in set 1. The 28-day strength was 9660psi based on standard 6 by 12-inch cylinders. Compressive strengths at release are provided in Table 5-3 along with the time elapsed between mixing the concrete and testing cylinders. Prestressing strands were cut a few minutes after compressive strength tests were conducted. According to the table, strengths measured based on standard 6 by 12-inch

95

cylinders were approximately 20 percent lower than those measured using match-cured 4 by 8-inch cylinders.

The ratio between concrete strength at release and 28-day strength ranged from 0.59 to 0.65 for the specimens in set 1. As mentioned in Section 3-2, this ratio is typical of what is experienced in precast plants.

Table 5-3: Compressive strengths at transfer (Set 1)

Time (hrs)	Specimens	Compressive Strength (psi)	
		Sure Cure 4x8" cylinder	Standard 6x12" cylinder
9.5	R1-60-1 (a) and (b)	5735	4500
10.7	R1-70-1 (a) and (b)	6025	4800
11.75	R1-75-1 (a) and (b)	6275	5300

5.4.3 Concrete Stresses at Transfer

As a result of late release of the prestress force, the desired concrete stresses were not attained. According to Table 5-4, extreme fiber concrete stresses at transfer ranged from $0.46f'_{ci}$ to $0.52f'_{ci}$. This table also shows the cross-sectional dimensions of the specimens, concrete properties, strand stresses, and measured and predicted cambers.

Concrete stresses at release were computed using the effective prestress force inferred from strain gauge measurements on prestressing strands. Low release stresses were also due to the inferred force being approximately 10 percent lower than the design prestress force obtained by assuming 7.5 percent losses between jacking and transfer. As indicated in Section 3-4, the design effective prestress force for these specimens was 172 kips. In reality, the measured prestress force ranged from 150 to 155 kips.

96

Strand stresses remained constant following jacking until initiation of the casting operation, at which point a gradual decrease was observed. The decreases in strand stress are thought to be due to temperature increases in the strand. In addition to the losses that occurred before transfer, elastic shortening losses of less than 8 percent of the initial jacking stress were measured. These losses were correctly predicted by the simplified PCI method illustrated in Section 5.3 (PCI, 1999).

Table 5-4: Summary of results (Set 1)

Specimen	R1-60-1 (a)	R1-60-1 (b)	R1-70-1 (a)	R1-70-1 (b)	R1-75-1 (a)	R1-75-1 (a)
Cross-sectional properties						
A_g (in2)	108	108	108	108	108	108
I_g (in4)	2916	2916	2916	2916	2916	2916
h (in)	18	18	18	18	18	18
y_b (in)	9	9	9	9	9	9
y_t (in)	9	9	9	9	9	9
Aps (in2)	0.92	0.92	0.92	0.92	0.92	0.92
e (in)	3.25	3.25	3.25	3.25	3.25	3.25
yb/h	0.50	0.50	0.50	0.50	0.50	0.50
Concrete properties						
Concrete Mix	No. 1 (modified - w/cm = 0.31)					
Release compressive strength - f'ci (psi)	5735	5735	6025	6025	6275	6275
Eci (ksi) (calculated as 57 f'ci$^{1/2}$)	4317	4317	4424	4424	4515	4515
f'c 28d (psi)	9660					
wc (lbs/ft3)	not measured / 150lbs/ft³ assumed					
Ec 28d (ksi) - Measured	not measured					
Ec 28d (ksi) - 33 wc$^{1.5}$ f'c$^{1/2}$	5959					
Ec 28d (ksi) - (40 f'c $^{1/2}$+1E3) (wc/145)$^{1.5}$	5189					
Average tensile stress in the strands						
Immediately before transfer (ksi) *	181	182	181	178	177	180
Immediately after transfer (ksi) *	168	169	168	166	164	168
Effective prestress force Po (kips)	154	155	154	152	150	155
Revision by nonlinear analysis **	156	157	159	154	153	156
Revision by PCI recommended method ***	155	156	157	152	151	155
Extreme fiber concrete stresses at transfer						
Compression (allowable stress design approach in Section 3.3.1.1)	0.52 f'ci	0.52 f'ci	0.5 f'ci	0.49 f'ci	0.46 f'ci	0.48 f'ci
Compression (strain compatibility approach in Section 3.3.1.2)	0.53 f'ci	0.53 f'ci	0.51 f'ci	0.49 f'ci	0.47 f'ci	0.48 f'ci
Compression (nonlinear approach Section in 3.3.2)	0.53 f'ci	0.53 f'ci	0.51 f'ci	0.49 f'ci	0.47 f'ci	0.48 f'ci
Tension x f'ci$^{1/2}$ (allowable stress design approach in Section 3.3.1.1)	1.6	1.6	1.6	1.5	1.5	1.5
Tension x f'ci$^{1/2}$ (strain compatibility approach in Section 3.3.1.2)	1.6	1.6	1.6	1.5	1.5	1.5
Tension x f'ci$^{1/2}$ (nonlinear approach Section in 3.3.2)	1.7	1.7	1.7	1.5	1.5	1.5
Camber						
Measured initial camber	0.53	-0.87	not measured			
Initial reading after installing linear potentiometers			1.08	0.21	0.70	-0.43
Predicted initial camber (procedure illustrated in Section 5.3 (7-a))	0.15	0.15	0.15	0.15	0.14	0.15
Predicted initial camber (procedure illustrated in Section 5.3 (8))	0.16	0.16	0.15	0.15	0.15	0.15
Measured camber 10 days after transfer	0.55	-0.86	1.08	0.24	0.75	-0.38
Predicted 10-day camber (procedure illustrated in Section 5.3 (7-b))	0.20	0.20	0.20	0.19	0.19	0.19
Measured camber 90 days after transfer	0.59	-0.82	1.12	0.27	0.78	-0.34
Predicted 90-day camber (procedure illustrated in Section 5.3 (7-b))	0.26	0.26	0.25	0.25	0.24	0.25
Predicted long-term camber (procedure illustrated in Section 5.3 (6-b))	0.37	0.37	0.36	0.35	0.34	0.35

* Inferred from strain gauge measurements
** From procedure discussed in section 3.3.2 and illustrated in section 5.3 (5)
*** From procedure illustratred in section 5.3 (1-b)

5.4.4 Camber

The initial cambers of Specimens R1-70-1 and R1-75-1 were not measured because linear potentiometers used to monitor deflection were installed after prestress transfer due to the unexpected high rate of strength gain in the beam concrete. In addition, the data acquisition system was programmed to collect data every 30 minutes. Consequently, data were not collected immediately after releasing the prestress force onto Specimens R1-60-1 (a) and (b). The fact that researchers were working on top of the prestressing bed when initial cambers were recorded for these beams could explain why measured initial cambers were 0.53 and -0.87 inches, which was significantly different from those predicted. While removing the forms for other specimens, the frames supporting displacement potentiometers could have been accidentally moved resulting in erroneous readings.

Behavior of the beams after transfer was evaluated by assuming the initial cambers were equal to the predicted values. For example, the camber response for Specimen R1-60-1(a) was displaced downward so that the initial camber was 0.15 inches instead of 0.53 inches. This was done for all the specimens in the first set. The resulting curves are shown in Figures 5-5, 5-6, and 5-7. Specimens were moved from the prestressing bed to the laboratory floor after approximately 12 days of monitoring by the data acquisition system.

Assuming that the initial cambers were predicted correctly, the behavior of Specimens R1-75-1(a) and (b) was predicted quite well by the first method described in Section 5.3 (Strain Compatibility). The same cannot be said about the response of Specimens R1-60-1 and R1-70-1, especially for the portion of the response curves measured while the beams were located on the prestressing bed. However, the slopes of measured and predicted response curves were similar after the specimens were moved to the laboratory floor.
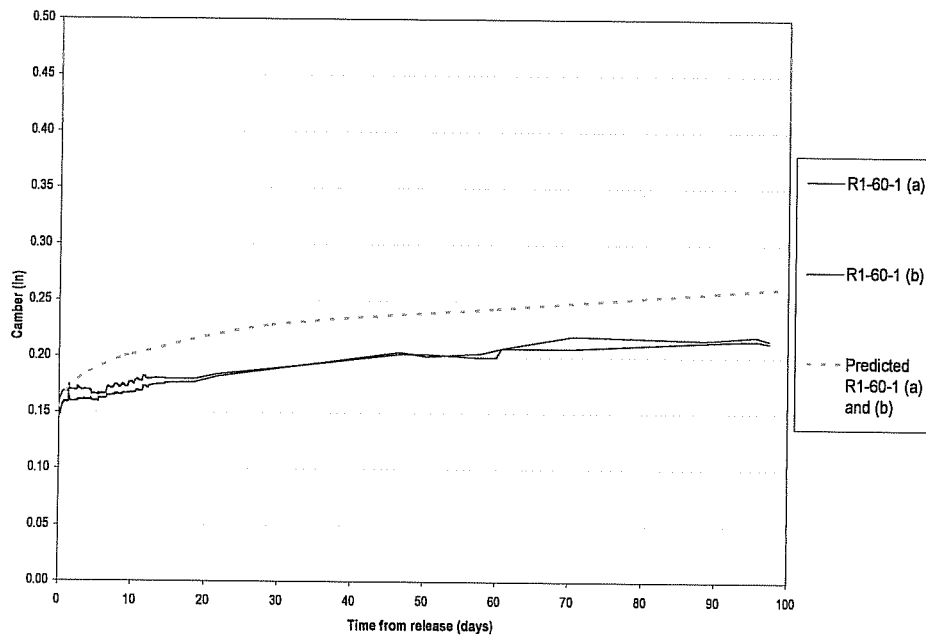
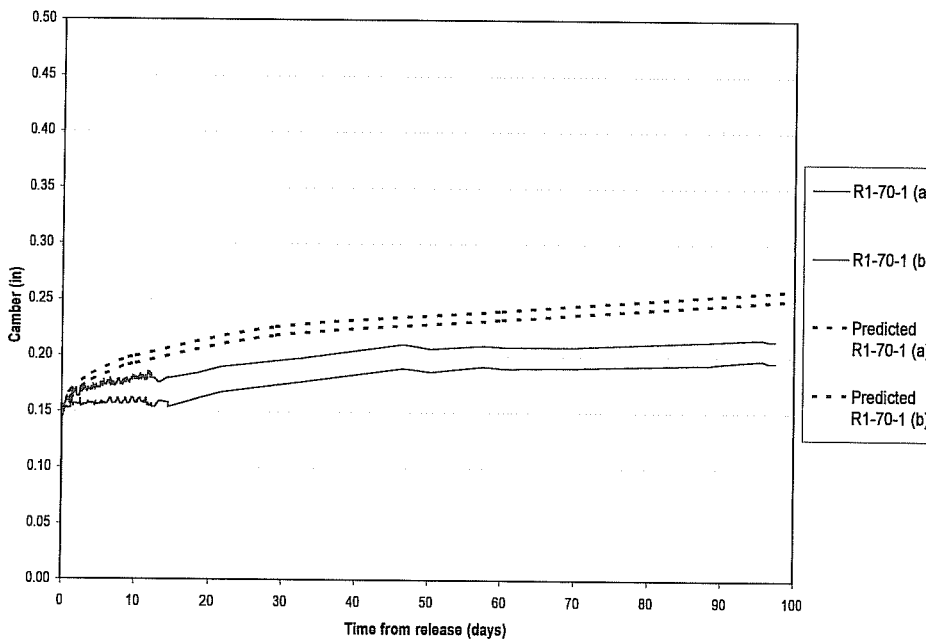*Figure 5-5: Adjusted camber for Specimens R1-60-1(a) and (b)*

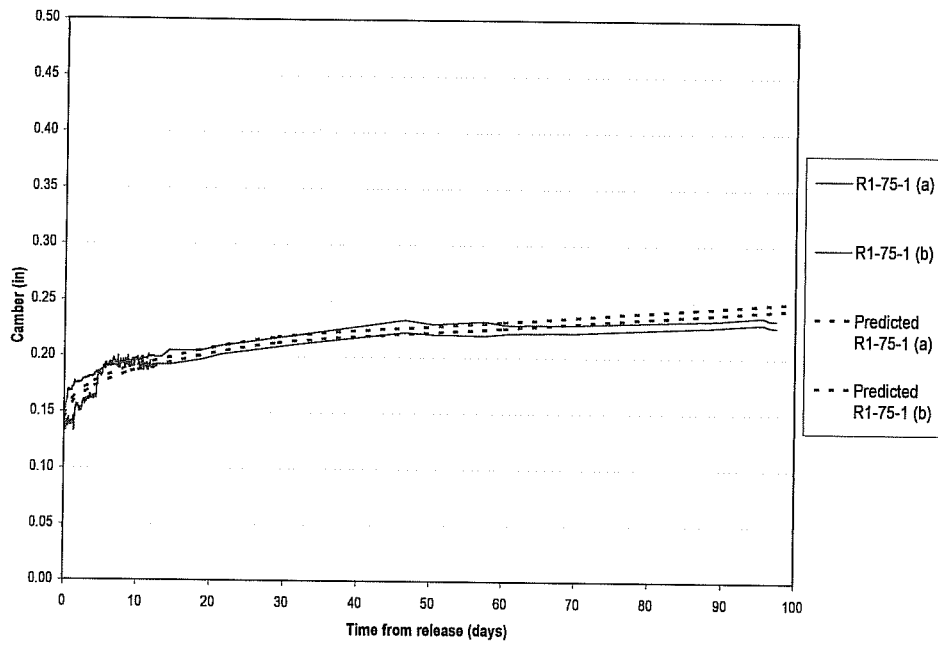*Figure 5-6: Adjusted camber for Specimens R1-70-1(a) and (b)*

99

Figure 5-7: Adjusted camber for Specimens R1-75-1(a) and (b)

5.5 Presentation of Results for Set Number 2

5.5.1 General

After completing the first set of beams, the research team became aware of work conducted by Noppakunwijai, Tadros, Ma, and Mast (Noppakunwijai et al, 2001), which suggested allowable release stresses should be a function of beam section properties. In light of this publication and the problems encountered by the research team during fabrication and release of the first set of beams, new test specimens were designed to examine the behavior of three cross sections at elevated release stresses, and to provide a sufficient interval between the release of the prestress force for each type of beam to facilitate installation of the instruments used to monitor camber. Set 2 included Specimens R2-75-2, R2-85-2, T1-74-2, T1-82-2, IT1-76-2, and IT1-84-2. These beams were cast on August 13, 2002 with nominally the same concrete mix used in set 1, but with better control on the mix proportions.

The instrumentation used to monitor this set of beams was similar to that used for the first set, except that concrete strains were not monitored with surface mounted gages or DEMEC points. In addition, only one strain gauge per strand, per beam, was installed for a total of 42 strain gauges. The frames used to support linear potentiometers for monitoring variations in camber of the first set of beams were used again.

The rate of strength gain was still a concern before casting the specimens so the formwork was redesigned to allow for easy removal. However, insufficient bracing and restraint were provided and, as a result, the forms expanded outward during the casting operation. Steel clamps were used with limited success to squeeze the forms back to the intended position. The resulting cross sections were different from those assumed in design. The actual dimensions of Specimen

R2-85-2 were furthest from the nominal dimensions and resulted in a beam with such irregular dimensions and unintended transverse eccentricity of the strands that the beam could not be used to study allowable release stresses.

As for the first set of beams, the ends of these specimens were not reinforced to resist bursting stresses that develop during release. Significant cracking occurred at the release ends of Specimens R2-75-2 and R2-85-2 as a result of the bursting stresses that developed due to the applied prestress force (Figure 5-8). This force was approximately 67 percent higher than that applied on the first set of specimens. No cracking was observed in the ends of the other specimens in set 2.
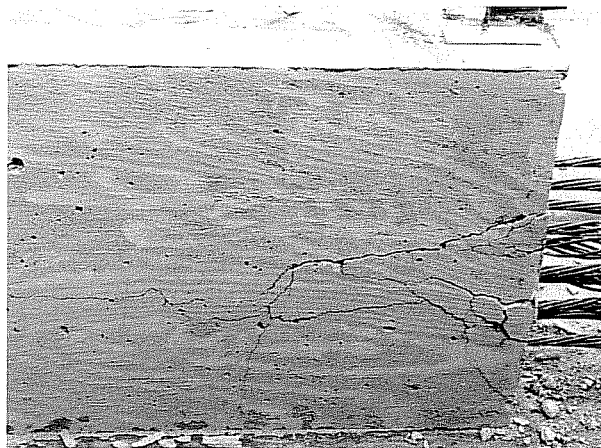

Figure 5-8: Cracking at release end due to bursting stresses (R2-75-2)

5.5.2 Concrete Compressive Strength

Although specimens with different cross sections were cast in set 2, Figure 5-9 indicates that measured concrete temperatures were similar for all specimens. The average temperature inside Ferguson Laboratory was approximately 85°F on August 13, 2002, and the maximum concrete temperatures measured during hydration were 137°F for the tee beams and 140°F for the inverted tee and

102

rectangular beams. As done in Figure 5-3, the times at which the prestress forces were transferred to the beam specimens in set 2 are shown in Figure 5-9 with dashed lines. Again, the prestress forces were not released simultaneously.

The actual mix proportions for this set of beams were very similar to those specified in Table 4-4 for concrete mix type 1. The amount of cement and water were slightly different resulting in a water/cementitious materials ratio of 0.35 instead of 0.34. In addition, 615 lbs of cement and 214 lbs of water per cubic yard were used. These small changes resulted in a slower rate of strength gain that lead to a concrete compressive strength of 4700 psi at 9.5 hours instead of the 5700 psi measured for set 1.
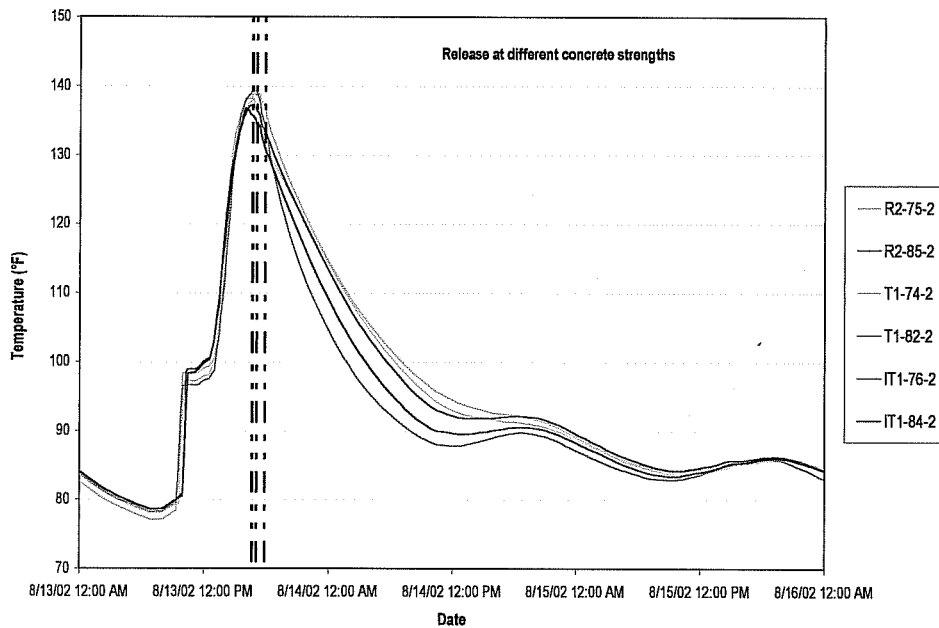

Figure 5-9: Measured temperatures (Set 2)

11000

10000

9000

8000

7000

Strength (psi)

6000

5000

4000

3000

2000

1000

0

0   5   10   15   20   25   30

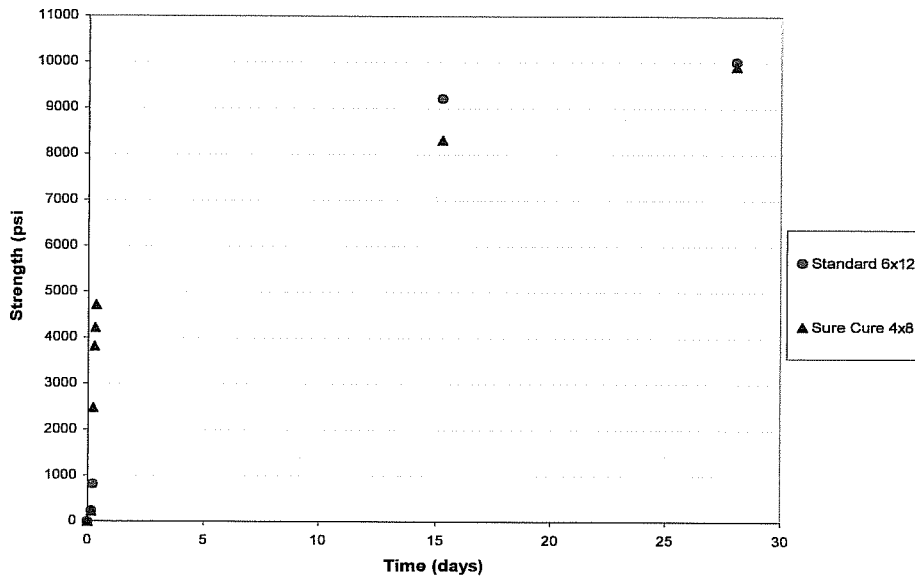Time (days)

● Standard 6x12

▲ Sure Cure 4x8

Figure 5-10: Concrete compressive strength vs. time (Set 2)

Figure 5-10 presents the development of strength with time for the concrete used in set 2. In addition, Table 5-5 shows the compressive strength at transfer for each pair of specimens. Except for Specimens T1-74-2 and T1-82-2, release strengths were close to those required by design to produce the desired extreme fiber concrete stresses. At the time, it was not possible to perform compressive strength tests on 6 by 12-inch cylinders immediately prior to prestress release, so it was not possible to evaluate the difference between match-cured and standard cylinders at an early age. However, using tests performed according to ASTM C39 on standard 6 by 12-inch cylinders, the 28-day concrete compressive strength was estimated to be 10015 psi. The ratio of concrete strength at release and the 28-day strength for these beams ranged from 0.38 to 0.47, and the ratio of 28-day strength of Sure-Cure cylinders to 28-day strength of standard cylinders was 0.99.

Table 5-5: Compressive strengths at transfer (Set 2)

Time (hrs)	Specimens	Compressive Strength (psi)	
		Sure Cure 4x8" cylinder	Standard 6x12" cylinder
8.0	IT1-76-2 / IT1-84-2	3815	Not measured
8.5	T1-74-2 / T1-82-2	4220	
9.5	R2-75-2 / R2-85-2	4720	

5.5.3 Concrete Stresses at Transfer

As discussed in Section 5.5.1, actual cross-section dimensions of the specimens in set 2 were different from the nominal dimensions used in design. Consequently, they were measured every 12 inches along the length of each beam, and average cross-section dimensions were used to estimate the concrete stresses at transfer shown in Table 5-6. For instance, the average estimated cross-section area and moment of inertia for beam R2-75-2 were 119 in^2 and 3360 in^4 instead of the nominal values of 108 in^2 and 2916 in^4.

The desired extreme concrete fiber stresses were not achieved due to the increase in cross-section dimensions. In addition, by comparing the information provided in Tables 3-7 and 5-6, it is clear that the inferred effective prestress forces were again lower than those used in design of test specimens. As a result, actual extreme bottom fiber stresses at transfer ranged from $0.62f'_{ci}$ to $0.73f'_{ci}$.

The objective of fabricating Specimens R2-75-2 and R3-85-2 was to evaluate the effect of a low stress gradient on the time-dependent response of pretensioned members subjected to high stresses at transfer. Table 5-6 indicates that the top fiber stress in Specimen R2-75-2 was $0.27f'_{ci}$ in compression while tensile stresses were generated in the top fiber of the rest of the beams. The tensile limit of $6\sqrt{f'_{ci}}$ was exceeded only in Specimen IT-84-2, which exhibited

cracking in the top of the beam. The average crack depth and spacing were 2.3 and 9.6 inches, respectively. The crack widths were too small to be measured with any accuracy.

Three approaches were used to compute the extreme concrete fiber stresses at transfer. Through comparison of results, it can be concluded that stresses computed based on gross-section properties are reasonably accurate for stresses near $0.6f'_{ci}$. The nonlinear method discussed in Section 3.3.2 generally lead to slightly lower estimates of compressive stresses and higher estimates of tensile stresses. The exception was Specimen IT1-84-2. Stresses computed using gross-section properties or the strain-compatibility approach did not include the effects of cracking.

Table 5-6: Summary of results (Set 2)

Specimen	R2-75-2	T1-74-2	T1-82-2	IT1-76-2	IT1-84-2
Cross-sectional properties					
A_g (in2)	119	106	113	153	152
I_g (in4)	3360	2280	2470	4350	4320
h (in)	18.4	15.5	15.5	18.3	18.3
y_b (in)	9.19	10.3	10.1	7.69	7.57
y_t (in)	9.19	5.17	5.36	10.56	10.68
Aps (in2)	1.53	0.46	0.46	1.22	1.22
e (in)	1.29	5.53	6.09	3.19	3.82
yb/h	0.50	0.67	0.65	0.42	0.41
Concrete properties					
Concrete Mix	No. 1 (modified - w/c = 0.35)				
Release compressive strength - f'ci (psi)	4720	4220	4220	3815	3815
Eci (ksi) (calculated as 57 f'ci$^{1/2}$)	3916	3703	3703	3521	3521
f'c 28d (psi)	10015				
wc (lbs/ft3)	not measured / 150lbs/ft^3 assumed				
Ec 28d (ksi) - Measured	not measured				
Ec 28d (ksi) - 33 wc$^{1.5}$ f'c$^{1/2}$	6067				
Ec 28d (ksi) - (40 f'c $^{1/2}$+1E3) (wc/145)$^{1.5}$	5264				
Average tensile stress in the strands					
Immediately before transfer (ksi) *	188	191	185	191	192
Immediately after transfer (ksi) *	169	180	168	174	171
Effective prestress force Po (kips)	259	83	77	213	209
Revision by nonlinear analysis **	263	82	79	217	216
Revision by PCI recommended method ***	261	81	79	215	214
Extreme fiber concrete stresses at transfer					
Compression (allowable stress design approach in Section 3.3.1.1)	0.65 f'ci	0.68 f'ci	0.62 f'ci	0.68 f'ci	0.73 f'ci
Compression (strain compatibility approach in Section 3.3.1.2)	0.67 f'ci	0.67 f'ci	0.64 f'ci	0.7 f'ci	0.76 f'ci
Compression (nonlinear approach Section in 3.3.2)	0.66 f'ci	0.65 f'ci	0.62 f'ci	0.67 f'ci	0.75 f'ci
Tension x f'ci$^{1/2}$ (allowable stress design approach in Section 3.3.1.1)	comp = 0.27 f'ci	3.9	5.2	4.1	9.8
Tension x f'ci$^{1/2}$ (strain compatibility approach in Section 3.3.1.2)	comp = 0.27 f'ci	3.9	5.3	4.2	10.2
Tension x f'ci$^{1/2}$ (nonlinear approach Section in 3.3.2)	comp = 0.27 f'ci	4.2	5.6	5.1	18.0
Cracked in reality	no	no	no	no	yes
Camber					
Measured initial camber	0.45	0.52	0.50	0.41	0.36
Predicted initial camber (procedure illustrated in Section 5.3 (7-a))	0.09	0.20	0.20	0.17	0.28
Predicted initial camber (procedure illustrated in Section 5.3 (8))	0.10	0.21	0.21	0.19	0.23
Eci$_{ADJ}$	822	1448	1478	1493	2264
ε'ci $_{ADJ}$	0.009	0.005	0.005	0.004	0.003
Measured camber 10 days after transfer	0.49	0.61	0.63	0.45	0.46
Predicted 10-day camber (procedure illustrated in Section 5.3 (7-b))	0.12	0.29	0.28	0.21	0.35
Measured camber 90 days after transfer	0.49	0.64	0.68	0.46	0.46
Predicted 90-day camber (procedure illustrated in Section 5.3 (7-b))	0.15	0.37	0.36	0.27	0.44
Predicted long-term camber (procedure illustrated in Section 5.3 (6-b))	0.22	0.50	0.47	0.41	0.49

* Inferred from strain gauge measurements

** From procedure discussed in Section 3.3.2 and illustrated in Section 5.3 (5)

*** From procedure illustratred in Section 5.3 (1-b)

5.5.4 Camber

The second set of beams was moved from the prestressing bed to the laboratory floor 10 days after releasing the prestress force. Changes in camber were measured for an additional 157 days using mechanical dial gauges once the beams were moved to the laboratory floor. In total, camber response of the beams was observed for 5.5 months. The resulting camber versus time curves are presented in Figures 5-11 through 5-13.

For this set of beams, the data acquisition system was programmed to collect data every 5 seconds to avoid inaccurate initial camber measurements as occurred for the first set of beams. In spite of this, initial measured and predicted cambers were significantly different. As shown in Table 5-6, measured initial cambers were considerably larger than predicted, ranging from 1.3 to five times as much. In addition, the initial camber measured for IT1-84-2 was less than that for IT1-76-2, even though the former specimen was cracked at the top as a result of higher tensile stresses imposed during transfer.

As mentioned earlier, beam cross-section dimensions were carefully measured and average dimensions were used to predict behavior of the members. The adjusted moment of inertia, area, and distance to extreme fibers are shown in Table 5-6 for each beam. The data in Table 5-6 demonstrate that differences in camber cannot be explained by irregularities in the cross sections. In addition, because cross sections tended to be larger near midspan than at the ends of beams, use of measured dimensions at discrete locations, rather than average measured dimensions, would have resulted in even smaller predicted initial cambers.

Because the research team was busy releasing forms, installing support frames and displacement transducers used to monitor camber, and testing concrete cylinders to monitor strength gain, determination of the modulus of elasticity of concrete, according to ASTM C469, at the time of each release was not possible.

Consequently, the ACI 318-02 equation for estimating elastic modulus based on the compressive strength of concrete was utilized. Having an accurate estimate of the elastic modulus was necessary for correctly predicting deflections of the prestressed concrete beams. The research team evaluated elastic modulus values different from those predicted by the ACI Code equation to determine whether the concrete modulus was responsible for the differences between calculated and measured initial cambers.

Table 5-6 lists elastic moduli (Eci_{ADJ}) and corresponding strains at peak stress ($\varepsilon'ci_{ADJ}$) used in the nonlinear analysis model in order to match measured camber values. Because the $\varepsilon ci'_{ADJ}$ values required to produce correct cambers ranged from 0.003 to 0.009, in contrast to strains corresponding with peak concrete stresses (which typically range from as low as 0.0015 to as high as 0.0025), it was concluded that differences in camber values could not be resolved by employing different elastic moduli in the camber calculations.

The reason for inconsistencies between measured and predicted initial cambers is not clear. It was quite clear that the ends of pretensioned beams displaced a significant amount when prestress force was released onto the beams. It is speculated that camber readings were affected by rigid body translation of beams at release, which resulted in significant longitudinal movement (along the axis of respective beams) of plates positioned beneath the displacement transducers.

Initial camber for each beam was offset to match the predicted initial camber, as was done for the first set of beams. Figure 5-11 illustrates the behavior of Specimen R2-75-2. The figure indicates that camber increased during the first three days then remained virtually constant for several months. This might be indicative of damage suffered at the release end resulting in a drastic reduction of tension in the strands along a significant portion of the member.

Measured response of the inverted tee and tee beams more closely resembled predicted response. Figures 5-12 and 5-13 illustrate a rapid increase in camber during the first few days followed by a gradual reduction in the rate of camber increase (slope of the response curves) with time. The reduction in rate of camber increase was more pronounced for Specimens IT1-76-2 and IT1-84-2. For both the inverted tee and tee beam specimens, the predicted rate of camber increase tended to be less than the measured response during the early life of the beams, and was significantly greater following the first ten to 15 days of response.
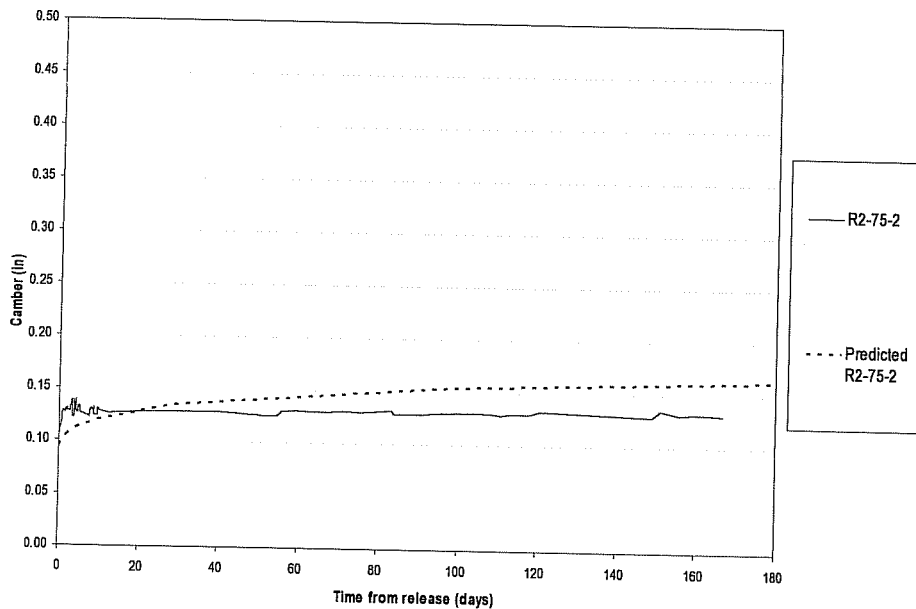
Figure 5-11: Adjusted camber for Specimen R2-75-2
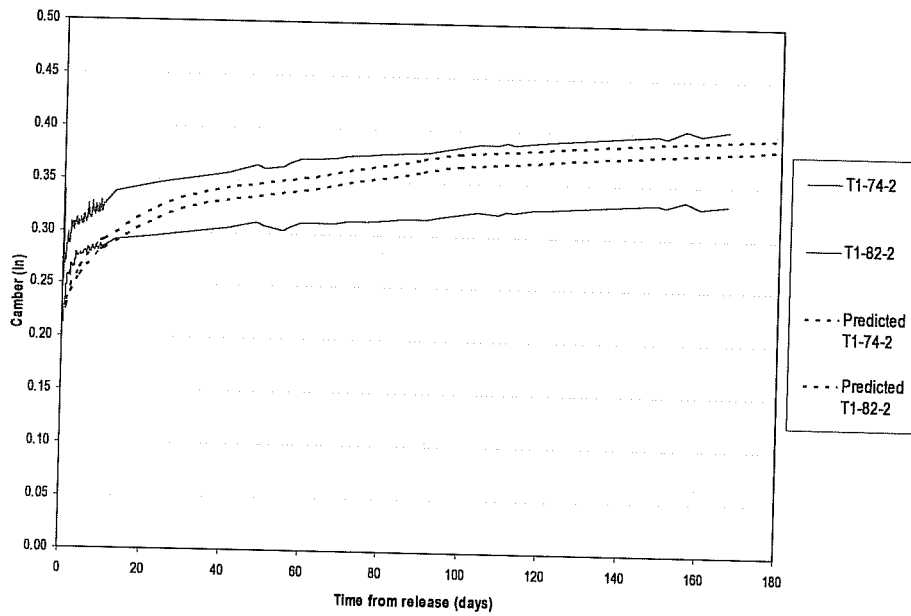
Figure 5-12: Adjusted camber for Specimens T1-74-2 and T1-82-2
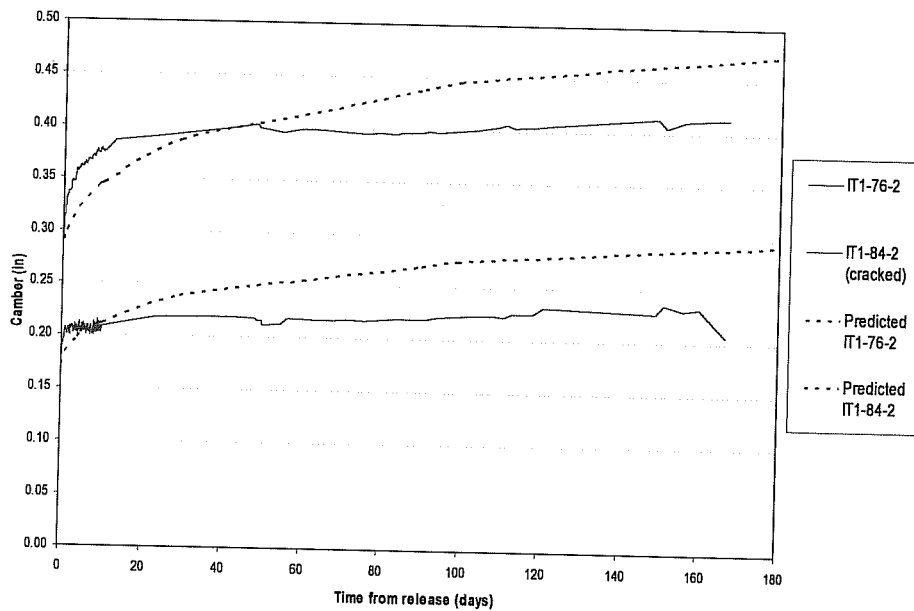
Figure 5-13: Adjusted camber for Specimens IT1-76-2 and IT1-84-2

111

5.6 PRESENTATION OF RESULTS FOR SET NUMBER 3

5.6.1 General

Beam specimens were redesigned to prevent splitting cracks at the ends during the release process. Transverse reinforcement was placed at the ends of beams to provide the required bursting resistance during transfer (AASHTO, 1998) as shown in Appendix C. In addition, cross-section dimensions and the amount and location of prestressing steel were modified so that the prestress force for all beams could be released when the same target concrete strength was reached. The two inverted tee specimens had basically the same cross-section properties, except Specimen IT3-85-3 contained non-prestressed reinforcement in the top of the beam to control flexural cracking caused by application of the prestress force.

Concrete mix number 1 with 1-inch river gravel for coarse aggregate was used to cast these specimens. This is a typical mix used in many Texas precast manufacturing plants for pretensioned concrete applications. As for earlier sets of beams, the modulus of elasticity of concrete at transfer was not measured. However, standard 4 by 8-inch cylinders were tested 28 days after casting, and results demonstrated that this mix resulted in concrete that was significantly stiffer than the concrete produced with crushed limestone coarse aggregate. This will be discussed further in the following section.

Along with redesign of the test specimens, the most important modification made as a result of experience with the second set of specimens was changing the frame system used to support the transducers for camber measurements. The simplified frame (modified configuration) presented in Figure 4-9 was successfully used for this set of beams. Also, measures were taken to ensure specimen dimensions remained dimensionally stable during

112

casting. Ties made up of threaded rods were used to hold the forms together during casting and curing of concrete. The ties were designed for easy removal so that forms could be loosened rapidly before transfer. Cross-section dimensions and location of strands were verified after removing the forms.

5.6.2 Concrete Compressive Strength

The average ambient temperature inside Ferguson Laboratory was approximately 81°F on September 24, 2002. Heat generated during concrete hydration differed for each type of beam. Figure 5-14 shows that curing conditions for cylinders linked to the two tee beams were comparable. Also, conditions for cylinders cured based on reference temperatures measured in Specimens IT3-85-3 and R3-82-3 were roughly the same before release. Specimens IT2-85-3 and R3-76-3 reached the highest temperatures at release of 127°F and 129°F, respectively. However, the difference in temperature associated with R3-76-3 relative to R3-82-3 and IT3-85-3 was not significant until approximately two hours before release. Consequently, tests to determine compressive strength indicated that similar concrete strengths had been achieved in these specimens at transfer.
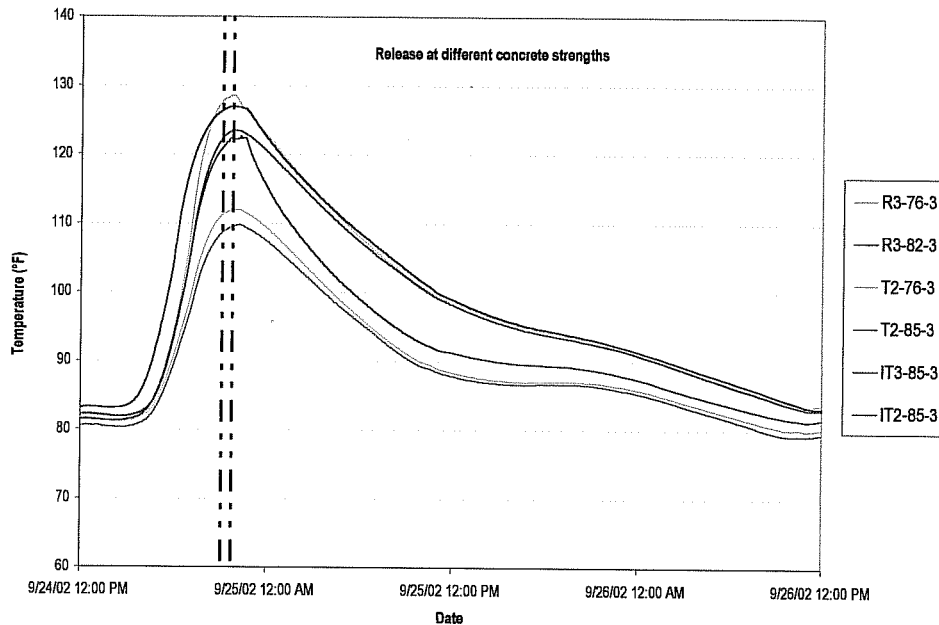
Figure 5-14: Measured temperature histories (Set 3)

Measured concrete strengths at release are presented in Table 5-7. Additionally, compressive strengths determined with concrete cylinders during the first 16 hours are plotted in Figure 5-15. Standard 4 by 8-inch cylinders were also tested during this period to evaluate the effects of match-curing of cylinders. Even though temperatures measured in these small-scale beams were not as high as those commonly experienced in precast manufacturing facilities, there was a difference of approximately 10 to 15 percent between strengths determined using match-cured and standard cylinders. Basing the release of pretensioned concrete members on tests performed using standard cylinders will likely lead to actual extreme fiber stresses at release that are lower than intended. Larger differences would be expected for higher curing temperatures typical in actual pretensioned bridge beams.

114
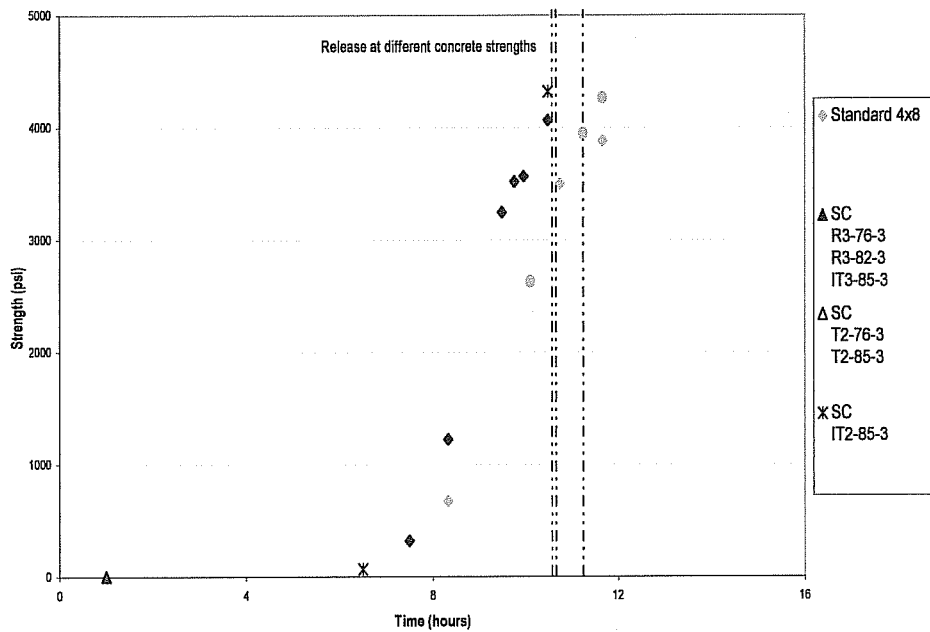
Figure 5-15: Concrete strength during first 16 hours (Set 3)

Table 5-7: Compressive strengths at transfer (Set 3)

Time (hrs)	Specimens	Compressive Strength (psi)	
		Sure Cure 4x8 cylinder	Standard 4x8 cylinder
10.5	R3-76-3/ R3-82-3/ IT3-85-3	4065	3500 psi at 10.75 hours 3900 psi at 11.67 hours
10.5	IT2-85-3	4320	
11.25	T2-76-3/ T2-85-3	3950	

Twenty-eight-day compressive strengths of 10,050 psi and 10,015 psi were determined based on standard 4 by 8-inch and 6 by 12-inch cylinders. The 28-day concrete stiffness was also determined according to ASTM C469 using 4 by 8-inch and 6 by 12-inch cylinders resulting in elastic modulus values of 5900 ksi and 6050 ksi. A significantly lower value of 5460 ksi was calculated using the ACI 363-R92 expression presented in Chapter 2. Although this equation is

115

recommended for high-strength concrete, it underestimated the actual modulus by approximately 8 percent. As will be discussed further in Section 5.7.2, the measured 28-day stiffness of the concrete made with river rock was considerably higher than that for concrete made with crushed limestone.
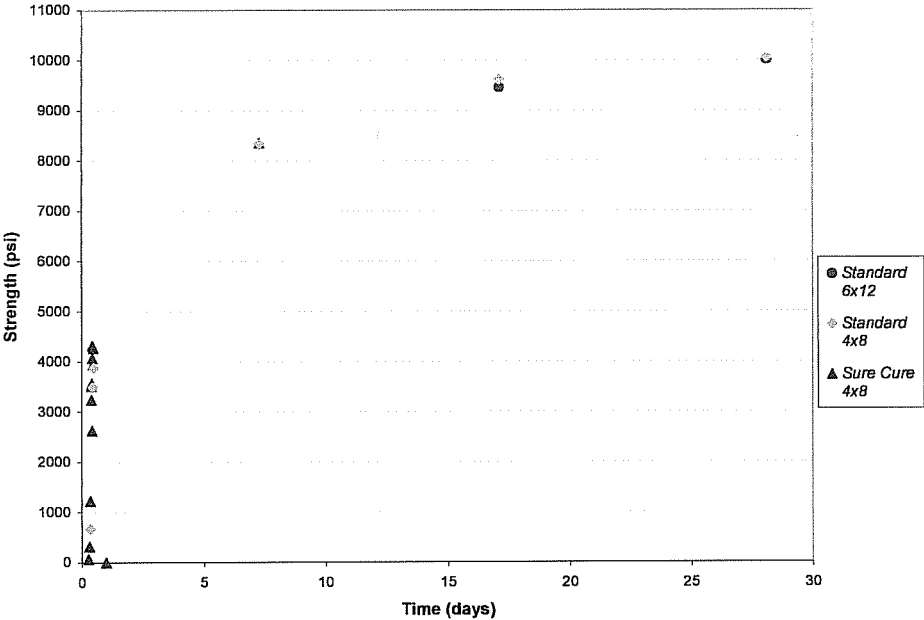
Figure 5-16: Concrete compressive strength vs. time (Set 3)

5.6.3 Concrete Stresses at Transfer

Based on the results from the first two sets of beams, 10 percent additional prestress losses were considered when designing these beams. As a result, the actual effective prestress forces were equal to or higher than expected. Considering these inferred forces and concrete strengths at transfer, compressive stresses at release were slightly lower than desired but considerably higher than the specified limit. Extreme fiber compressive stresses between $0.75f'_{ci}$ and $0.86f'_{ci}$ were applied to the specimens.

116

Beams R3-82-3, IT3-85-3, and IT2-85-3 exhibited flexural cracking at the top as a consequence of the high, imposed tensile stresses. However, the extreme fiber tensile stress calculated with the assumption of linear-elastic uncracked behavior for Specimen R2-82-3 was lower than the modulus of rupture estimated with the expressions included in Table 2-4. Despite this, Specimen R2-82-3 exhibited, on average, 1.75-inch deep cracks spaced at 10 inches. Tensile stresses calculated for Specimens IT3-85-3 and IT2-85-3 were approximately $9\sqrt{f'_{ci}}$. As indicated earlier, only Specimen IT3-85-3 had top non-prestressed reinforcement to control the effects of cracking. This beam experienced 2-inch deep cracks spaced at 8.5 inches, while Specimen IT2-85-3 developed 2.25-inch deep cracks spaced at 11 inches. As for the specimens in set 2, the cracks were extremely fine.

The applied compressive and tensile stresses were higher for this set of beams than they were for any of the previous sets. Consequently, the assumption of linear behavior of the materials may not accurately represent the conditions in the members. Differences in stresses calculated based on linear-elastic assumptions and a nonlinear approach are notable in these beams. For instance, extreme fiber stresses of $0.86f'_{ci}$ in compression and $4.2\sqrt{f'_{ci}}$ in tension were computed for Specimen T2-85-3 using a linear-elastic approach. The corresponding values calculated with a nonlinear approach were $0.81f'_{ci}$ and $5\sqrt{f'_{ci}}$. This demonstrates that estimating compressive stresses in highly stressed pretensioned members with a linear-elastic approach results in overestimation of those stresses, as suggested by Huo and Tadros (1997). However use of a linear-elastic approach for estimation of extreme tensile fiber stresses may result in underestimation of those stresses.

Table 5-8: Summary of results (Set 3)

Specimen	R3-76-3	R3-82-3	T2-76-3	T2-85-3	IT3-85-3	IT2-85-3
Cross-sectional properties						
A_g (in2)	144	144	104	104	156	156
I_g (in4)	3888	3888	2251	2251	4706	4706
h (in)	18	18	15.5	15.5	19	19
y_b (in)	9	9	10.27	10.27	7.88	7.88
y_t (in)	9	9	5.23	5.23	11.12	11.12
Aps (in2)	1.22	1.22	0.61	0.61	1.53	1.53
e (in)	3.50	4	4.52	5.27	3.66	3.66
yb/h	0.5	0.5	0.66	0.66	0.41	0.41
Concrete properties						
Concrete Mix			No. 1 (w/c = 0.34)			
Release compressive strength - f'ci (psi)	4065	4065	3950	3950	4065	4320
Eci (ksi) (calculated as 57 f'ci$^{1/2}$)	3630	3630	3580	3580	3630	3750
f'c 28d (psi) - Based on 6x12-inch / 4x8-inch standard cylinders			10015 / 10050			
wc (lbs/ft3)			154			
Ec 28d (ksi) - Based on 6x12-inch / 4x8-inch standard cylinders			6050 / 5900			
Ec 28d (ksi) - 33 wc$^{1.5}$ f'c$^{1/2}$ - (6x12-inch / 4x8-inch cylinders)			6300 / 6310			
Ec 28d (ksi) - (40 f'c $^{1/2}$+1E3) (wc/145)$^{1.5}$ - (6x12-inch / 4x8-inch cylinders)			5460 / 5470			
Average tensile stress in the strands						
Immediately before transfer (ksi) *	181	178	182	181	189	188
Immediately after transfer (ksi) *	165	159	168	165	168	170
Effective prestress force Po (kips)	201	195	103	101	257	260
Revision by nonlinear analysis **	200	194	103	101	262	261
Revision by PCI recommended method ***	203	197	102	100	260	259
Extreme fiber concrete stresses at transfer						
Compression (allowable stress design approach in Section 3.3.1.1)	0.75 f'ci	0.78 f'ci	0.79 f'ci	0.86 f'ci	0.79 f'ci	0.76 f'ci
Compression (strain compatibility approach in Section 3.3.1.2)	0.76 fci	0.8 fci	0.79 fci	0.87 fci	0.82 fci	0.77 fci
Compression (nonlinear approach Section in 3.3.2)	0.71 fci	0.74 fci	0.75 fci	0.81 fci	0.79 fci	0.75 fci
Tension x f'ci$^{1/2}$ (allowable stress design approach in Section 3.3.1.1)	3.7	7.1	1.5	4.2	9.0	8.8
Tension x f'ci$^{1/2}$ (strain compatibility approach in Section 3.3.1.2)	3.7	7.2	1.5	4.3	9.1	9.0
Tension x f'ci$^{1/2}$ (nonlinear approach Section in 3.3.2)	4.4	8.5	2.0	5.0	13.9	13.3
Cracked in reality	no	yes	no	no	yes	yes
Top reinforcement	no	no	no	no	yes	no
Camber						
Measured initial camber	0.18	0.20	0.15	0.20	0.18	0.21
Predicted initial camber (procedure illustrated in Section 5.3 (7-a))	0.19	0.22	0.22	0.25	0.26	0.24
Predicted initial camber (procedure illustrated in Section 5.3 (8))	0.20	0.23	0.24	0.28	0.24	0.23
Eci$_{ADJ}$	4185	4186	5625	5080	4957	4032
ε'ci $_{ADJ}$	0.0017	0.0017	0.0012	0.0013	0.0014	0.0018
Measured camber 10 days after transfer	0.28	0.31	0.23	0.31	0.31	0.29
Predicted 10-day camber (procedure illustrated in Section 5.3 (7-b))	0.24	0.27	0.31	0.36	0.30	0.30
Measured camber 90 days after transfer	0.32	0.36	0.27	0.34	0.35	0.33
Predicted 90-day camber (procedure illustrated in Section 5.3 (7-b))	0.30	0.34	0.40	0.45	0.36	0.38
Predicted long-term camber (procedure illustrated in Section 5.3 (6-b))	0.46	0.51	0.53	0.61	0.52	0.51

* Inferred from strain gauge measurements
** From procedure discussed in Section 3.3.2 and illustrated in Section 5.3 (5)
*** From procedure illustratred in Section 5.3 (1-b)

5.6.4 Camber

The primary objective of this research program was to determine whether subjecting prestressed concrete members to stresses exceeding current design limits would adversely affect behavior at and after prestress transfer. Adverse behavior such as concrete microcracking and large creep deformations could lead to excessive camber and, perhaps, even failure. The beams in this set were subjected to compressive stresses at transfer in excess of $0.75f'_{ci}$ with no obvious negative effects observed. As illustrated in Figures 5-17, 5-18, and 5-19, the rate at which members deflected during the first two to three days following release was higher than predicted. However, this rate decreased gradually, leading to cambers that were equal to or lower than predicted values after six months of continuous monitoring. Furthermore, cambers measured at that time were significantly lower than long-term cambers estimated using multipliers suggested by the PCI. In addition, the trend of the camber measurements indicated that it was unlikely that specimens would reach the levels of deformation predicted by the PCI multipliers (PCI, 1999).

Although predicted initial camber values were larger than measured values, differences were within hundredths of an inch. The accuracy of the analytical models is only as good as the validity of the assumptions invoked in the models and the accuracy of the input parameters used. For instance, the difference between actual and estimated concrete stiffness at transfer could account for the small differences in initial camber. Previous researchers have indicated that the ACI 318-02 and ACI 363-R92 expressions relating concrete stiffness to compressive strength must be used cautiously with early-age high-strength concrete. At this stage in the life of concrete, the rate of gain of the

119

elastic modulus is higher than the rate at which strength increases. Furthermore, the measured 28-day elastic modulus for the concrete used to cast this set of beams was considerably higher than the modulus estimated using the expression recommended by ACI 363R-92.
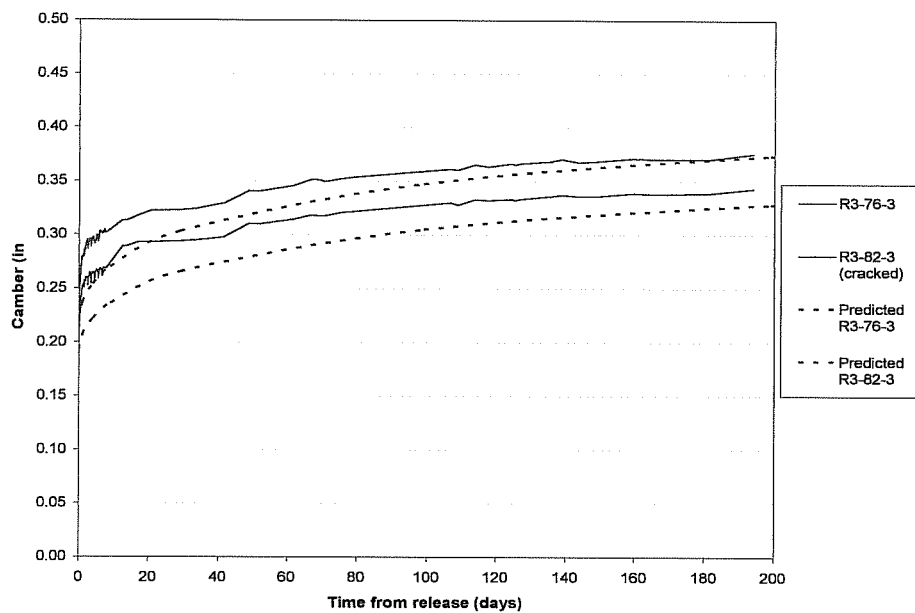
Figure 5-17: Camber response for Specimens R3-76-3 and R3-82-3
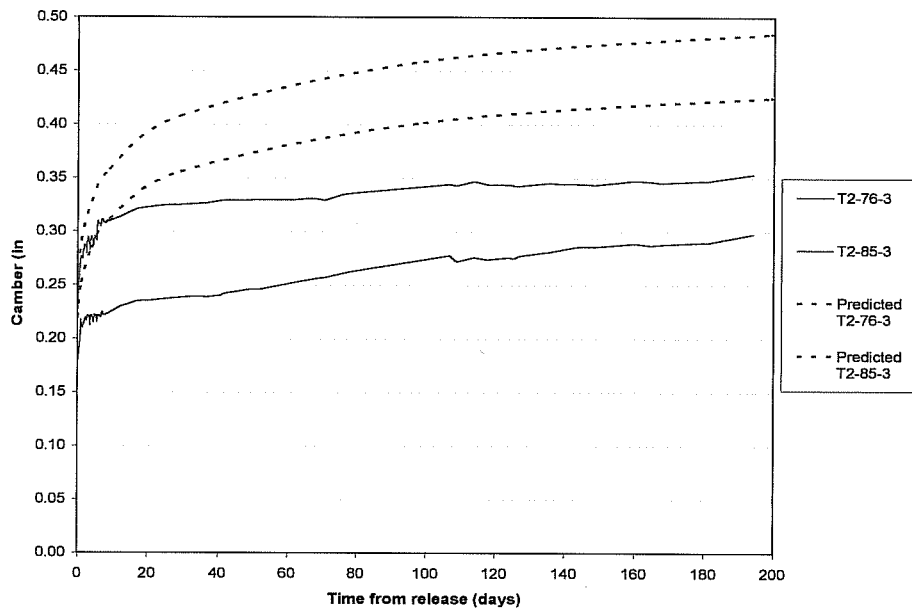
Figure 5-18: Camber response for Specimens T2-76-3 and T2-85-3
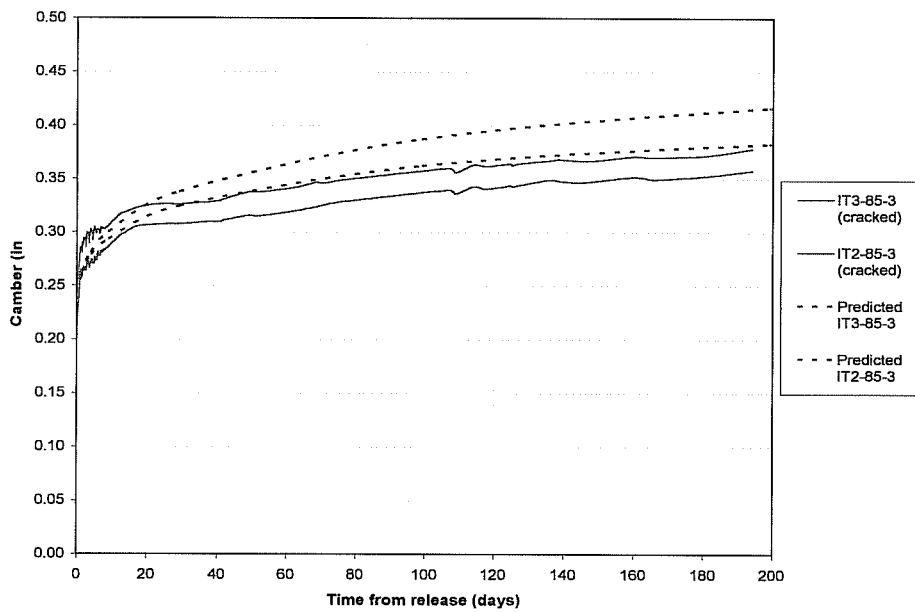
Figure 5-19: Camber response for Specimens IT2-85-3 and IT3-85-3

121

5.7 PRESENTATION OF RESULTS FOR SET NUMBER 4

5.7.1 General

Six specimens were cast on December 5, 2002. The only nominal difference between these beams and those in the third set was the type of coarse aggregate used in the concrete. Beams in this set were cast using mix 2 in Table 4-4, which had 1-inch crushed limestone instead of river gravel.

After removing the forms, honeycomb concrete was found at midspan of Specimen IT2-85-4. A similar defect was found over 23 inches at one end of Specimen T2-85-4 in the vicinity of the strands. Camber and stress data for these two beams will be presented in this section. However, these specimens will not be considered in the analyses performed in Section 5.9.

5.7.2 Concrete Compressive Strength

Due to a technical problem encountered with the data acquisition system, temperatures measured inside the specimens were not recorded properly. Therefore, temperature history curves are not presented for this set of beams as was done for the previous sets. Nonetheless, the highest temperatures observed in the rectangular, tee, and inverted tee specimens were 120°F, 115°F, and 119°F, respectively. The average ambient temperature inside Ferguson Laboratory was approximately 72°F on the day of this casting.

Results from compressive strength tests performed during the first 20 hours after batching are shown in Figure 5-20. Strength values measured at 7, 14, and 28 days are shown in Figure 5-21. Match-cured and standard 4 by 8-inch and 6 by 12-inch cylinders were tested. The compressive strength of concrete at transfer was 3800 psi based on tests of match-cured cylinders. At this point in time, concrete compressive strength was less than 2400 psi according to tests performed on non match-cured cylinders. Finally, Table 5-9 shows that while the

122

28-day compressive strengths of concrete used for this set of beams and for the third set of beams were similar, the elastic modulus was considerably lower for concrete used in the fourth set.
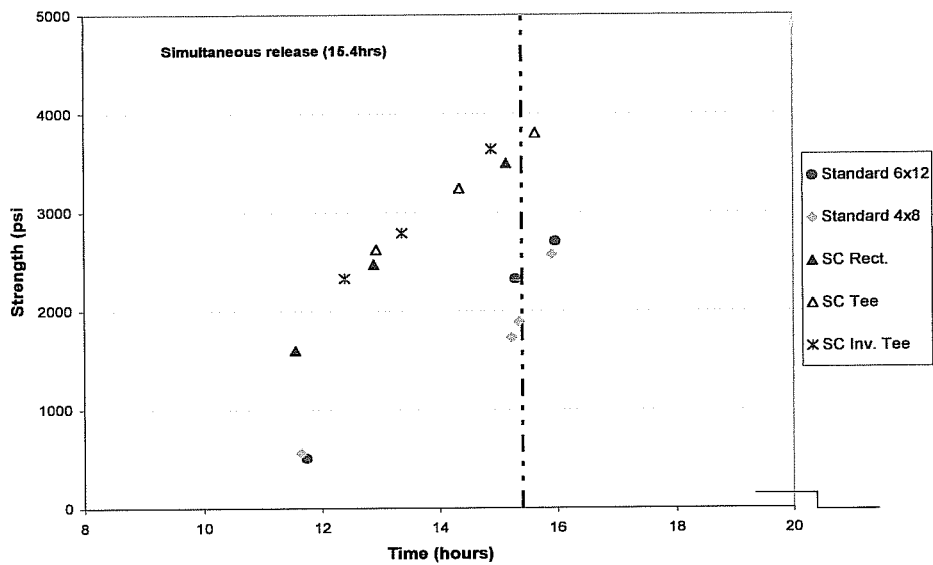
Figure 5-20: Concrete strength during first 20 hours (Set 4)
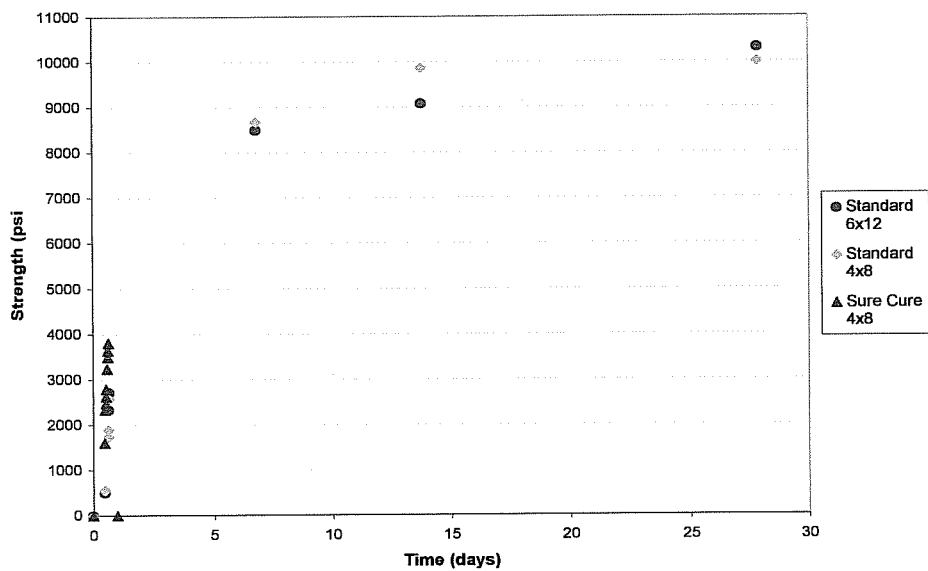
Figure 5-21: Concrete compressive strength vs. time (Set 4)

123

5.7.3 Concrete Stresses at Transfer

Computed concrete stresses at prestress force transfer are presented in Table 5-9. The values shown for Specimens T2-85-4 and IT2-85-4 were calculated ignoring the aforementioned fabrication defects.

Table 5-9: Summary of results (Set 4)

Specimen	R3-76-4	R3-82-4	T2-76-4	T2-85-4	IT3-85-4	IT2-85-4
Cross-sectional properties						
A_g (in2)	144	144	104	104	156	156
I_g (in4)	3888	3888	2251	2251	4706	4706
h (in)	18	18	15.5	15.5	19	19
y_b (in)	9	9	10.27	10.27	7.88	7.88
y_t (in)	9	9	5.23	5.23	11.12	11.12
Aps (in2)	1.22	1.22	0.61	0.61	1.53	1.53
e (in)	3.50	4	4.52	5.27	3.66	3.66
yb/h	0.5	0.5	0.66	0.66	0.41	0.41
Concrete properties						
Concrete Mix	No. 2 (w/c = 0.33)					
Release compressive strength - f'ci (psi)	3800	3800	3800	3800	3800	3800
Eci (ksi) (calculated as 57 f'ci$^{1/2}$)	3514	3514	3514	3514	3514	3514
f'c 28d (psi) - Based on 6x12-inch / 4x8-inch standard cylinders	10300 / 10000					
wc (lbs/ft3)	158					
Ec 28d (ksi) - Based on 4x8-inch standard cylinders	4850					
Ec 28d (ksi) - 33 wc$^{1.5}$ f'c$^{1/2}$ - (6x12-inch / 4x8-inch cylinders)	6650 / 6560					
Ec 28d (ksi) - (40 f'c $^{1/2}$+1E3) (wc/145)$^{1.5}$ - (6x12-inch / 4x8-inch cylinders)	5760 / 5690					
Average tensile stress in the strands						
Immediately before transfer (ksi) *	180	180	184	182	191	195
Immediately after transfer (ksi) *	161	159	167	158	164	164
Effective prestress force Po (kips)	197	194	102	96	251	251
Revision by nonlinear analysis **	201	199	104	101	260	259
Revision by PCI recommended method ***	201	199	103	101	261	268
Extreme fiber concrete stresses at transfer						
Compression (allowable stress design approach in Section 3.3.1.1)	0.78 f'ci	0.83 f'ci	0.81 f'ci	0.85 f'ci	0.83 f'ci	0.83 f'ci
Compression (strain compatibility approach in Section 3.3.1.2)	0.81 fci	0.86 fci	0.83 fci	0.9 fci	0.88 fci	0.9 fci
Compression (nonlinear approach Section in 3.3.2)	0.76 fci	0.81 fci	0.78 fci	0.83 fci	0.83 fci	0.86 fci
Tension x f'ci$^{1/2}$ (allowable stress design approach in Section 3.3.1.1)	3.7	7.3	1.5	4.1	9.1	9.1
Tension x f'ci$^{1/2}$ (strain compatibility approach in Section 3.3.1.2)	3.8	7.6	1.5	4.4	9.4	9.9
Tension x f'ci$^{1/2}$ (nonlinear approach Section in 3.3.2)	5.0	10.8	2.2	5.2	15.9	18.5
Cracked in reality	no	yes	no	no	yes	yes
Top reinforcement	no	no	no	no	yes	no
Camber						
Measured initial camber	0.24	0.26	0.23	0.26	0.26	0.34
Predicted initial camber (procedure illustrated in Section 5.3 (7-a))	0.20	0.24	0.23	0.26	0.28	0.36
Predicted initial camber (procedure illustrated in Section 5.3 (8))	0.22	0.25	0.25	0.27	0.26	0.29
Eci$_{ADJ}$	3173	3462	3729	3567	3579	3000
ε'ci $_{ADJ}$	0.0021	0.0019	0.0018	0.0019	0.0019	0.0022
Measured camber 10 days after transfer	0.34	0.38	0.32	0.40	0.40	0.48
Predicted 10-day camber (procedure illustrated in Section 5.3 (7-b))	0.24	0.30	0.32	0.37	0.35	0.45
Measured camber 90 days after transfer	0.37	0.43	0.38	0.48	0.44	0.53
Predicted 90-day camber (procedure illustrated in Section 5.3 (7-b))	0.31	0.37	0.41	0.46	0.44	0.57
Predicted long-term camber (procedure illustrated in Section 5.3 (6-b))	0.46	0.53	0.54	0.59	0.52	0.52

* Inferred from strain gauge measurements
** From procedure discussed in Section 3.3.2 and illustrated in Section 5.3 (5)
*** From procedure illustratred in Section 5.3 (1-b)

124

5.7.4 Camber

The variation of camber with time is presented in Figures 5-22, 5-23, and 5-24. Despite the change in coarse aggregate and resulting changes in concrete properties, no catastrophic behavior due to the high concrete stresses at transfer was observed. As for earlier sets of specimens, an initial rapid increase in camber followed by a gradual decrease in the rate at which camber grows was observed. As shown in Table 5-9, measured initial camber values were similar to respective predicted values, with the largest difference being only 0.04 inches for Specimen R3-76-4. This implies that the modulus of elasticity at transfer, E_{ci}, was estimated reasonably well using the ACI 318-02 expression. In contrast, E_{ci} was apparently underestimated for the third set of beams. The trajectory of camber response curves for Specimens R3-76-4, R3-82-4, and T2-85-4 suggests that long-term responses may exceed predicted responses.
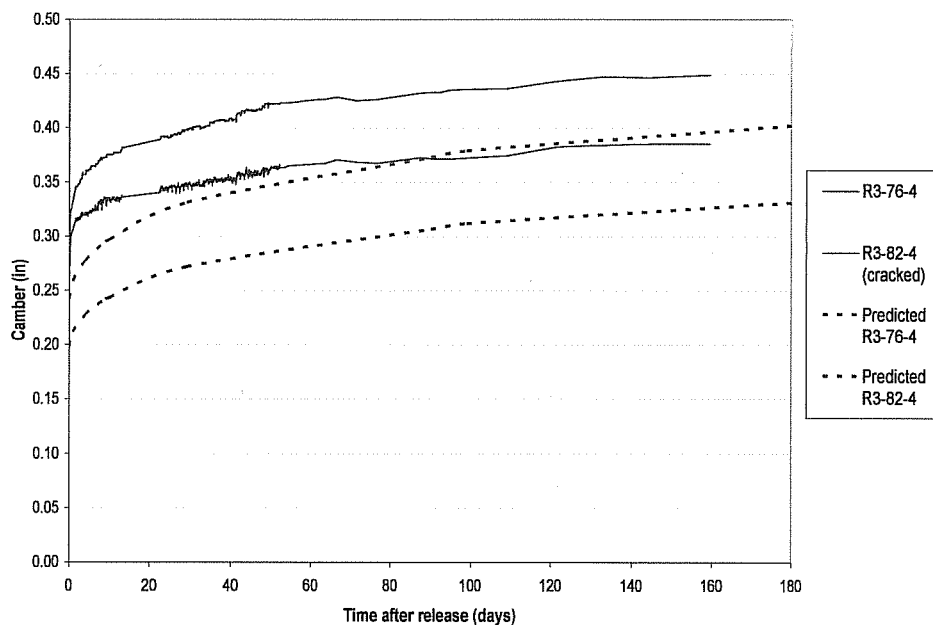
Figure 5-22: Camber response for Specimens R3-76-4 and R3-82-4

125
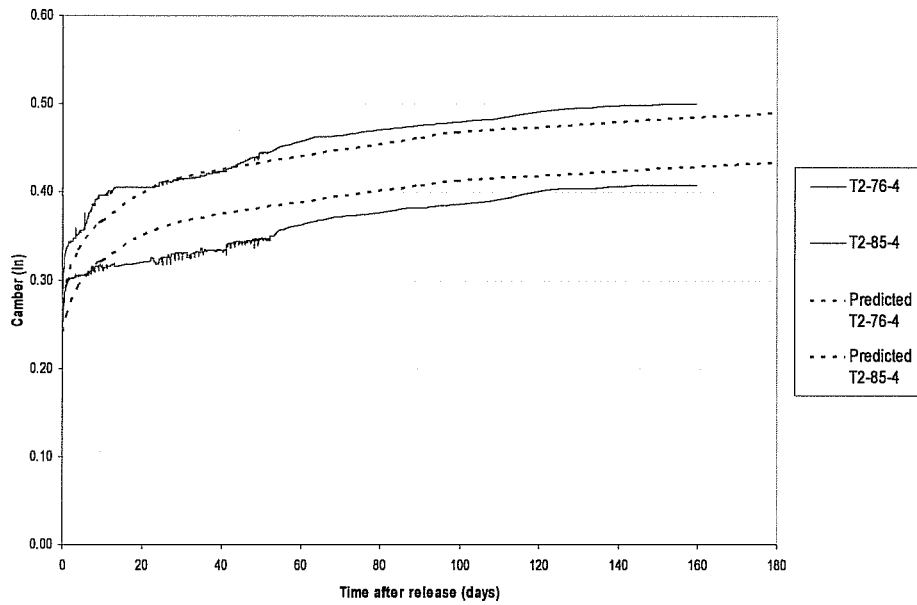
Figure 5-23: Camber response for Specimens T2-76-4 and T2-85-4
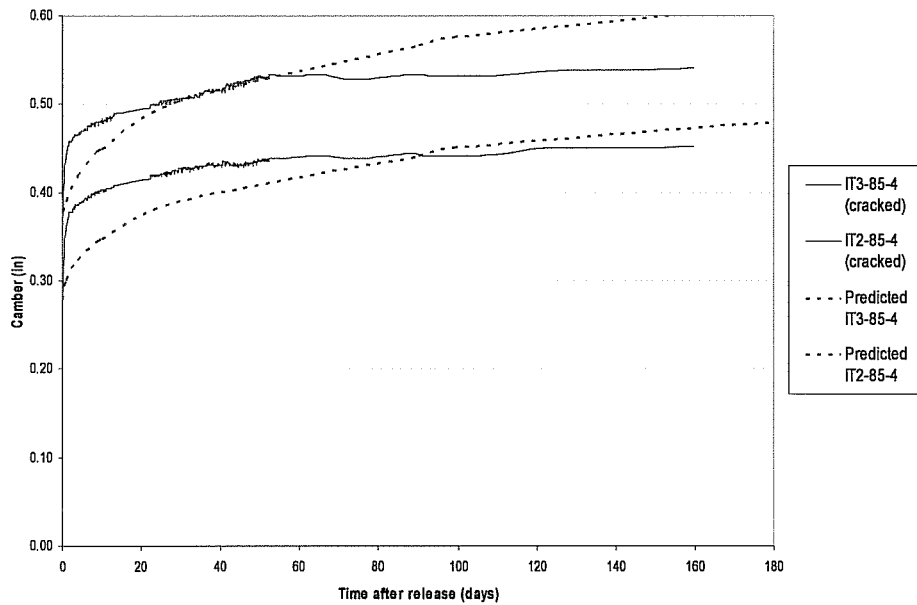
Figure 5-24: Camber response for Specimens IT2-85-4 and IT3-85-4

126

5.8 PRESENTATION OF RESULTS FOR SET NUMBER 5

5.8.1 General

This set of beams, cast on March 4, 2003, included specimens having the same characteristics as those in the third and fourth sets. Concrete mix 3 was used for this series of specimens to evaluate the effect of rate of concrete strength gain on specimen behavior. This concrete was expected to hydrate slower and generate less heat than the mixes 1 and 2 due to its reduced cement content and use of Class C fly ash as replacement for some of the cement. The temperatures measured inside the beams are presented in Figure 5-25. Crushed limestone was used again to produce a concrete with low modulus of elasticity that would have the highest likelihood to result in higher creep deformations leading to increased cambers.

Once again, poor consolidation of concrete resulted in honeycomb concrete at the level of the strands over an approximate length of 16 inches at one end of Specimen T2-85-5. As a result, this beam will not be considered in the analysis presented in Section 5.9.

5.8.2 Concrete Compressive Strength

Figure 5-25 presents the temperatures measured inside the specimens of set 5. The temperatures in Specimen R3-82-3 are also shown for the purpose of comparing the heat generated during hydration of the conventional precast and reduced-heat concrete mixes. In fact, while temperatures in sets 3 and 4 reached 115°F to 130°F, the highest observed in set 5 were 94°F, 88°F, and 95°F for the rectangular, tee, and inverted tee beams, respectively. Consequently, it was necessary to wait approximately 27 hours after casting in order to release the prestress forces. As shown in Table 5-10, the estimated concrete compressive

strengths at transfer were 3465 psi in the tee beams and 4045 psi in the rectangular and inverted tee beams. Compressive strength values are plotted in Figures 5-26 and 5-27. By interpolation between results of compressions tests conducted an hour before and an hour after release, the compressive strength based on standard cylinders was approximately 2500 psi. The compressive strength and the elastic modulus for this concrete at 28 days were 7390 psi and 5000 ksi, respectively.
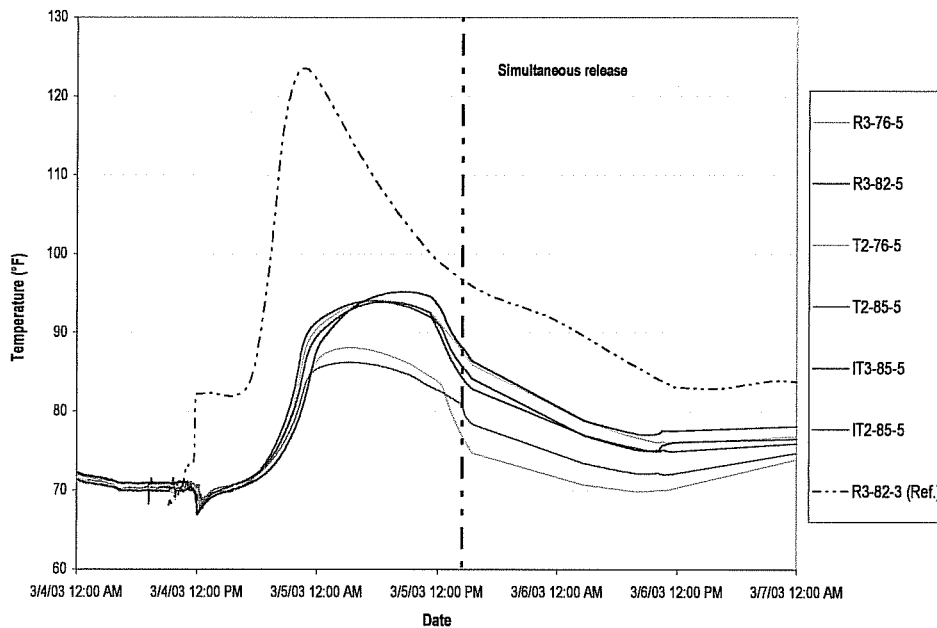
Figure 5-25: Measured temperature (Set 5)

Table 5-10: Compressive strengths at transfer (Set 5)

Time (hrs)	Specimens	Compressive Strength (psi)	
		Sure Cure 4x8 cylinder	Standard cylinders
26.8	R3-76-5/ R3-82-5 IT3-85-5/ IT2-85-5	4045	2500 psi (4x8 cyl.) 2570 psi (6x12cyl.)
	T2-76-5/ T2-85-5	3465	
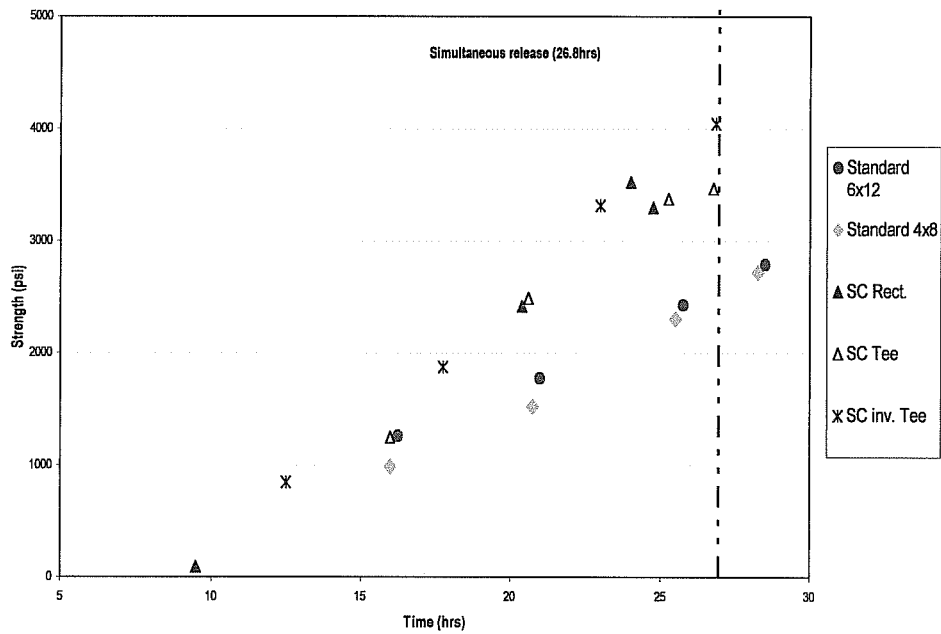
Figure 5-26: Concrete strength during first 30 hours (Set 5)
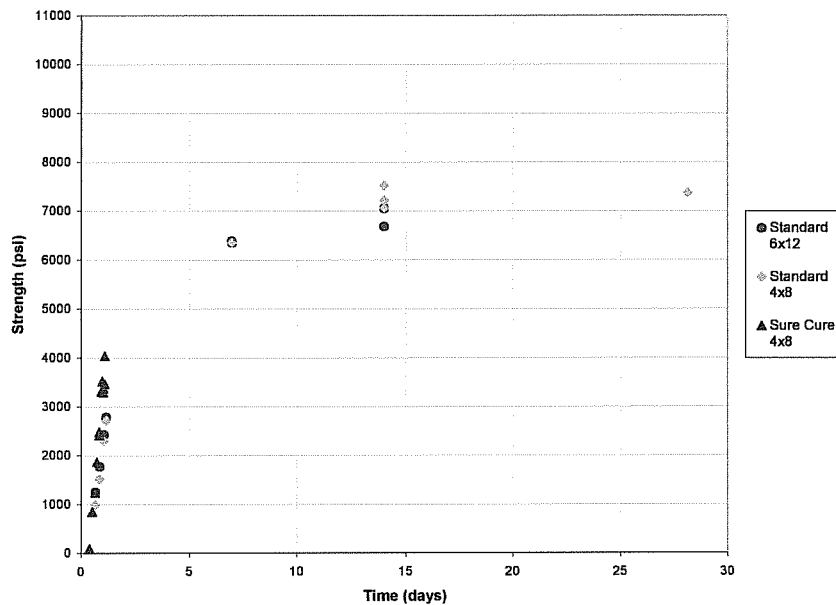
Figure 5-27: Concrete compressive strength vs. time (Set 5)

5.8.3   Concrete Stresses at Transfer

Concrete stresses at prestress force transfer are shown in Table 5-11. As for set 4, the values shown for Specimen T2-85-5 were computed without accounting for the honeycomb that appeared at one end of the specimen. Extreme compression fiber stresses, based on gross-section properties and assumed elastic behavior of the materials, ranged from 0.75 to $0.91f'_{ci}$ (excluding Specimen T2-85-5). These stresses ranged from 0.73 to $0.84f'_{ci}$ when a nonlinear analysis approach was used. Those beams with calculated tensile stresses exceeding $7\sqrt{f'_{ci}}$ (based on the linear-elastic model) presented cracking at the top of their cross sections. Extreme fiber tensile stresses as high as $9.3\sqrt{f'_{ci}}$ were computed when the linear-elastic model was used.

130

Table 5-11: Summary of results (Set 5)

Specimen	R3-76-5	R3-82-5	T2-76-5	T2-85-5	IT3-85-5	IT2-85-5
Cross-sectional properties						
A_g (in2)	144	144	104	104	156	156
I_g (in4)	3888	3888	2251	2251	4706	4706
h (in)	18	18	15.5	15.5	19	19
y_b (in)	9	9	10.27	10.27	7.88	7.88
y_t (in)	9	9	5.23	5.23	11.12	11.12
Aps (in2)	1.22	1.22	0.61	0.61	1.53	1.53
e (in)	3.48	3.97	4.60	5.29	3.69	3.67
yb/h	0.5	0.5	0.66	0.66	0.41	0.41
Concrete properties						
Concrete Mix	No. 3 (w/c = 0.34)					
Release compressive strength - f'ci (psi)	4045	4045	3465	3465	4045	4045
Eci (ksi) (calculated as 57 f'ci$^{1/2}$)	3625	3625	3355	3355	3625	3625
f'c 28d (psi) - Based on 4x8-inch standard cylinders	7390					
wc (lbs/ft3)	150					
Ec 28d (ksi) - Based on 4x8-inch standard cylinders	5010					
Ec 28d (ksi) - 33 wc$^{1.5}$ f'c$^{1/2}$	5200					
Ec 28d (ksi) - (40 f'c $^{1/2}$+1E3) (wc/145)$^{1.5}$	4660					
Average tensile stress in the strands						
Immediately before transfer (ksi) *	182	182	186	187	189	189
Immediately after transfer (ksi) *	165	164	168	167	167	167
Effective prestress force Po (kips)	201	200	103	102	256	255
Revision by nonlinear analysis **	204	201	104	103	259	259
Revision by PCI recommended method ***	203	202	104	103	260	261
Extreme fiber concrete stresses at transfer						
Compression (allowable stress design approach in Section 3.3.1.1)	0.75 fci	0.8 fci	0.91 fci	1 fci	0.79 fci	0.8 fci
Compression (strain compatibility approach in Section 3.3.1.2)	0.76 fci	0.82 fci	0.93 fci	1.02 fci	0.82 fci	0.83 fci
Compression (nonlinear approach Section in 3.3.2)	0.73 fci	0.78 fci	0.84 fci	0.9 fci	0.8 fci	0.79 fci
Tension x f'ci$^{1/2}$ (allowable stress design approach in Section 3.3.1.1)	3.5	7.1	1.9	4.6	9.3	9.0
Tension x f'ci$^{1/2}$ (strain compatibility approach in Section 3.3.1.2)	3.8	7.6	1.9	4.8	9.9	10.0
Tension x f'ci$^{1/2}$ (nonlinear approach Section in 3.3.2)	4.7	9.7	2.7	6.3	14.1	15.3
Cracked in reality	no	yes	no	no	yes	yes
Top reinforcement	no	no	no	no	yes	no
Camber						
Measured initial camber	0.20	0.23	0.20	0.23	0.23	0.27
Predicted initial camber (procedure illustrated in Section 5.3 (7-a))	0.19	0.23	0.24	0.28	0.26	0.27
Predicted initial camber (procedure illustrated in Section 5.3 (8))	0.21	0.24	0.27	0.33	0.24	0.25
Eci$_{ADJ}$	3817	3885	4676	4665	3804	3304
$\varepsilon'ci_{ADJ}$	0.0018	0.0018	0.0014	0.0014	0.0018	0.0021
Measured camber 10 days after transfer	0.30	0.35	0.30	0.34	0.35	0.42
Predicted 10-day camber (procedure illustrated in Section 5.3 (7-b))	0.25	0.29	0.37	0.42	0.33	0.34
Measured camber 90 days after transfer	0.36	0.42	0.40	0.45	0.40	0.47
Predicted 90-day camber (procedure illustrated in Section 5.3 (7-b))	0.32	0.38	0.47	0.54	0.44	0.45
Predicted long-term camber (procedure illustrated in Section 5.3 (6-b))	0.49	0.56	0.62	0.71	0.55	0.54

* Inferred from strain gauge measurements

** From procedure discussed in Section 3.3.2 and illustrated in Section 5.3 (5)

*** From procedure illustratred in Section 5.3 (1-b)

131

5.8.4 Camber

The variation of camber with time is presented in Figures 5-28, 5-29, and 5-30. Due to time limitations, only the results obtained after observing the behavior of these specimens during approximately 3 months are reported in this thesis. As for the previous set of beams, initial measured camber values were within 0.04 in. of predicted values. In addition, high rates of early camber growth, followed by rates of camber growth that gradually reduced with time, were observed. Long-term camber response for the T beams and for one of the inverted T beams (Specimen IT3-85-5) appeared to be bounded by the predicted response curves. After 96 days of monitoring camber responses, measured camber values for both rectangular beam specimens and one inverted T specimen (IT2-85-5) still exceeded predicted values. These larger-than-predicted camber values tended to occur because of the high rate of early camber growth. Camber growth of all beams after five to ten days of response tended to be equal to or lower than predicted.
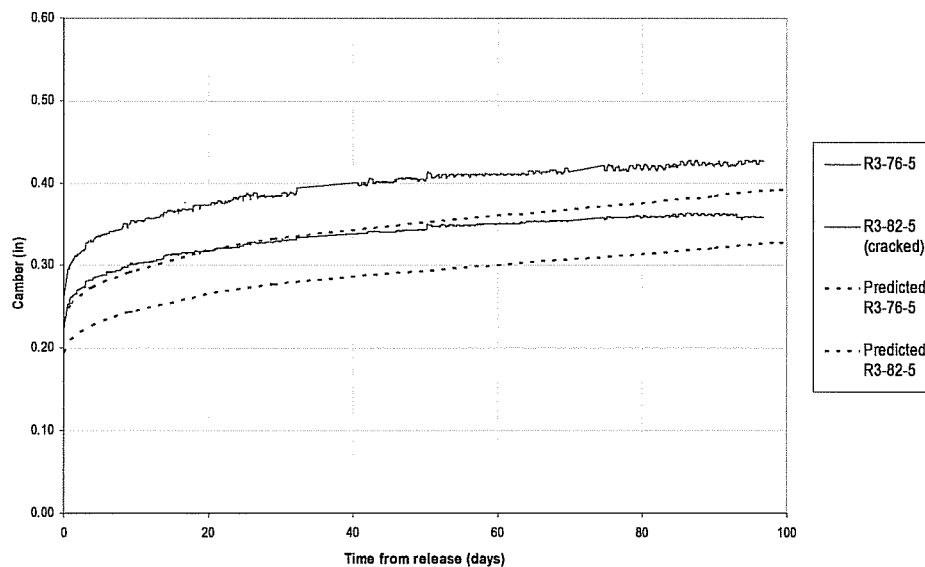
Figure 5-28: Camber response for Specimens R3-76-5 and R3-82-5

132
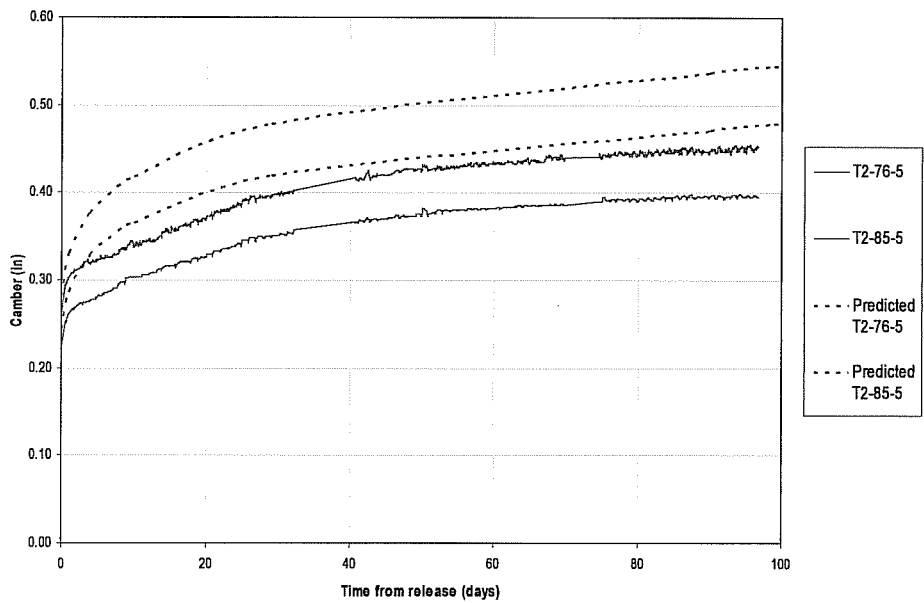
Figure 5-29: Camber response for Specimens T2-76-5 and T2-85-5
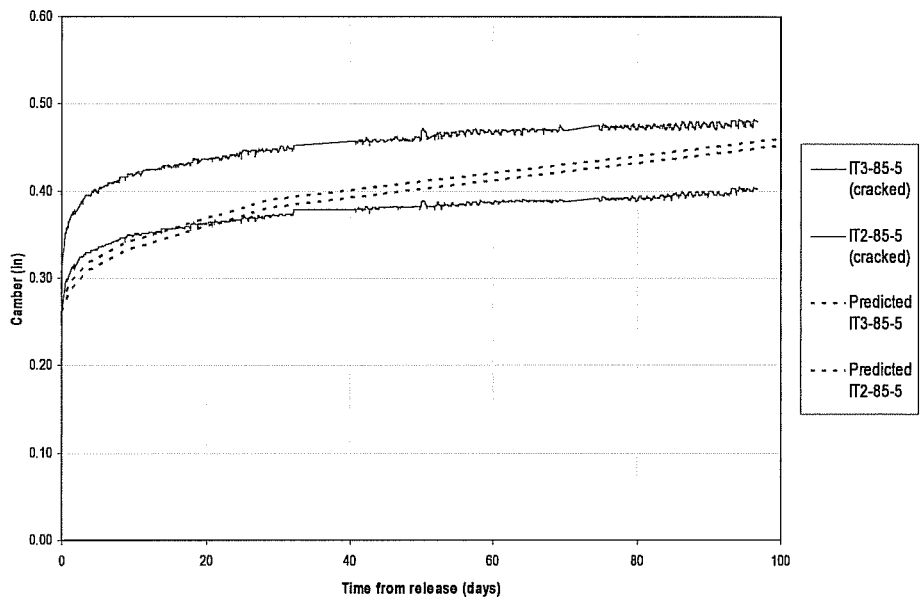
Figure 5-30: Camber response for Specimens IT2-85-5 and IT3-85-5

133

5.9 ANALYSIS OF RESULTS

Researchers have suggested previously the possibility of increasing the current compressive stress limit for pretensioned concrete beams at prestress force transfer. Noppakunwijai and Tadros (Noppankunwijai et al, 2001) recommended replacing the current limit of $0.6f'_{ci}$ with a relationship that is a function of member cross-section properties. This equation results in allowable stresses ranging from $0.66f'_{ci}$ to $0.75f'_{ci}$ for standard double-tee, rectangular, and inverted-tee cross-sections. In addition, a PCI Standard Design Practice report published in 1996 (PCI Technical Activities Council and PCI Committee on Building Code, 1996) affirmed that no problems had been observed by allowing extreme compressive fiber stresses as high as $0.75f'_{ci}$.

An analysis of laboratory results obtained during this study is presented in this section with the purpose of determining whether current allowable stress limits at prestress release can be increased beyond current limits. Several factors are believed to affect the behavior of prestressed beams at release. As discussed in Section 3.2, some of these factors are:

1. Stress gradient on the cross-section
2. Geometry of the cross-section
3. Concrete properties (stiffness, creep, rate of strength gain, etc.)

The first factor is not considered here because the specimens designed to study the effect of a low stress gradient (R2-75-2 and R2-85-2) experienced splitting cracks at one end due to a lack of transverse reinforcement for resisting bursting stresses that developed during prestress transfer. However, low stress gradients on standard cross sections used by TxDOT are not very common. As shown in Figures 3-2 through 3-4, typically the majority of prestressed

134

reinforcement is located near the bottom of girder cross sections resulting in stress gradients similar to those experienced by the other beam specimens.

Performance of specimens studied in this research project will be evaluated based on camber histories recorded during the first 90 days after transfer. Time-dependent deformations will be evaluated by comparing changes in camber exhibited by the specimens in the first 10 and 90 days (Δ_{10} and Δ_{90}) after prestress release. The quantities Δ_{10} and Δ_{90} were calculated by subtracting initial cambers from 10-day and 90-day cambers provided in Tables 5-4, 5-6, 5-8, 5-9, and 5-11. In an attempt to identify trends in the behavior of the beams, measured and predicted changes in camber, as well as their ratio, were plotted against extreme fiber compressive and tensile stresses at release, maximum temperatures achieved during hydration, as well as other measures of response. Performing the analysis in this manner allows the inclusion of specimens from Sets 1 and 2 for which initial camber readings are dubious.

Only those beams that did not experience fabrication defects, such as voids, severe honeycombed concrete, or severe cracking due to bursting stresses at transfer, are included in this analysis. Behavior of inverted-tee beam specimens is evaluated first, followed by rectangular beams, and finally tee beams.

5.9.1 Inverted-Tee Beam Specimens

As discussed in Section 2.2.3.3, the expression suggested by Noppakunwijai et al resulted in lower allowable compression stresses at release for inverted-tee sections than for rectangular and double-tee sections. This suggests that behavior of inverted-tee beams is likely to be more sensitive to elevated release stresses than the other two types of elements. Figure 5-31 presents the camber history recorded for inverted-tee specimens fabricated in Sets 3 through 5. The responses illustrated in Figure 5-31 are similar and demonstrate that camber did not increase in an uncontrolled manner with time despite specimens being subjected to extreme compressive and tensile stresses exceeding $0.76f'_{ci}$ and $8.8\sqrt{f'_{ci}}$, respectively.
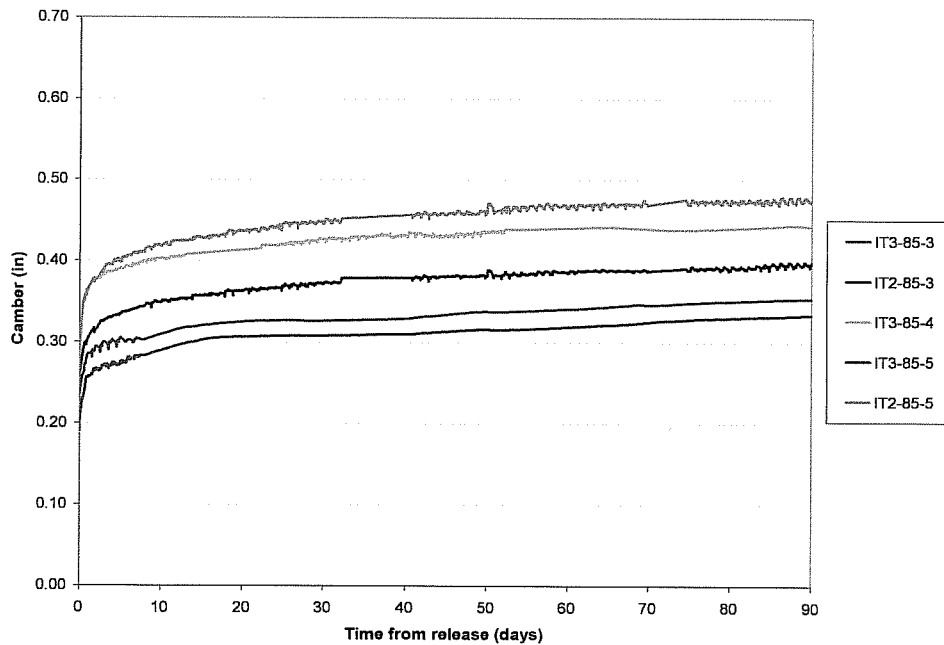
Figure 5-31: Camber history for inverted-tee beams (Sets 3, 4, and 5)

Results obtained by monitoring camber of inverted-tee beam specimens for Sets 2 through 5 are summarized in Table 5-12. Details associated with each beam, such as concrete mix, ratio between compressive strength at transfer and 28-day concrete compressive strength, highest measured temperature in concrete during hydration, extreme fiber stresses at release, and existence of top reinforcement for restraining flexural cracking at release, are presented in lines 2 through 8. Measured and predicted changes in camber at 10 and 90 days (Δ_{10} and Δ_{90}), changes in camber normalized with predicted values ($\Delta_{10}/\Delta_{10\text{-pred}}$ and $\Delta_{90}/\Delta_{90\text{-pred}}$), and normalized camber growth for the period following the initial 10 days of growth (($\Delta_{90}-\Delta_{10}$)/($\Delta_{90\text{-pred}}-\Delta_{10\text{-pred}}$)) are also included in this table. Normalized camber values were calculated with the objective of evaluating the accuracy of camber predictions for the different cross sections, concrete properties, and extreme fiber release stresses.

Table 5-12: Summary of results for inverted-tee specimens (Sets 2 through 5)

Specimen	IT1-76-2	IT1-84-2	IT3-85-3	IT2-85-3	IT3-85-4	IT3-85-5	IT2-85-5
Concrete Mix	1	1	1	1	2	3	3
f'ci / f'c	0.38	0.38	0.41	0.43	0.37	0.55	0.55
Max. Temp (°F)	140	140	123	127	119	94	95
Compressive stress at release (x f'ci)	0.68	0.73	0.79	0.76	0.83	0.79	0.80
Tensile stress at release (x f'ci$^{1/2}$)	4.1	9.8	9.0	8.8	9.1	9.3	9.0
Cracked at top	no	yes	yes	yes	yes	yes	yes
Top reinforcement	no	no	yes	no	yes	yes	no
Δ_{10}	0.04	0.10	0.13	0.08	0.15	0.12	0.15
$\Delta_{10\text{-pred}}$	0.05	0.04	0.04	0.06	0.07	0.07	0.07
Δ_{10} / $\Delta_{10\text{-pred}}$	0.84	2.20	3.33	1.31	2.18	1.60	2.02
Δ_{90}	0.05	0.10	0.18	0.12	0.19	0.17	0.21
$\Delta_{90\text{-pred}}$	0.10	0.16	0.18	0.17	0.19	0.18	0.18
Δ_{90} / $\Delta_{90\text{-pred}}$	0.51	0.61	0.98	0.72	1.00	0.92	1.14
($\Delta_{90}-\Delta_{10}$) / ($\Delta_{90\text{-pred}}-\Delta_{10\text{-pred}}$)	0.20	0.00	0.32	0.40	0.33	0.46	0.53

Figure 5-32 indicates that normalized cambers ($\Delta_{measured}/\Delta_{predicted}$) tend to increase as the extreme fiber compressive stresses increase. For instance, a $\Delta_{10}/\Delta_{10\text{-pred}}$ value of 1.31 was calculated for Specimen IT2-85-3 for which the maximum compressive stress at release was $0.76f'_{ci}$. A value of 2.02 was calculated for Specimen IT2-85-5 for which the maximum compressive stress at release was $0.80f'_{ci}$. The same general trend was observed for the $\Delta_{90}/\Delta_{90\text{-pred}}$ ratios. Specimens IT3-85-3 and IT1-84-2 exhibited $\Delta_{10}/\Delta_{10\text{-pred}}$ ratios substantially higher than indicated by the general trend for the other five inverted-tee specimens.

Long–term camber responses based on Δ_{90} were predicted significantly better than short-term responses. Table 5-12 indicates that $\Delta_{90}/\Delta_{90\text{-pred}}$ ranged from 0.51 to 1.14 with a mean value of 0.84, while $\Delta_{10}/\Delta_{10\text{-pred}}$ ranged from 0.84 to 3.33 with a mean value of 1.93. The mean for $\Delta_{10}/\Delta_{10\text{-pred}}$ reduces to 1.59 when the extreme ratios for Specimens IT3-85-3 and IT1-84-2 are excluded. It should also be noted that the substantially smaller difference between ratios of measured to computed camber at 10 and 90 days for Specimen IT1-76-2, which was subjected to extreme fiber stresses of $0.68f'_{ci}$ and $4.1\sqrt{f'_{ci}}$ at release, further reduced the computed mean ratios of measured to computed camber.

In general, the empirical model described in Section 3.3.3 underestimated the change in camber between days 1 and 10. Additionally, accuracy of short-term camber predictions (Δ_{10}) decreased as the extreme fiber compressive stress increased. However, 90-day camber predictions generally overestimated the measured response. This observation is consistent with the response observed in Figures 5-13, 5-19, 5-24, 5-30 and 5-31, where a rapid increase in camber during the first five to ten days after prestress release was followed by a gradual decrease in the rate of camber growth. Therefore, the majority of the time-dependent

deformations occurred during the initial five to ten days after tension forces in the prestressing steel were transferred to the concrete.
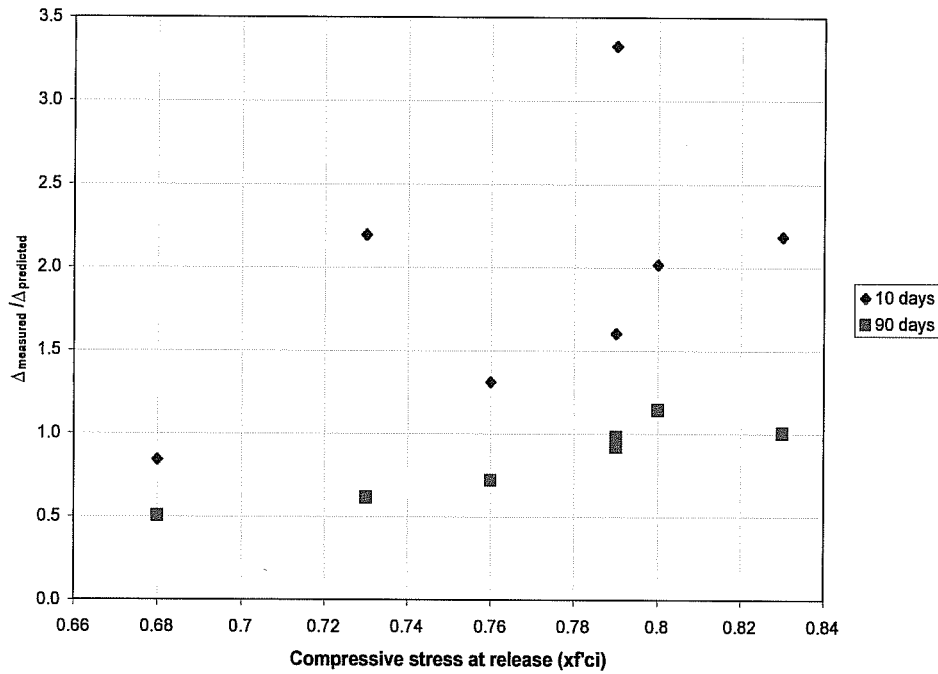
Figure 5-32: $\Delta_{measured}/\Delta_{pred}$ *versus compressive stress at release (IT beams)*

The ratio $((\Delta_{90}-\Delta_{10})/(\Delta_{90\text{-}pred}-\Delta_{10\text{-}pred}))$ was calculated for each beam with the objective of comparing normalized increases in camber after initial deflections (Δ_{10}) had occurred. Figure 5-33 illustrates that camber growth beyond ten days for beams fabricated using 1-inch crushed limestone (mixes 2 and 3) and replacement of Type-III cement with fly ash (mix 3) was greater than for beams fabricated using river gravel as the coarse aggregate (mix 1). Mean normalized ratios for mixes 1, 2, and 3 were 0.23, 0.33, and 0.50 respectively. This observation is consistent with the fact that rate of strength gain and 28-day compressive strength were significantly lower for the reduced-heat-of-hydration concrete mix.

139
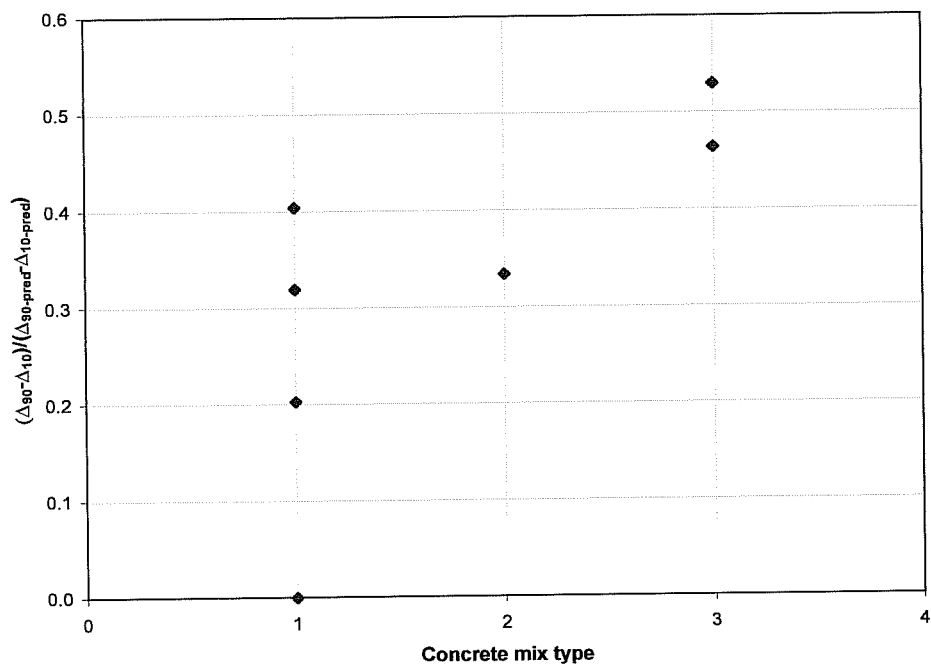
Figure 5-33: Camber growth beyond 10 days versus mix type (IT-beams)

Table 5-12 also shows that, despite the fact that reduced moments of inertia (Equation 5-2) were used in the calculations, measured Δ_{10} values for cracked beams exceeded, in most cases by a wide margin, corresponding predicted values. This is true for beams with and without non-prestressed reinforcement in the tops of beams. However, those having top reinforcement deflected less than those without it for comparable stress levels. For example, $\Delta_{10}/\Delta_{10\text{-pred}}$ values of 1.60 and 2.02 were calculated for Specimens IT3-85-5 and IT2-85-5, respectively. The extreme fiber compressive stress for both specimens was approximately $0.80f'_{ci}$.

Relationships between beam behavior and tensile stresses at release, maximum concrete temperatures during hydration, or f'_{ci} / f'_c were not identified. Plots of $\Delta_{10}/\Delta_{10\text{-pred}}$ and $\Delta_{90}/\Delta_{90\text{-pred}}$ can be found in Appendix D.

140

5.9.2 Rectangular Beam Specimens

Camber histories recorded for rectangular beam specimens of Sets 3 through 5 are presented in Figure 5-34. Despite having been subjected to extreme fiber compressive stresses exceeding $0.75f'_{ci}$ and extreme fiber tensile stresses as high as $7.1\sqrt{f'_{ci}}$, camber did not increase with time in an uncontrolled manner. Measured and predicted changes in camber, and normalized cambers (ratios of measured-to-predicted cambers) for rectangular beam specimens in Sets 1 through 5 are presented in Table 5-13. As before, beams with fabrication defects were not included in this table.
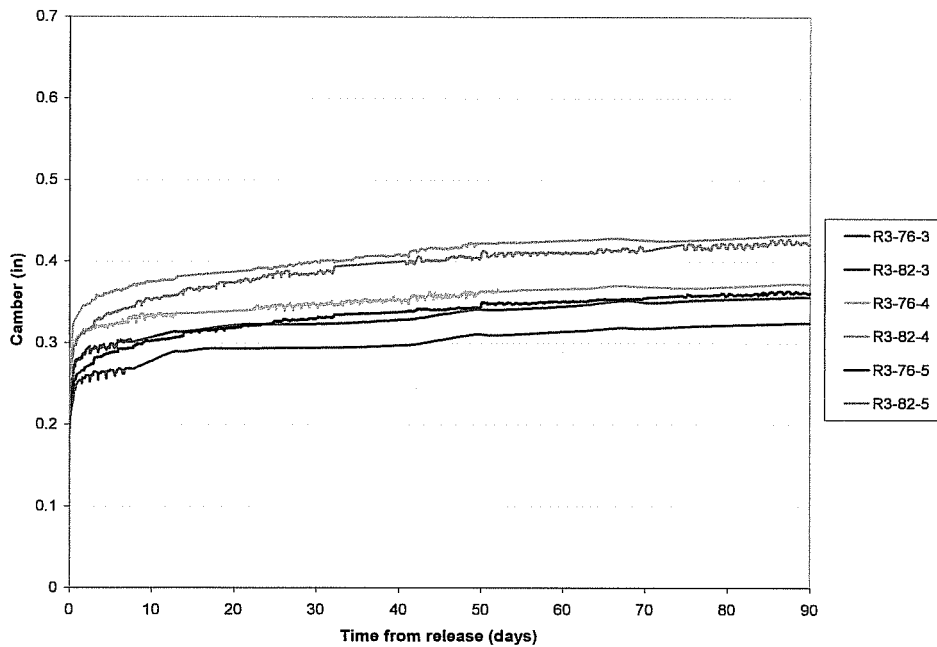
Figure 5-34: Camber history for rectangular beams (Sets 3, 4, and 5)

Table 5-13 shows that compressive release stresses imposed on rectangular beam specimens of Set 1 did not exceed $0.60f'_{ci}$. Mean $\Delta_{10}/\Delta_{10\text{-pred}}$ and $\Delta_{90}/\Delta_{90\text{-pred}}$ ratios for these beams were 0.64 and 0.70 respectively. Hence, camber response was overestimated by approximately 50 percent. In contrast, camber response of specimens with compressive stresses exceeding $0.60f'_{ci}$ (Sets 3, 4, and 5) was underestimated, as the mean values of $\Delta_{10}/\Delta_{10\text{-pred}}$ and $\Delta_{90}/\Delta_{90\text{-pred}}$ were 2.02 and 1.40, respectively.

Table 5-13: Summary of results for rectangular specimens (Sets 1 through 5)

Specimen	R1-70-1(a)	R1-60-1(b)	R1-60-1(a)	R1-70-1(b)	R1-75-1(a)	R1-75-1(a)	R3-76-3	R3-82-3	R3-76-4	R3-82-4	R3-76-5	R3-82-5
Concrete Mix	1	1	1	1	1	1	1	1	2	2	3	3
f'ci / f'c	0.62	0.59	0.59	0.62	0.65	0.65	0.41	0.41	0.37	0.37	0.55	0.55
Max. Temp (°F)	145	145	145	145	145	145	129	123	120	120	94	94
Compressive stress at release (x f'ci)	0.5	0.52	0.52	0.49	0.48	0.46	0.75	0.78	0.78	0.83	0.75	0.8
Tensile stress at release (x f'ci^1/2)	1.6	1.6	1.6	1.5	1.5	1.5	3.7	7.1	3.7	7.3	3.6	7.1
Cracked at top	no	no	no	no	no	no	no	yes	no	yes	no	yes
Top reinforcement	no	no	no	no	no	no	no	no	no	no	no	no
Δ_{10}	0.01	0.01	0.02	0.03	0.05	0.06	0.10	0.11	0.09	0.12	0.10	0.13
$\Delta_{10\text{-pred}}$	0.05	0.05	0.05	0.05	0.05	0.04	0.04	0.05	0.05	0.05	0.05	0.06
Δ_{10} / $\Delta_{10\text{-pred}}$	0.14	0.16	0.48	0.73	1.11	1.23	2.27	2.17	2.04	2.18	2.02	2.05
Δ_{90}	0.04	0.06	0.06	0.07	0.09	0.09	0.15	0.16	0.13	0.18	0.16	0.20
$\Delta_{90\text{-pred}}$	0.10	0.10	0.10	0.09	0.09	0.09	0.12	0.14	0.06	0.12	0.13	0.15
Δ_{90} / $\Delta_{90\text{-pred}}$	0.42	0.54	0.58	0.72	0.96	0.99	1.20	1.10	2.01	1.51	1.28	1.29
$(\Delta_{90}\text{-}\Delta_{10})$ / $(\Delta_{90\text{-pred}}\text{-}\Delta_{10\text{-pred}})$	0.66	0.86	0.66	0.72	0.81	0.74	0.60	0.53	1.94	0.92	0.78	0.77

Figure 5-35 and Table 5-13 show that, for Sets 3 through 5, $\Delta_{10}/\Delta_{10\text{-pred}}$ was typically greater than $\Delta_{90}/\Delta_{90\text{-pred}}$. Conversely, specimens in Set 1 did not present this behavior. This is consistent with the behavior observed for inverted-tee beams. It appears that the rapid increase in camber observed during the first ten days after prestress force transfer is a direct result of the maximum compressive stress level at release. However, high concrete release stresses did not appear to affect long-term response of the members.
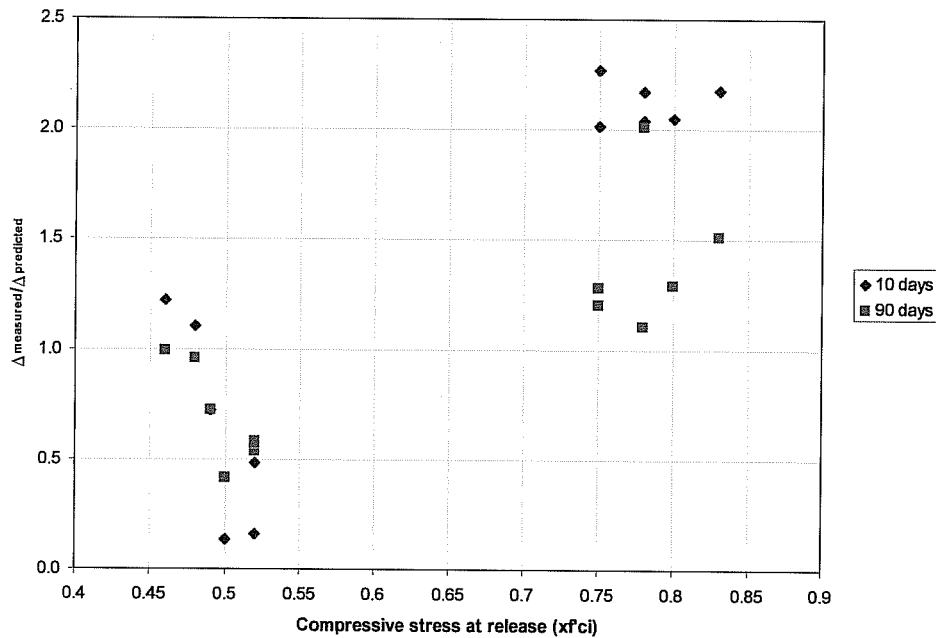
Figure 5-35: $\Delta_{measured}/\Delta_{pred}$ *versus compressive stress at release (Rect. beams)*

Long-term camber response (Δ_{90}) of Specimen R3-76-3 and R3-82-3 was estimated more accurately than the response of specimens in Sets 4 and 5, although not substantially more so for specimens in Set 5. Normalized Δ_{90} values of 1.20 and 1.10 were calculated for these two specimens, while ratios for R3-76-4, R3-82-4, R3-76-5, and R3-82-5 ranged from 1.28 to 2.01. Compressive stresses at release were similar for all beams. Normalized camber values for growth beyond 10 days $((\Delta_{90}-\Delta_{10})/(\Delta_{90\text{-pred}}-\Delta_{10\text{-pred}}))$ for these four specimens ranged from 0.77 to 1.94, which contrasts with the mean ratios of 0.56 for Specimens R3-76-3 and R3-82-3. This indicates that camber growth in beams from Sets 4 and 5 was greater than in beams from Set 3 after the first ten days following prestress release. This behavior was likely related to the lower concrete elastic moduli of mixes 2 and 3 and to the lower rate of strength gain for mix 3.

As discussed in Section 3.2, compressive strengths at prestress release in precast plants typically range from 55 to 60 percent of the 28-day strength. Values as low as 37 percent of f'_c were determined for Sets 3 and 4. Figure 5-36 indicates that measured camber changes, Δ_{10} and Δ_{90}, were underestimated for low f'_{ci}/f'_c values. Apparently, maturity of concrete at release can affect behavior of pretensioned beams after release. However, this trend was not observed for the inverted-tee beams.
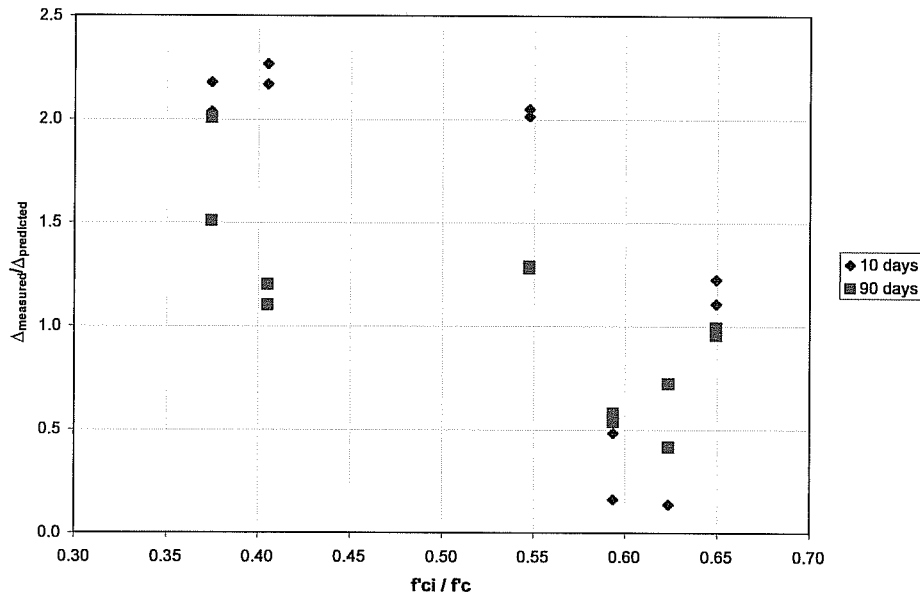
Figure 5-36: $\Delta_{measured}/\Delta_{pred}$ versus f'_{ci}/f'_c (Rectangular beams)

Additional plots of $\Delta_{10}/\Delta_{10\text{-}pred}$ and $\Delta_{90}/\Delta_{90\text{-}pred}$ are presented in Appendix D for different mix types, measured maximum temperatures during hydration, and other quantities.

5.9.3 Tee Beam Specimens

Camber histories for tee beam specimens of Sets 3 through 5 are presented in Figure 5-37. As for the other cross sections considered in this study, extreme fiber compressive release stresses between $0.79f'_{ci}$ and $0.91f'_{ci}$ did not result in unstable camber growth. Behavior of beams subjected to different maximum compressive release stresses differed mainly in the overall magnitude of the measured cambers. For instance, measured 90-day camber for Specimens T2-76-3 and T2-76-5 were 0.27 and 0.40 inches. Maximum compressive stresses at release for these beams, were $0.79f'_{ci}$ and $0.91f'_{ci}$, respectively.
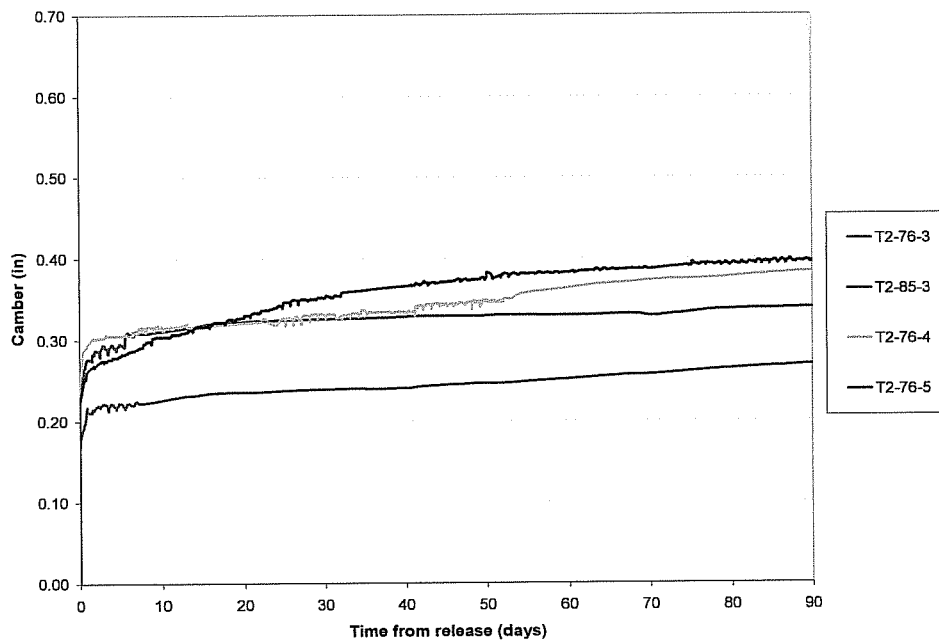
Figure 5-37: Camber history for tee beams (Sets 3, 4, and 5)

145

According to Table 5-14, short-term response (Δ_{10}) was predicted well for all but Specimens T1-82-2 and T1-74-2. Table 5-14 also shows that predicted long-term response was overestimated for Beams T2-76-3 and T2-85-3. Measured cambers at 90 days for these specimens (Δ_{90}), constructed using concrete mix 1 with river gravel, were approximately 50 percent of the corresponding predicted cambers. Normalized Δ_{90} values for these specimens were significantly smaller than those for specimens in Sets 4 and 5 perhaps as the result of the higher concrete stiffness associated with the river gravel concrete mix, as opposed to the crushed limestone concrete mix.

Table 5-14: Summary of results for tee-beam specimens (Sets 1 through 5)

Specimen	T1-82-2	T1-74-2	T2-76-3	T2-85-3	T2-76-4	T2-76-5
Concrete Mix	1	1	1	1	2	3
f'ci / f'c	0.42	0.42	0.39	0.39	0.37	0.47
Max. Temp (°F)	137	137	112	110	115	88
Compressive stress at release (x f'ci)	0.62	0.68	0.79	0.86	0.81	0.91
Tensile stress at release (x $f'ci^{1/2}$)	5.2	3.9	1.5	4.2	1.5	1.9
Cracked at top	no	no	no	no	no	no
Top reinforcement	no	no	no	no	no	no
Δ_{10}	0.13	0.08	0.07	0.12	0.08	0.11
$\Delta_{10\text{-pred}}$	0.05	0.05	0.09	0.11	0.10	0.12
Δ_{10} / $\Delta_{10\text{-pred}}$	2.65	1.73	0.79	1.08	0.84	0.88
Δ_{90}	0.18	0.11	0.12	0.14	0.15	0.20
$\Delta_{90\text{-pred}}$	0.16	0.17	0.24	0.26	0.17	0.23
Δ_{90} / $\Delta_{90\text{-pred}}$	1.13	0.68	0.48	0.56	0.86	0.88
$(\Delta_{90}-\Delta_{10})$ / $(\Delta_{90\text{-pred}}-\Delta_{10\text{-pred}})$	0.48	0.25	0.29	0.19	0.88	0.87

A plot of normalized camber for growth beyond the first ten days following prestress release $((\Delta_{90}-\Delta_{10})/(\Delta_{90\text{-pred}}-\Delta_{10\text{-pred}}))$ versus concrete mix type is presented in Figure 5-38. It is apparent that camber growth for beams fabricated using crushed limestone (mixes 2 and 3) was greater than for those constructed

146

using river gravel (mix 1). Excluding the tee beams with irregular cross-sections that were fabricated as part of Set 2, mean values of normalized camber growth beyond the first ten days for mixes 1, 2, and 3 were 0.24, 0.88, and 0.87 respectively.
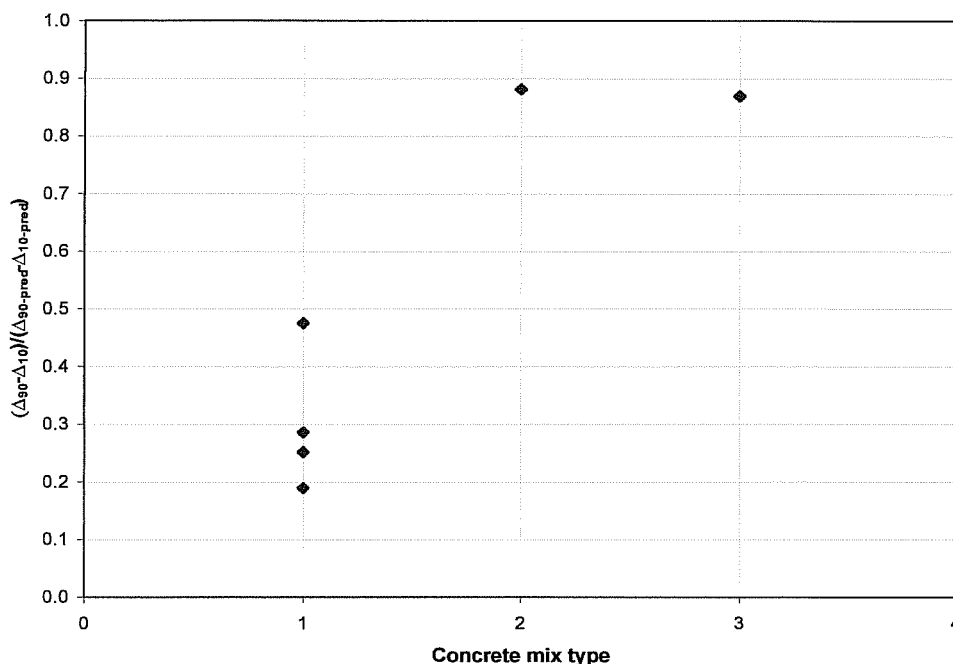
Figure 5-38: Camber growth beyond 10 days versus mix type (T-beams)

In summary, short-term response (Δ_{10}) was predicted well for tee beams in Sets 3, 4, and 5. However, the rate of camber growth decreased significantly for tee beams in Set 3 (concrete mix 1) after approximately three days, resulting in measured cambers that were lower than predicted values at 90 days after prestress release. The rate of camber growth and Δ_{90} were accurately estimated for Sets 4 and 5. Additional plots of $\Delta_{10}/\Delta_{10\text{-pred}}$ and $\Delta_{90}/\Delta_{90\text{-pred}}$ are presented in Appendix D.

5.9.4 Cross Section Effect on Beam Response

Noppakunwijai and Tadros (Noppankunwijai et al, 2001) indicated that allowable concrete stresses at prestress release should be a function of pretensioned beam cross-section properties, and recommended replacing the current compressive release stress limit with Equation 2-11. This equation was established based on a proposed strength design method that considered immediate effects of prestress force transfer but did not directly consider long-term effects such as concrete creep and relaxation of prestressing strands. In order to attempt to evaluate the influence of different cross-section properties on the response of pretensioned beams subjected to elevated release stresses, normalized short and long-term cambers ($\Delta_{10}/\Delta_{10\text{-pred}}$ and $\Delta_{90}/\Delta_{90\text{-pred}}$) were plotted versus y_b/h in Figures 5-39 and 5-40.

Specimens from Sets 3 through 5 experienced the highest concrete release stresses. When only those specimens are considered, Figure 5-39 indicates that short-term response (Δ_{10}) for only the tee beams is predicted reasonably well, while response of inverted-tee and rectangular beams is underestimated, by a substantial amount in some cases. It is interesting that the converse is true when only the beams that experienced compressive stresses at or below the current allowable limit are considered.

Long-term camber response (Δ_{90}) was predicted reasonably well for all beam types from all sets of beams, except rectangular beams from Sets 3 through 5. In general, a clear relationship between camber response and cross-section shape was not indicated by the response of specimens in this study.
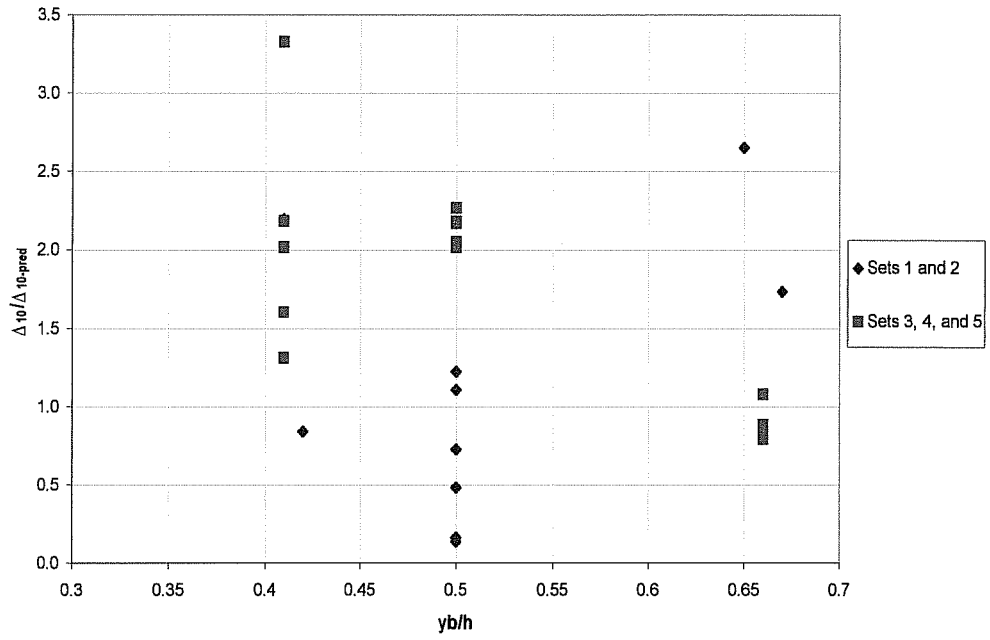
Figure 5-39: Normalized Δ_{10} versus y_b/h
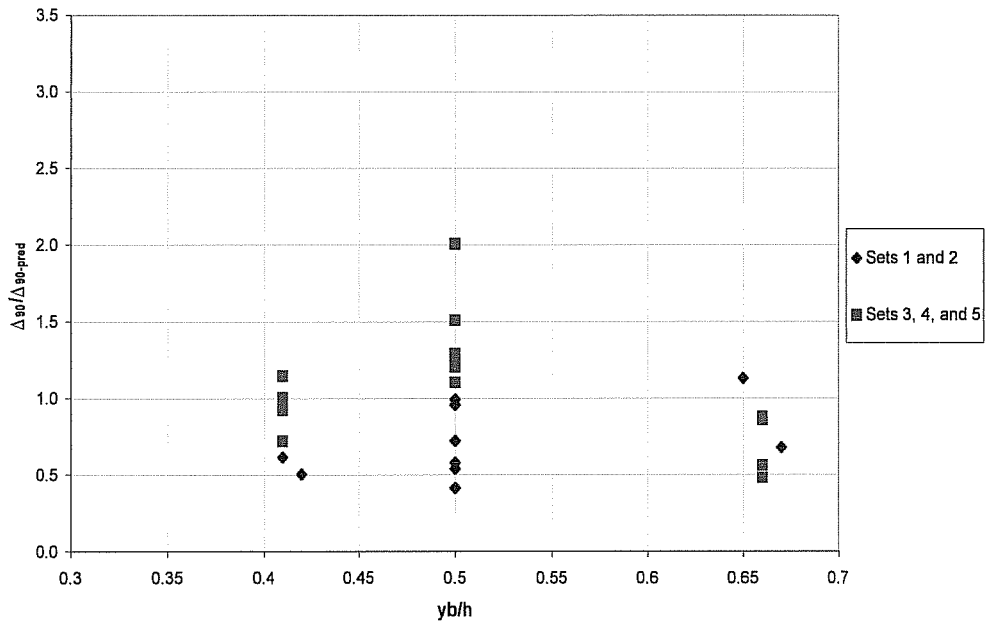
Figure 5-40: Normalized Δ_{90} versus y_b/h

149

5.9.5 General Observations

Five sets of six pretensioned beams per set were cast and monitored at Ferguson Laboratory between June 2002 and March 2003. All but the first set included specimens representing standard double-tee, U, and I girders. Analysis of camber response collected for a minimum of 90 days for each specimen permitted the identification of trends in the response of these beams to elevated release stresses. However, revised compressive and tensile stress limits at prestress release could not be determined because, despite being subjected to stresses exceeding the current specified limits, no specimens exhibited behavior indicative of uncontrolled or unstable response. In general, camber increased with increases in maximum compressive stress at release regardless of the cross-section geometry and type of concrete used to fabricate the specimens. This trend is illustrated in Figures 5-41 and 5-42 where measured and predicted changes in camber for 10 and 90 days (Δ_{10} and Δ_{90}) are plotted versus the extreme compressive fiber stresses at transfer.

Comparisons of measured and predicted values in Figures 5-41 and 5-42 indicate that short-term response (Δ_{10}) for specimens with extreme compressive fiber stresses exceeding the current allowable limit was generally underestimated by the prediction model described in Section 3.3.3. In contrast, the long-term response (Δ_{90}) was estimated more accurately, although not conservatively so for all specimens. Apparently, elevated release stresses resulted in a high rate of camber growth in the first days after prestress force transfer but did not affect the expected long-term response of the members. This suggests that pretensioned concrete beams can be subjected to elevated compressive stress levels at prestress release as long as long-term camber response is adequately predicted and values are acceptable to the engineer of record.
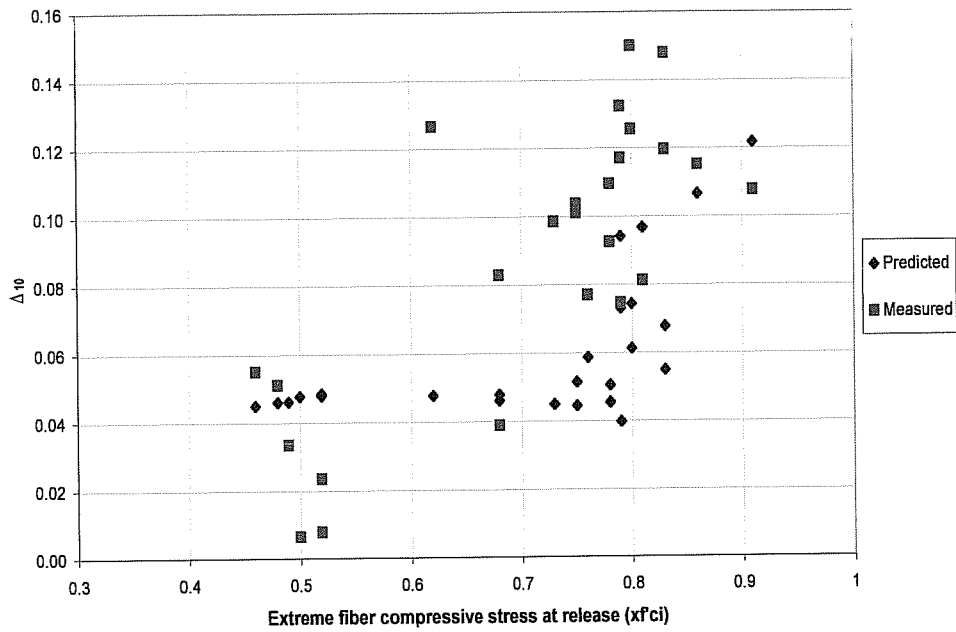
Figure 5-41: Δ_{10} versus compressive release stress
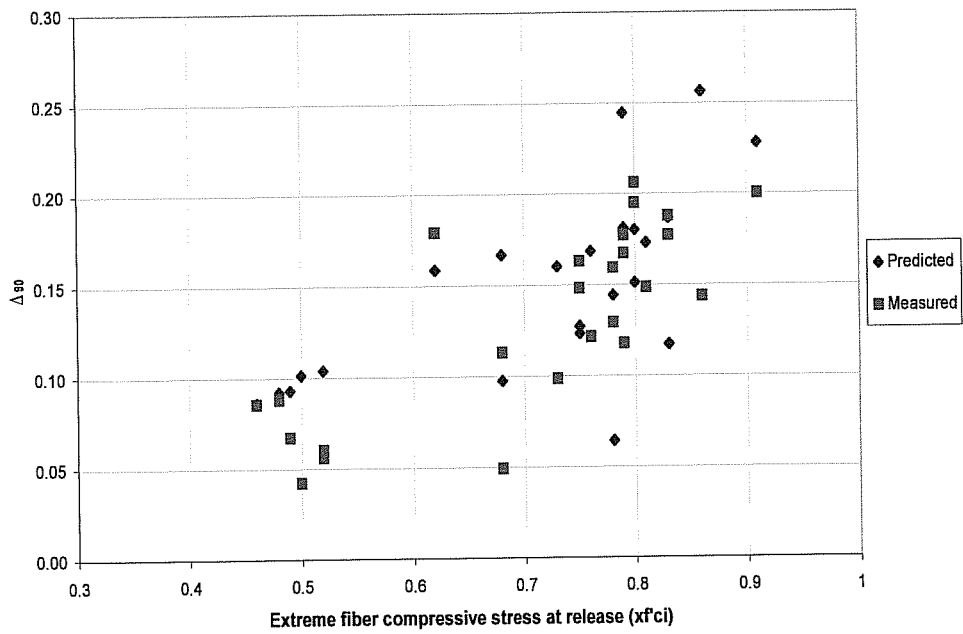
Figure 5-42: Δ_{90} versus compressive release stress

151

In order to adequately predict camber response of pretensioned beams, it is necessary to employ good prediction models for creep, shrinkage, and relaxation. According to ACI Committee 209, creep deformations at 122°F can double or triple those at 70°F (ACI Committee 209, 1992). ACI Committee 209 indicates that accurate results can only be expected if the predictions are made based on experimental data for the actual materials. Although temperatures measured in most of the specimens during concrete hydration were comparable to those typically experienced in precast plants, the specimens monitored in this study were fabricated inside the laboratory, while actual bridge girders will typically remain outdoors where temperatures can easily exceed 100°F during the summer.

The research team also investigated the effects of elevated extreme tensile fiber stresses in combination with elevated extreme compressive fiber stresses at prestress release. Flexural cracking was experienced in specimens with tensile stresses as low as $7.1\sqrt{f'_{ci}}$, and measured cambers tended to be greater than for uncracked specimens with a comparable level of extreme compressive fiber stress. In addition, specimens with flexural cracking but lacking non-prestressed reinforcement in the tensile region to control crack widths experienced even greater camber growth. Although specimens with flexural cracking exhibited enhanced camber growth, neither specimens containing non-prestressed reinforcement or lacking this reinforcement demonstrated behavior that was unstable or unpredictable. However, flexural cracks in these specimens developed to a depth not greater than 15% of the depth of the specimens. Because of the shallow depth of these cracks and the distributed nature of the prestressing force in the specimens (relative to what is typically used in actual prestressed bridge girders), the research team does not recommend reducing the tensile stress limits at release that are currently used in design.

In order to investigate the impact of elevated concrete stresses at prestress release on the behavior of pretensioned beams, some aspects of precast, pretensioned concrete manufacturing could not be accurately reproduced in the laboratory. As was mentioned earlier, ambient temperatures in the laboratory following prestress release may have been lower than what can be experienced in a precast concrete manufacturing facility. In addition, concrete compressive strengths at transfer typically range from 55 to 60 percent of the 28-day strength in precast plants. However, in order for some of the concrete mixes used in the research study to be representative of mixes used currently in precast, prestressed concrete manufacturing facilities in Texas, while also investigating the effect of elevated concrete stresses at release, ratios of concrete compressive strength at transfer to 28-day strength as low as 0.37 were experienced. This low ratio indicates that the rate of strength gain when prestress forces were released onto the specimens was quite different from what is typically encountered in the current manufacturing process for full-size bridge beams. This may have been one factor that affected the early-age camber development in the test specimens. Behavior of actual bridge beams following prestress transfer could differ significantly from that observed during this research project, and as a result, fabrication and monitoring of full-size members subjected to elevated concrete stresses at release is recommended to verify the behavior observed in the laboratory testing program.

5.10 Summary

A research project was conducted at Ferguson Structural Engineering Laboratory to determine whether pretensioned concrete beams could be subjected to elevated allowable concrete stresses at prestress release without adversely affecting their behavior. Extreme compressive fiber stresses are currently limited to $0.60f'_{ci}$ by ACI and AASHTO. Small-scale beams were subjected to elevated compressive and tensile stresses at transfer, and results presented in this chapter indicate that pretensioned concrete beams can be exposed to higher stress levels at prestress release as long as camber is adequately predicted and the amount is acceptable. Differences between laboratoryconditions and conditions in a typical precast concrete manufacturing plant suggest that full-size members should be manufactured in a precast facility and be subjected to elevated concrete stresses at release to verify the behavior observed in the laboratory testing program.

CHAPTER 6

Summary, Conclusions, and Recommendations

6.1 SUMMARY OF THE RESEARCH PROGRAM

A research program was conducted in Ferguson Structural Engineering Laboratory at The University of Texas at Austin to determine whether elevated concrete stresses at extreme flexural fibers, relative to current allowable stresses, can be applied to pretensioned concrete beams at transfer. A thorough review of documents related to allowable stresses in prestressed concrete was followed by the construction of a prestressing bed capable of accommodating six fifteen-foot-long beam specimens.

Five sets of six pretensioned beams were cast and monitored between June 2002 and May 2003. These sets included specimens that were representative of standard U beams, I girders, and double-tee beams. Instrumentation for these beams consisted of strain gauges on prestressing strands and linear potentiometers supported on steel frames to measure changes in camber. At prestress force transfer, extreme fiber compressive stresses in these specimens ranged from $0.46f'_{ci}$ to $0.91f'_{ci}$. Tensile stresses ranged from $1.5\sqrt{f'_{ci}}$ to $9.3\sqrt{f'_{ci}}$. Concrete compressive strengths at release were determined based on cylinders cured using a match-curing system called Sure Cure. This method provided for a better assessment of the actual concrete strength in the members. Measured response of test specimens and a thorough evaluation of specimen response were presented in this thesis.

6.2 CONCLUSIONS AND RECOMMENDATIONS

The following conclusions and recommendations can be drawn from this investigation:

1- Based on the five sets of pretensioned beams fabricated and monitored in this study, camber increased with increases in maximum compressive stress at release, expressed as a function of f'_{ci}, regardless of the cross-section geometry and type of concrete used to fabricate the specimens.

2- Fifteen beam specimens were subjected to extreme compressive fiber stresses greater than or equal to $0.75f'_{ci}$. As indicated in Figure 5-41, their short-term response (Δ_{10}) was generally underestimated. Higher release stresses appear to result in high rates of camber growth in the first days after prestress force transfer. However, long-term response (Δ_{90}) was estimated more accurately, although not conservatively for all specimens. This suggests that pretensioned concrete beams can be subjected to elevated compressive stress levels at prestress release as long as long-term camber response is adequately predicted and values are acceptable to the engineer of record.

3- A relationship between cross-section geometry of pretensioned beams and camber response was not identified.

4- Accuracy of predicted 10-day changes in camber (Δ_{10}) for inverted-tee beams decreased as the maximum compressive stress at transfer, expressed as a function of f'_{ci}, increased. In general, camber growth between days 1 and 10 was underestimated.

5- Camber growth between days 10 and 90 was higher for those inverted-tee beams constructed using crushed limestone and replacement of cement with fly ash than for those fabricated using river gravel. This behavior

156

was likely related to differences in concrete elastic moduli and rates of strength gain.

6- Ninety-day changes in camber for inverted-tee beams were more accurately estimated than ten-day changes in camber.

7- Both 10-day and 90-day changes in camber for rectangular beams were underestimated. However, 90-day changes in camber were significantly better predicted as was the case for the inverted-tee beams. As before, camber growth between days 10 and 90 was higher for beams constructed with concrete containing crushed limestone and fly ash rather than cement and river gravel.

8- Short-term camber response (Δ_{10}) of tee beams was slightly overestimated by the theoretical models employed. Long-term response (Δ_{90}) was overestimated, especially for specimens constructed with river gravel as the coarse aggregate.

9- The use of match-curing systems can significantly enhance productivity at precast plants. Even though temperatures measured in some of the test specimens were not as high as those commonly experienced in precast plants, compressive strengths at prestress transfer determined using standard cylinders were at least 10 percent lower than strengths determined using match-cured 4 by 8-inch cylinders.

10- The allowable stress design method typically overestimates extreme fiber compressive stresses at transfer. However, this approach may not be conservative for calculating extreme fiber tensile stresses. For example, the extreme fiber tensile stress in Specimen R3-82-3, calculated based on linear-elastic assumptions, was lower than the assumed modulus of rupture ($7.5\sqrt{f'_{ci}}$). In reality, this beam exhibited flexural cracks, as predicted by the nonlinear analysis approach. This observed behavior might have been

157

further exacerbated by differences between assumed and actual concrete tensile strength at the very early age at which the prestressing force was released.

11- Simulating typical curing and storage conditions in a precast concrete manufacturing facility was not possible in Ferguson Laboratory. In addition, test specimens used in the laboratory study were only 15 ft long, and were not replicas of actual U, I, and double-tee girder sections, but were developed to simulate the geometric properties of the cross sections. It is recommended that actual girders be fabricated and subjected to elevated concrete stresses at release in a precast manufacturing facility in order to verify the behavior of the laboratory specimens.

12- Transverse reinforcement for resisting bursting stresses at beam ends during prestress transfer resulted in satisfactory performance at stress levels exceeding currently-specified limits. This reinforcement was designed according to AASHTO provisions (AASHTO, 1998).

APPENDIX A

Tensile Stresses in the Strands
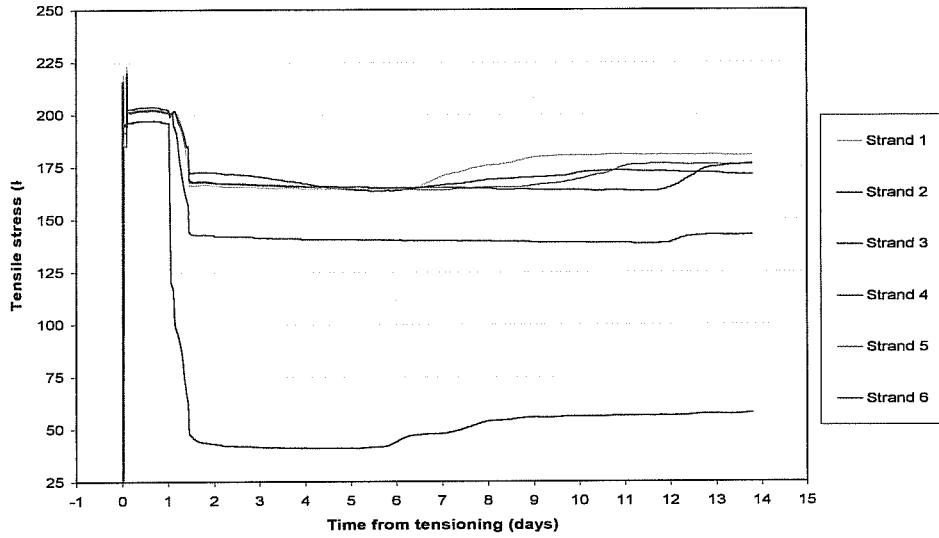
Figure A.1: Specimen R1-60-1 (a)
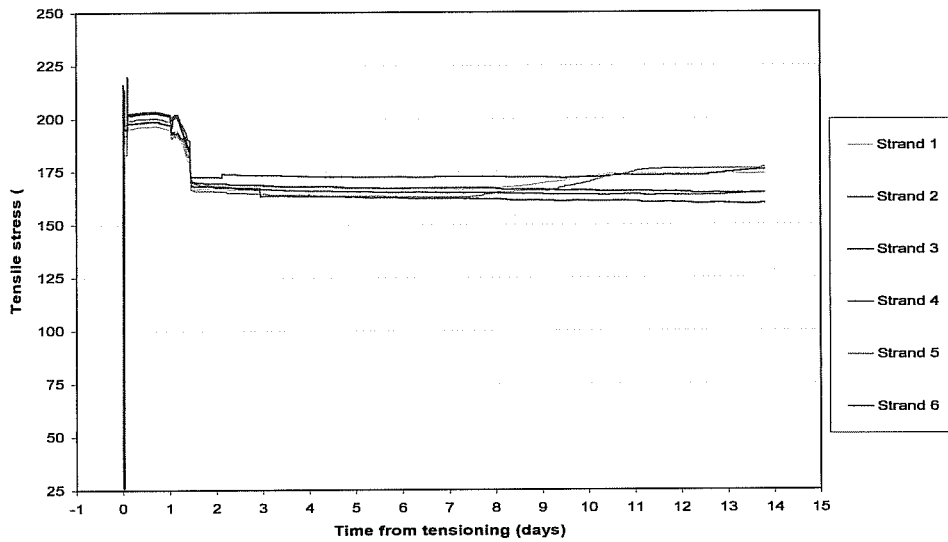
Figure A.2: Specimen R1-60-1 (b)
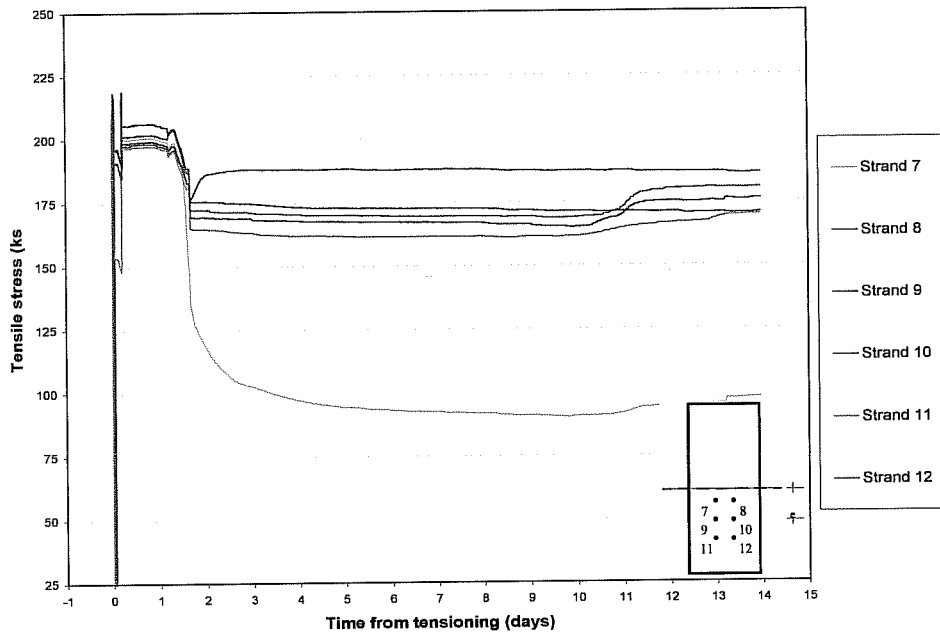
Figure A.3: Specimen R1-70-1 (a)
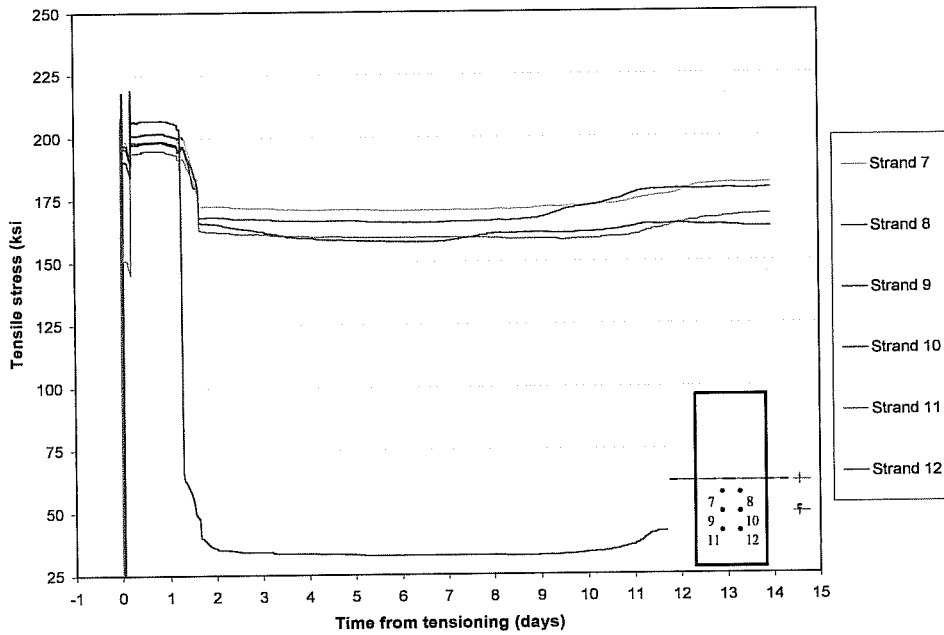
Figure A.4: Specimen R1-70-1 (b)

160
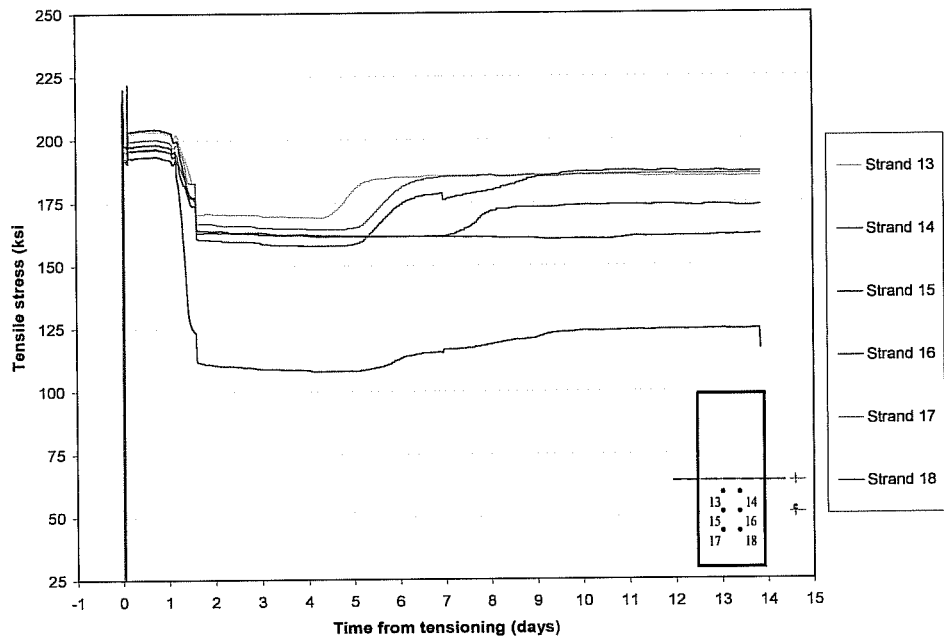
Figure A.5: Specimen R1-75-1 (a)
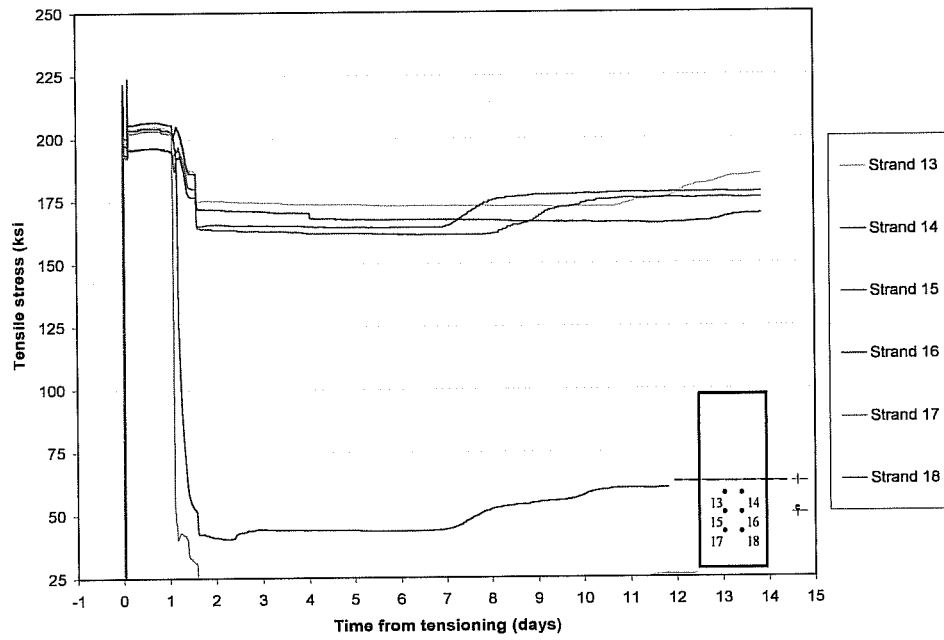
Figure A.6: Specimen R1-75-1 (b)

161
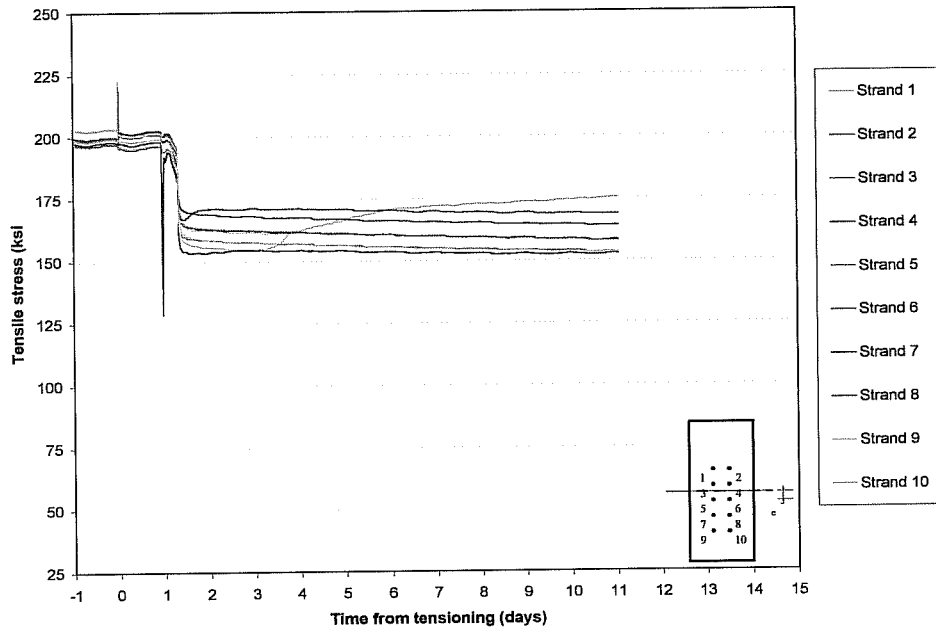
Figure A.7: Specimen R2-75-2
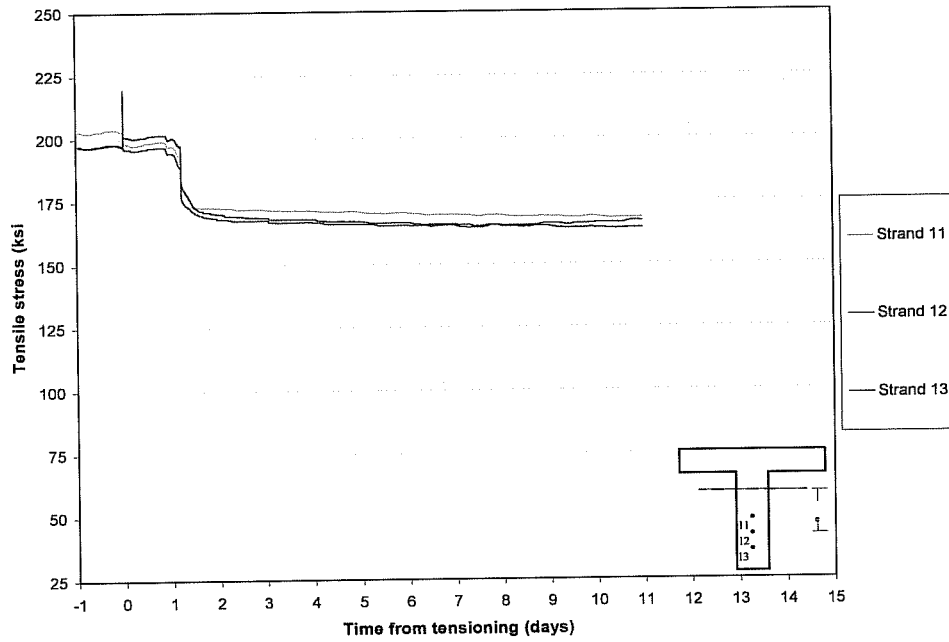
Figure A.8: Specimen T1-74-2

162
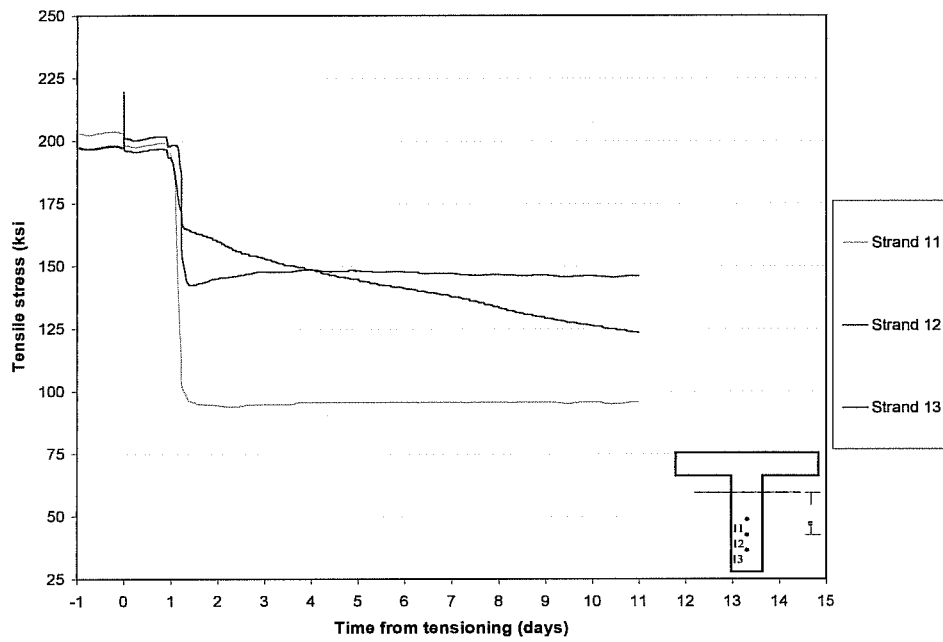
Figure A.9: Specimen T1-82-2
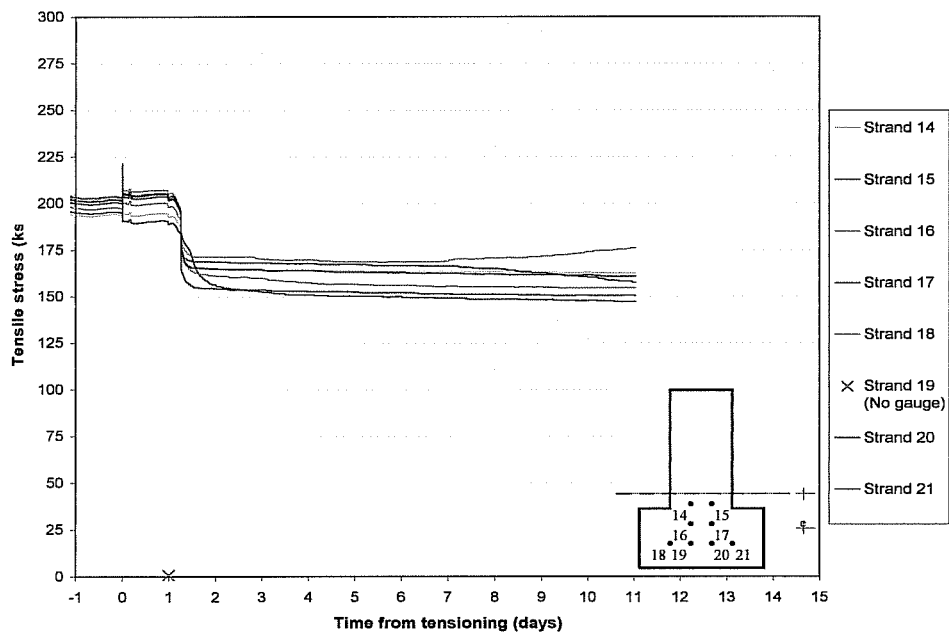
Figure A.10: Specimen IT1-76-2

163
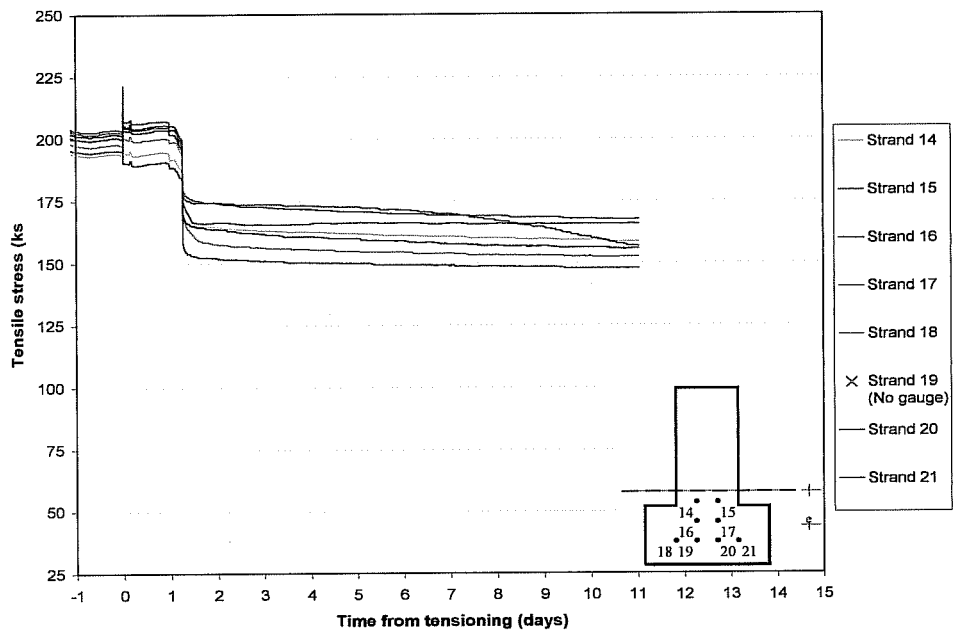
Figure A.11: Specimen IT1-84-2
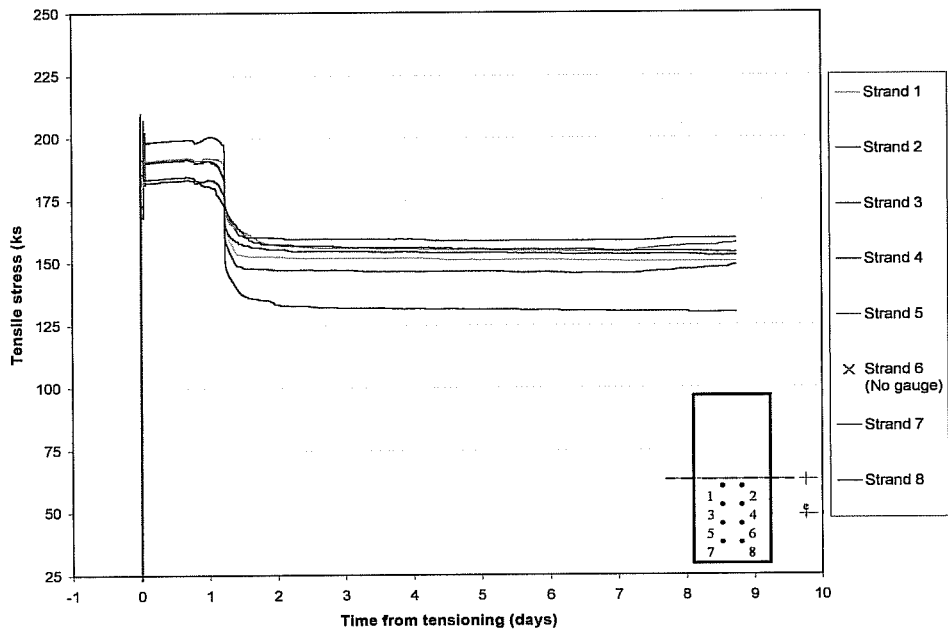
Figure A.12: Specimen R3-76-3

164
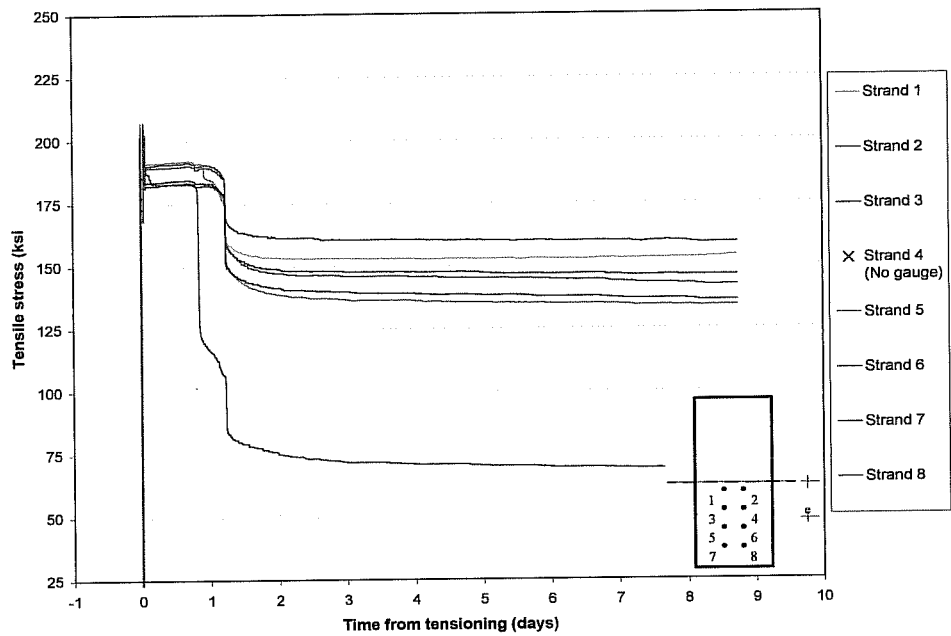
Figure A.13: Specimen R3-82-3
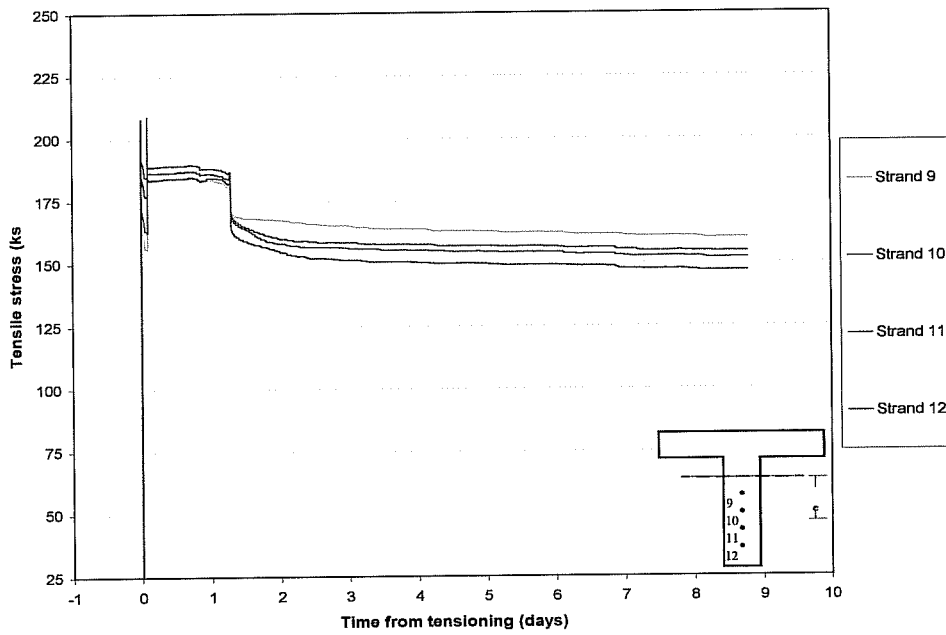
Figure A.14: Specimen T2-76-3

165
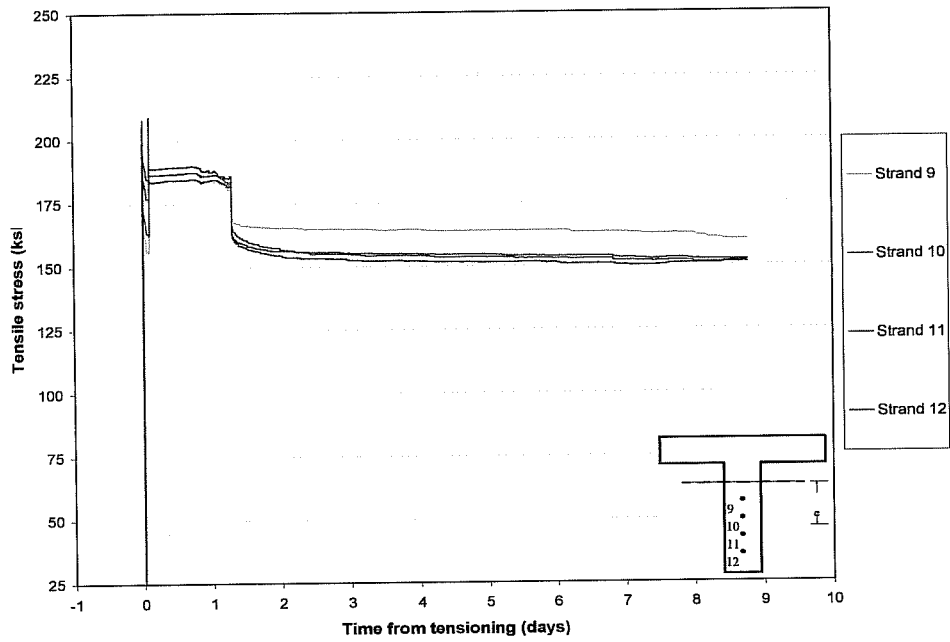
Figure A.15: Specimen T2-85-3
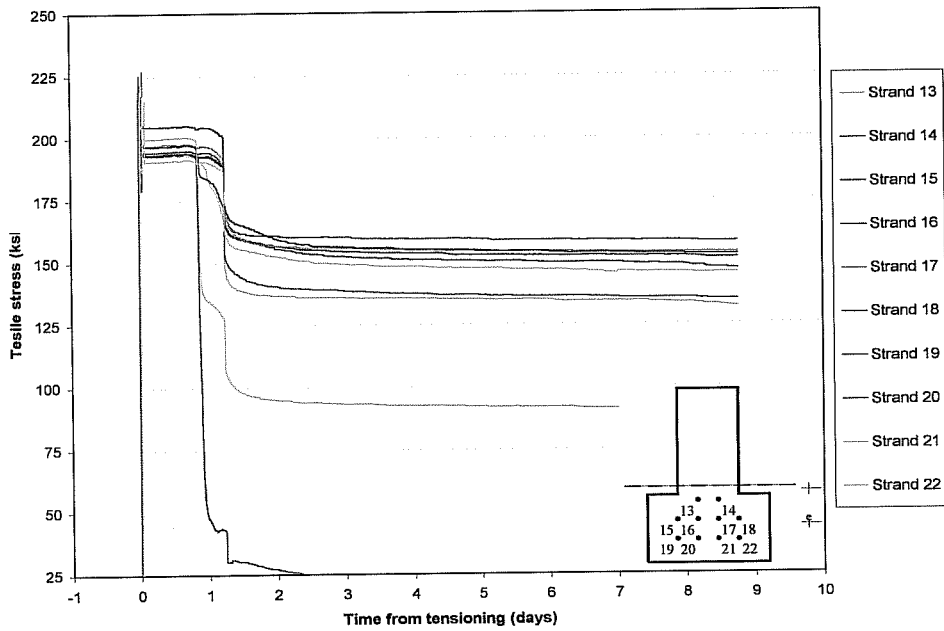
Figure A.16: Specimen IT3-85-3

166
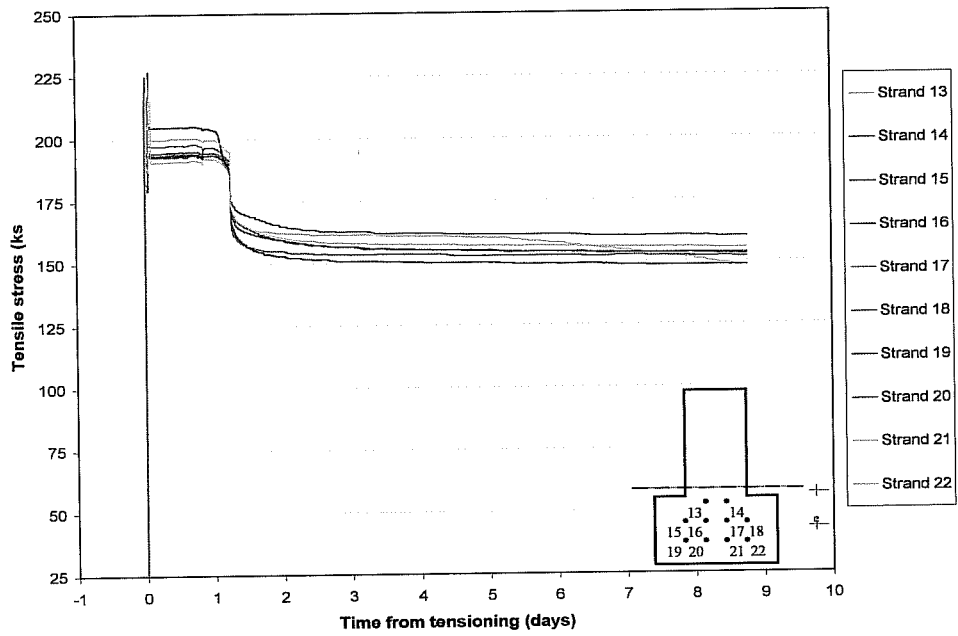
Figure A.17: Specimen IT2-85-3
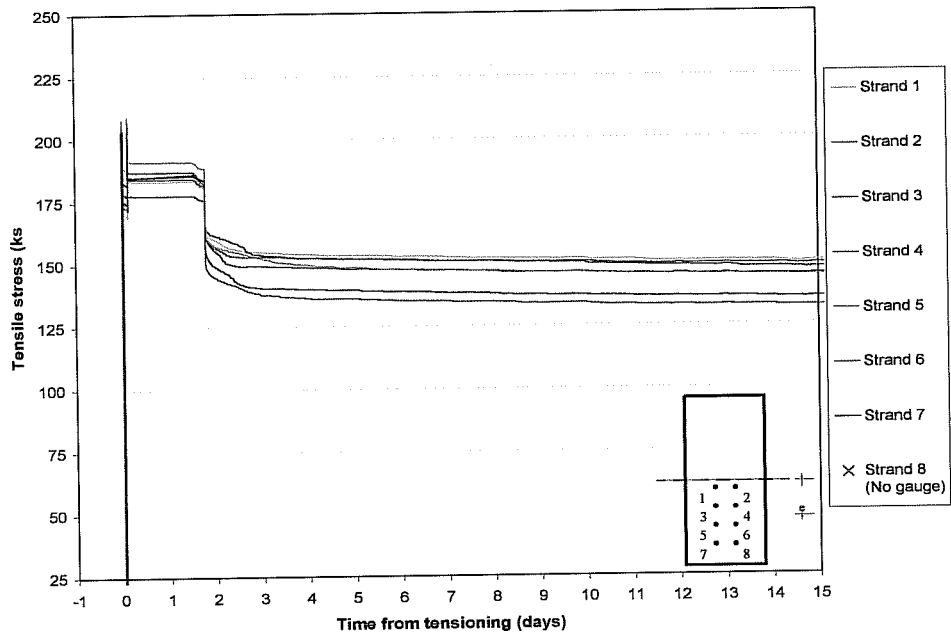
Figure A.18: Specimen R3-76-4

167
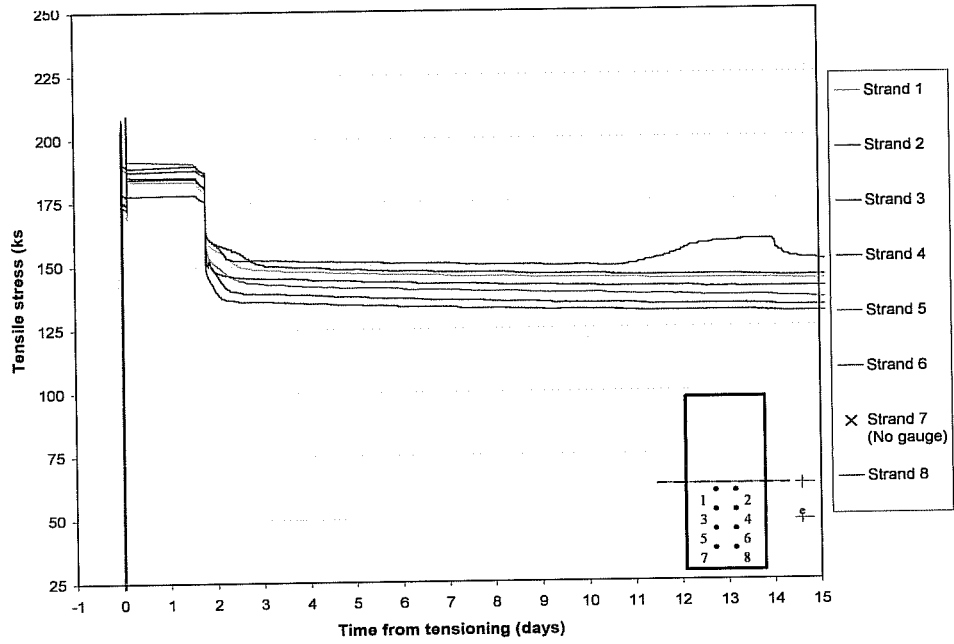
Figure A.19: Specimen R3-82-4
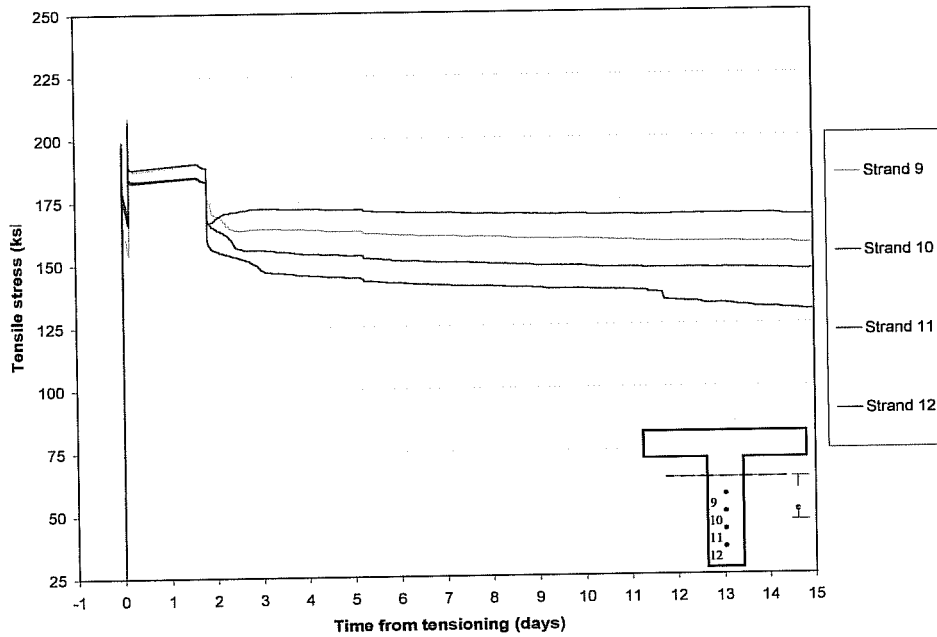
Figure A.20: Specimen T2-76-4

168
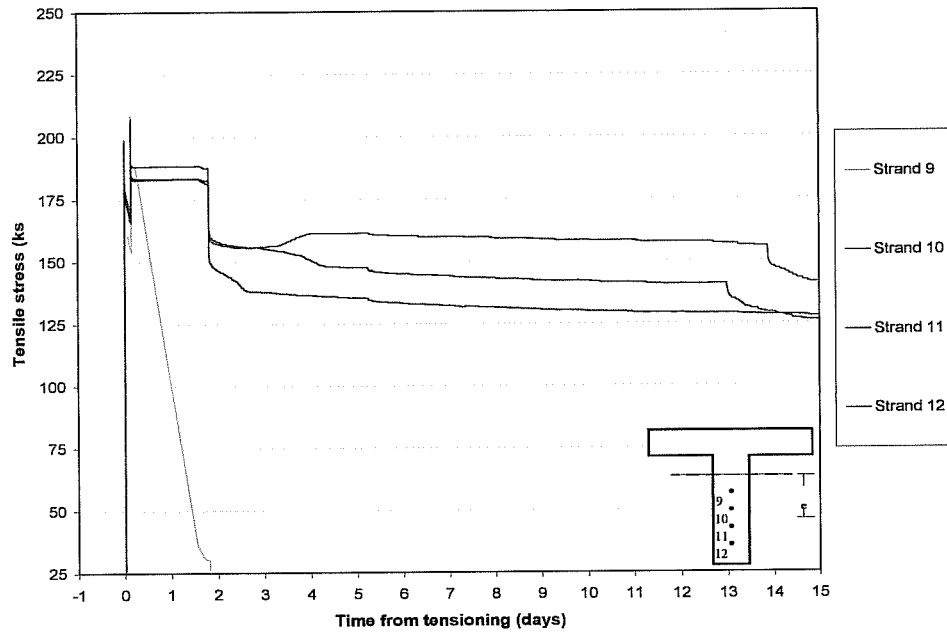
Figure A.21: Specimen T2-85-4
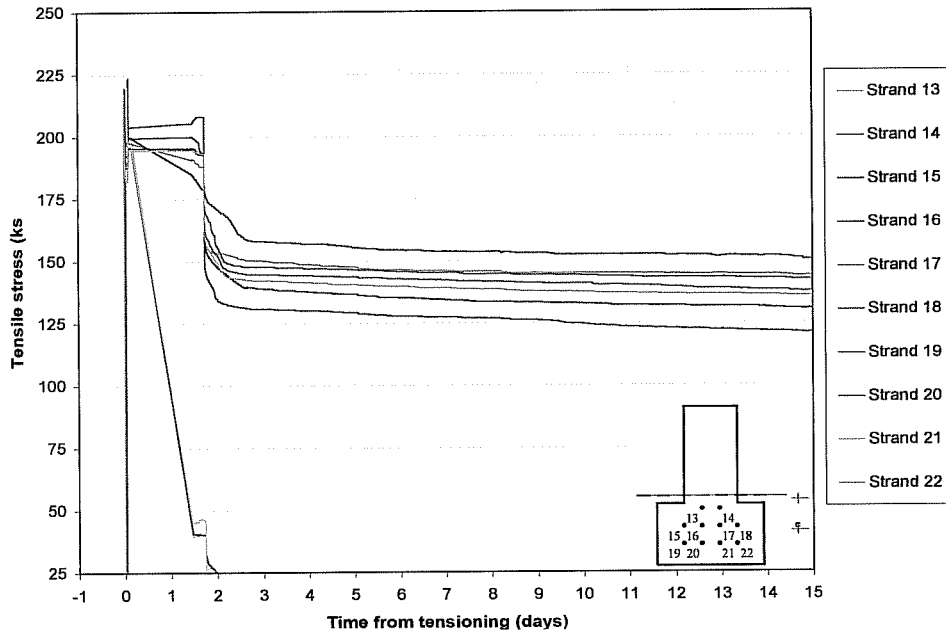
Figure A.22: Specimen IT3-85-4

169
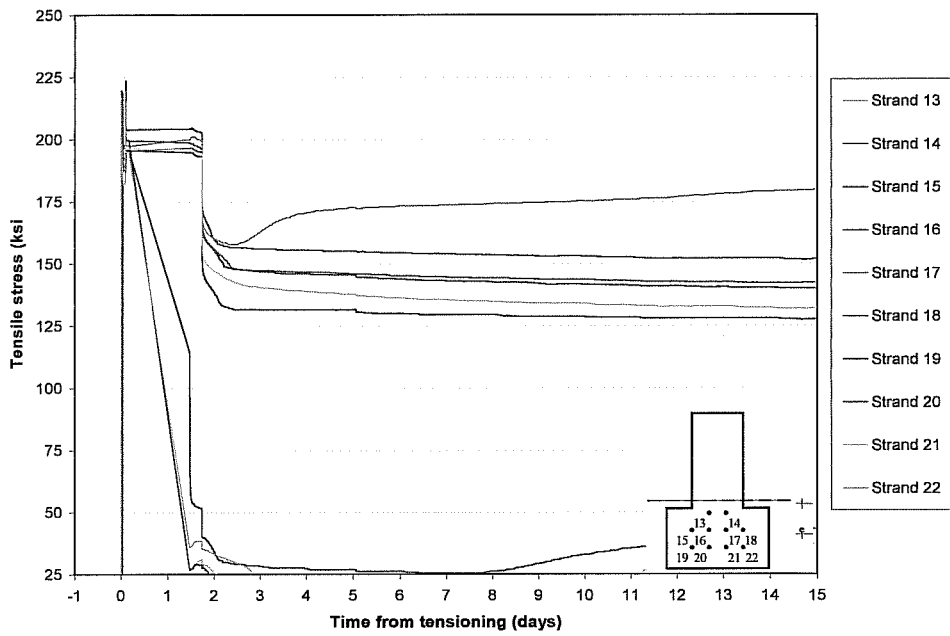
Figure A.23: Specimen IT2-85-4
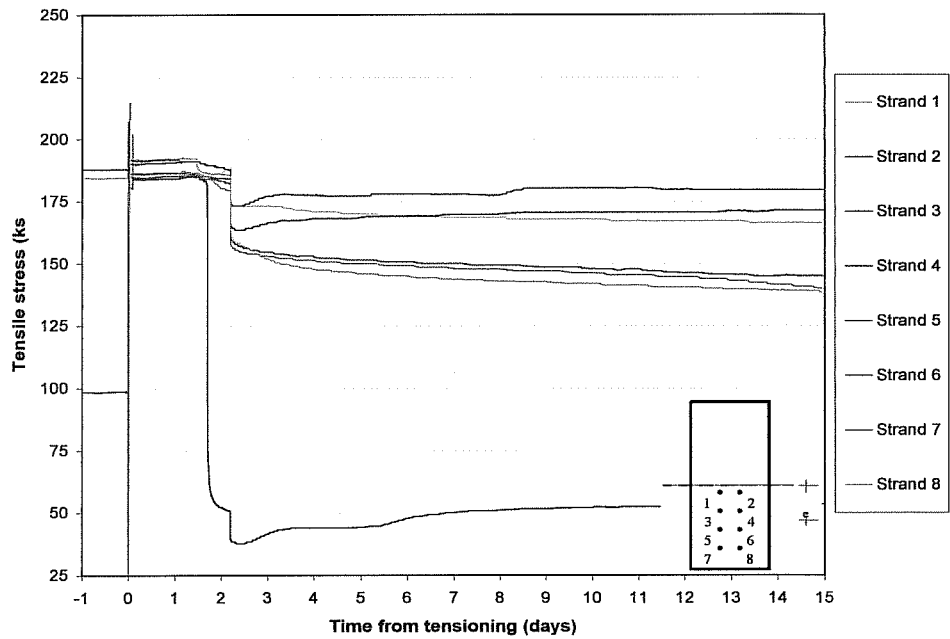
Figure A.24: Specimen R3-76-5
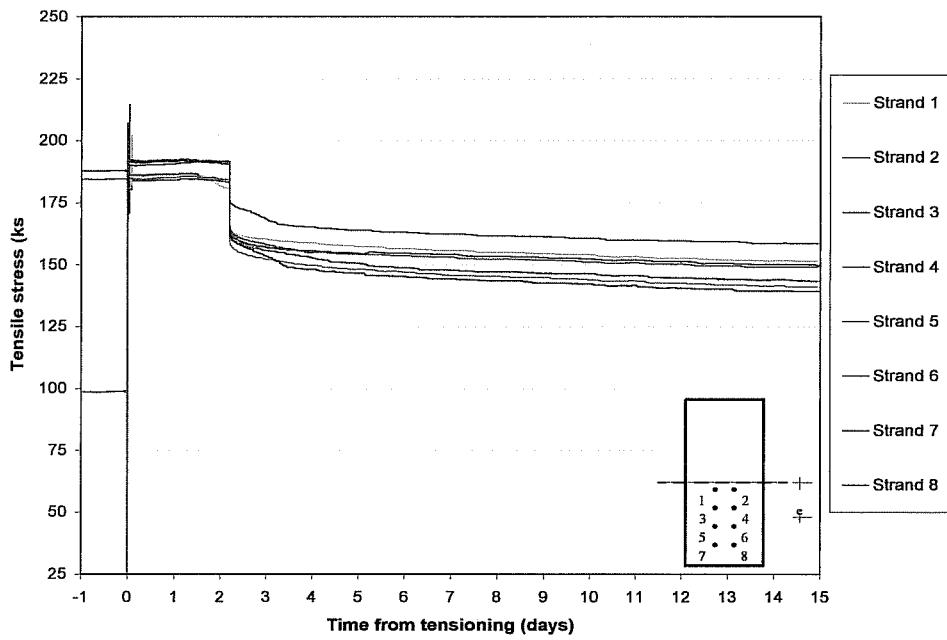
Figure A.25: Specimen R3-82-5
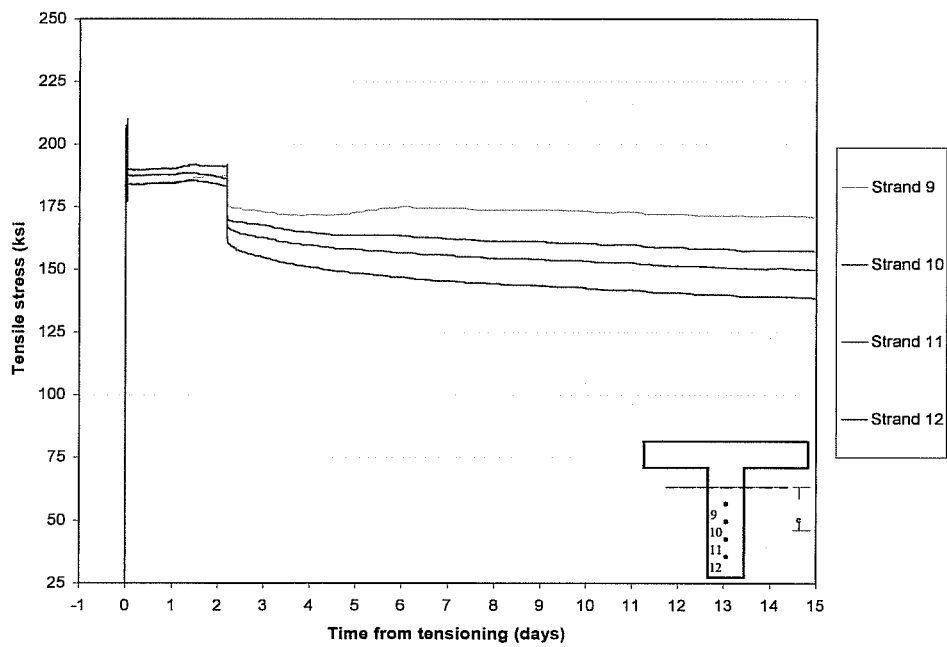
Figure A.26: Specimen T2-76-5

171
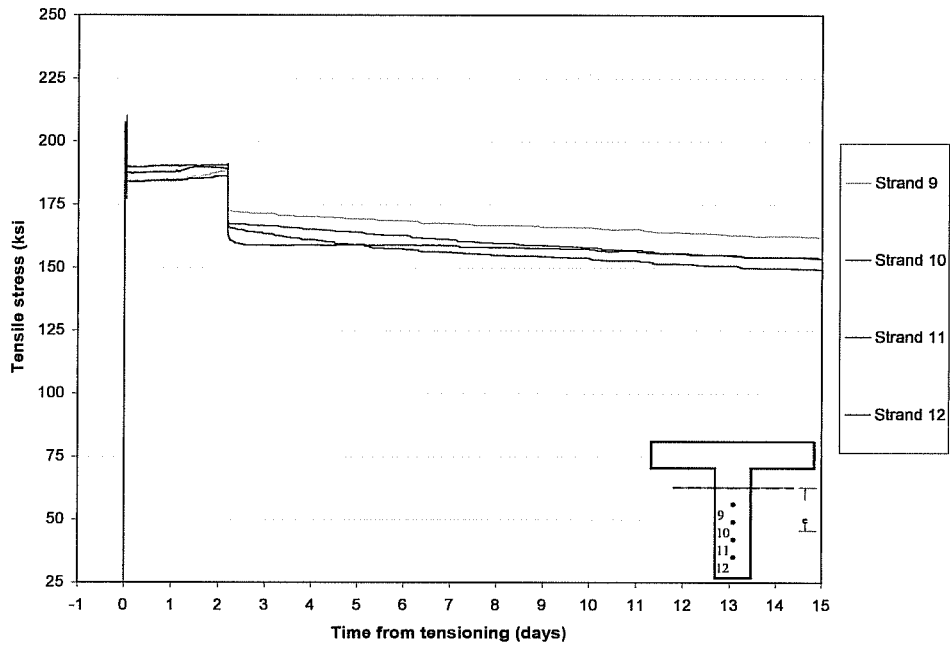
Figure A.27: Specimen T2-85-5
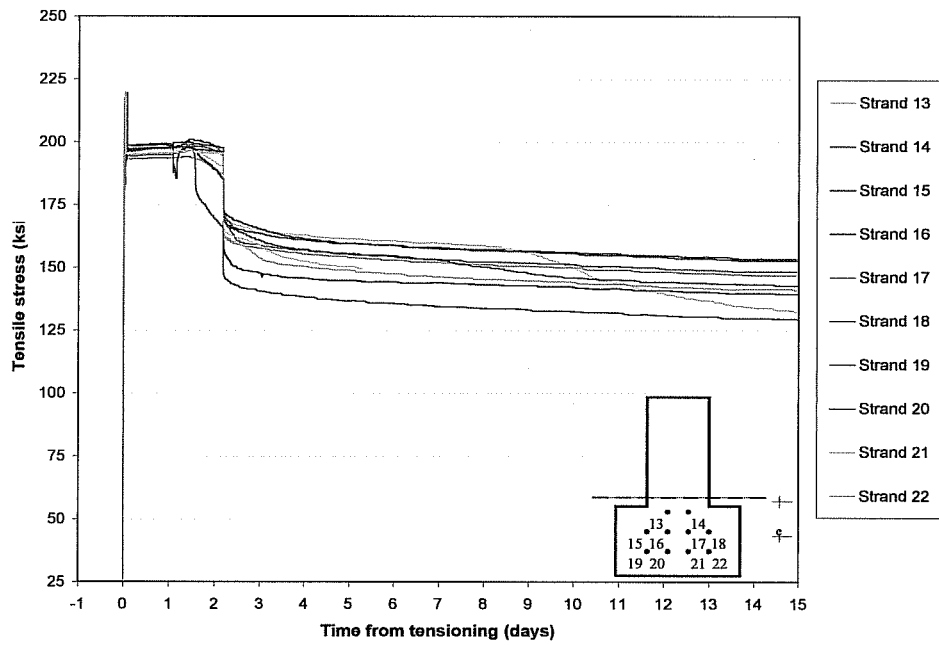
Figure A.28: Specimen IT3-85-5

172
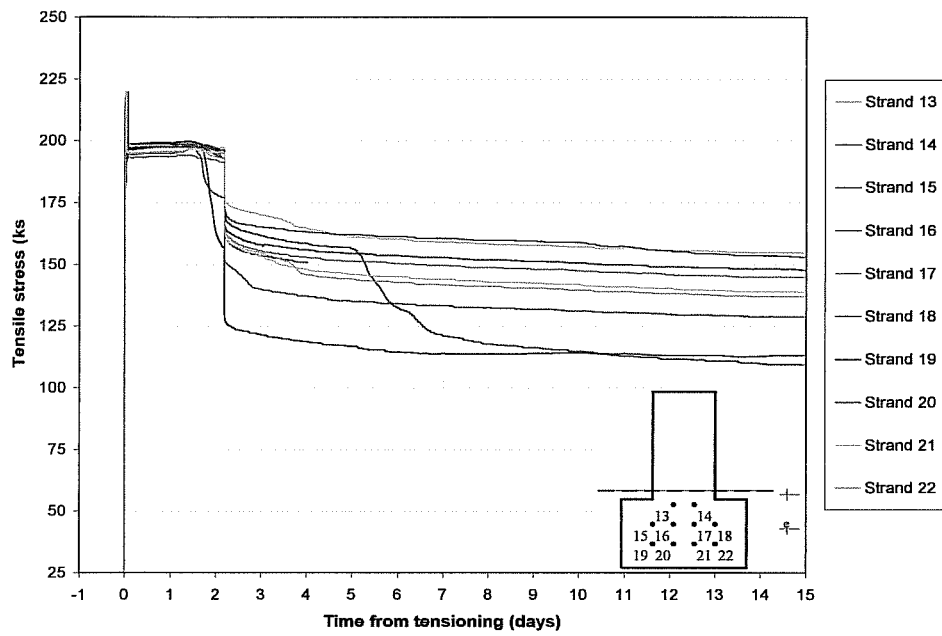
Figure A.29: Specimen IT2-85-5

APPENDIX B

Additional Photographs
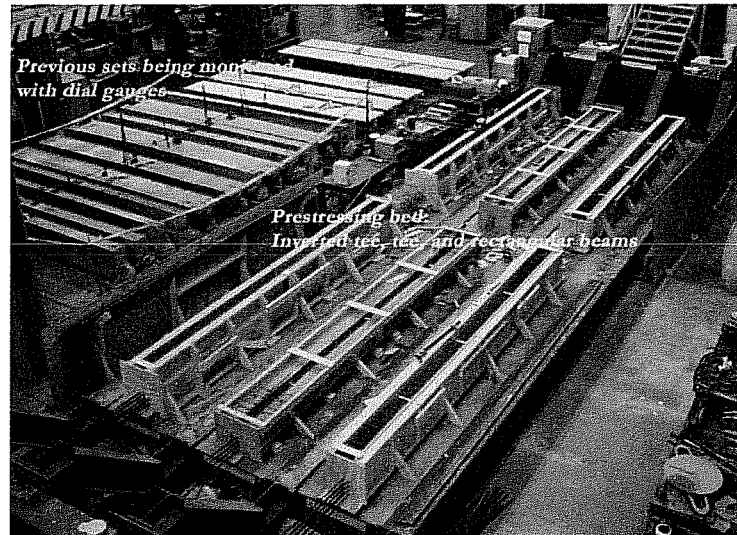
Figure B.1: Prestressing bed at Ferguson Laboratory
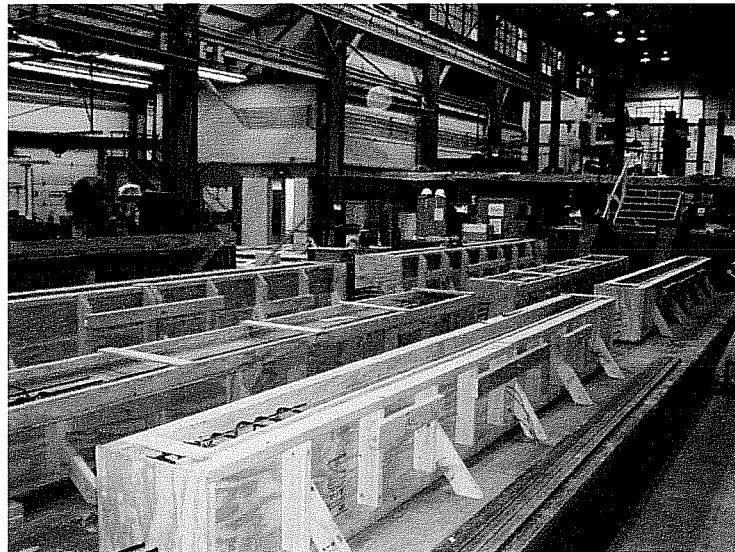
Figure B.2: Prestressing bed at Ferguson Laboratory 2
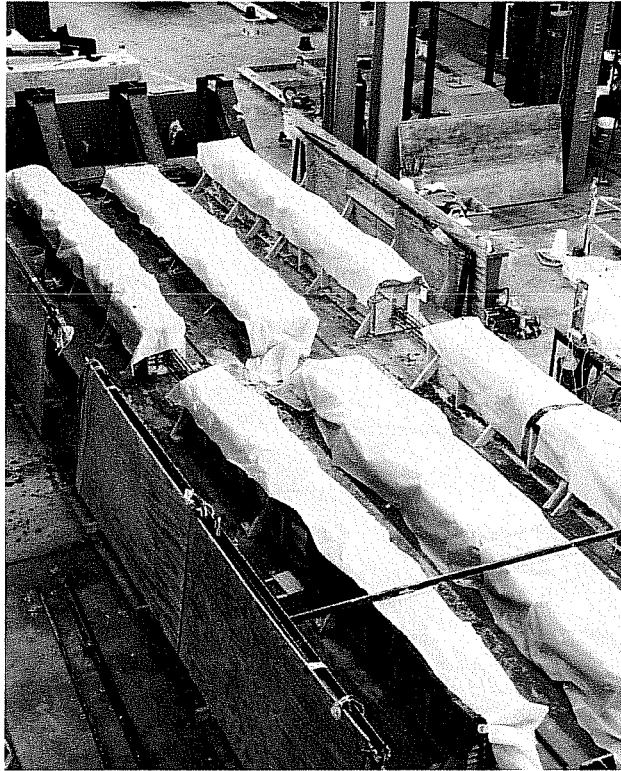
Figure B.3: Beams covered with wet burlap and plastic
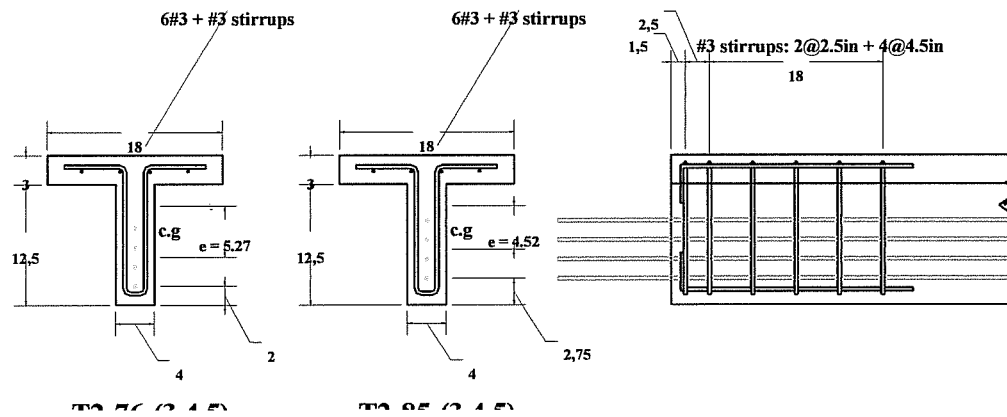
APPENDIX C

Reinforcement Details

R3-82-(3,4,5)   R3-76-(3,4,5)
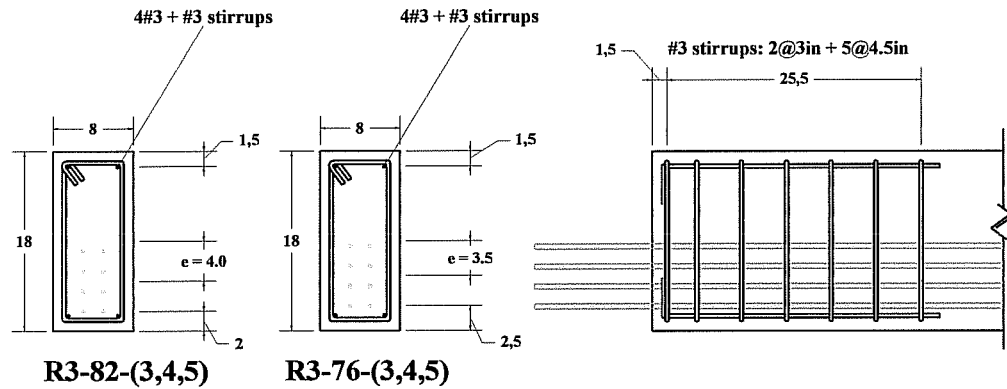
Figure C.1: Rectangular beams

Figure C.2: Tee beams
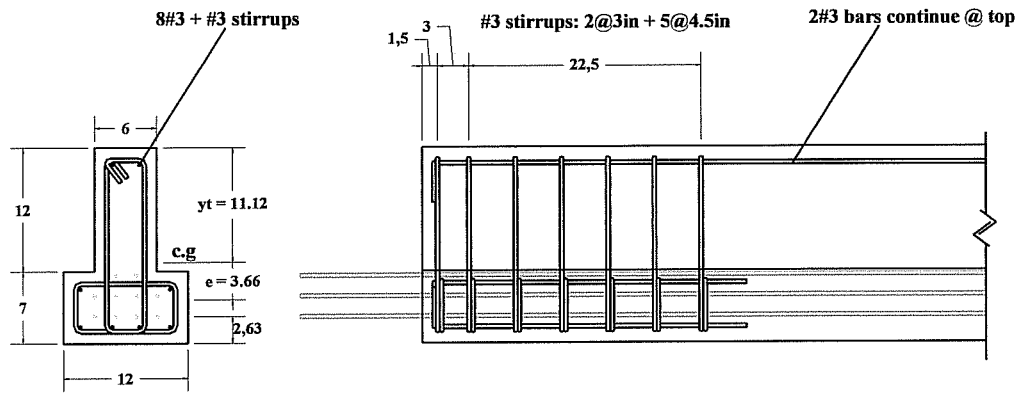
Figure C.3: Inverted tee beams with top nonprestressed reinforcement
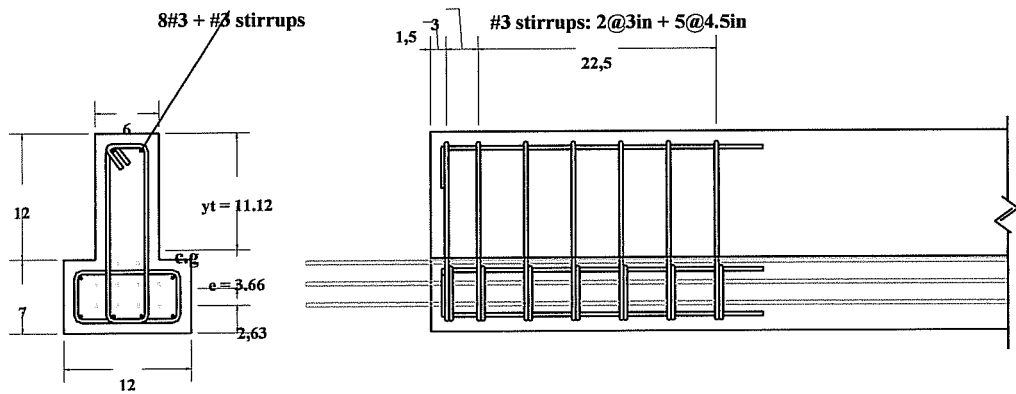
(IT3-85-3, IT3-85-4, and IT3-85-5)

Figure C.4: Inverted tee beams without top nonprestressed reinforcement

(IT2-85-3, IT2-85-4, and IT2-85-5)

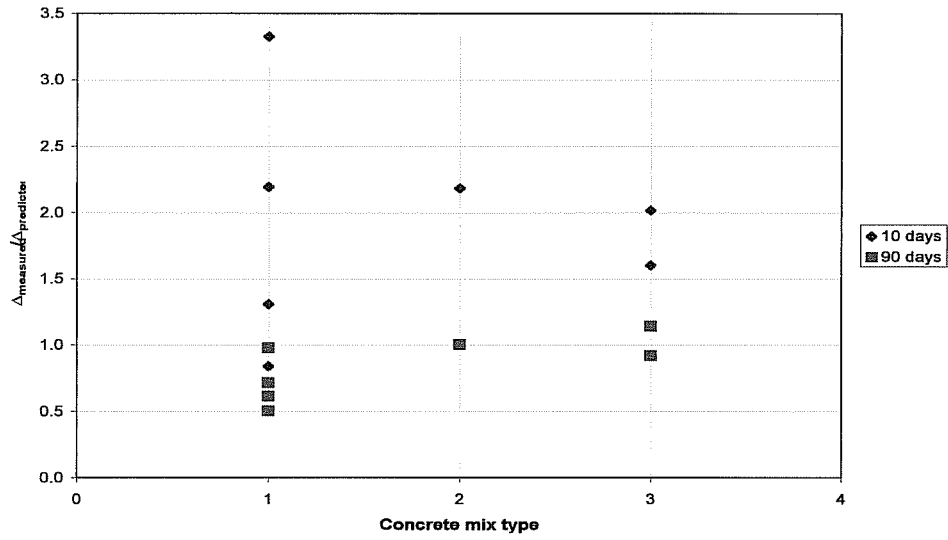# APPENDIX D

Additional Figures for Chapter 5

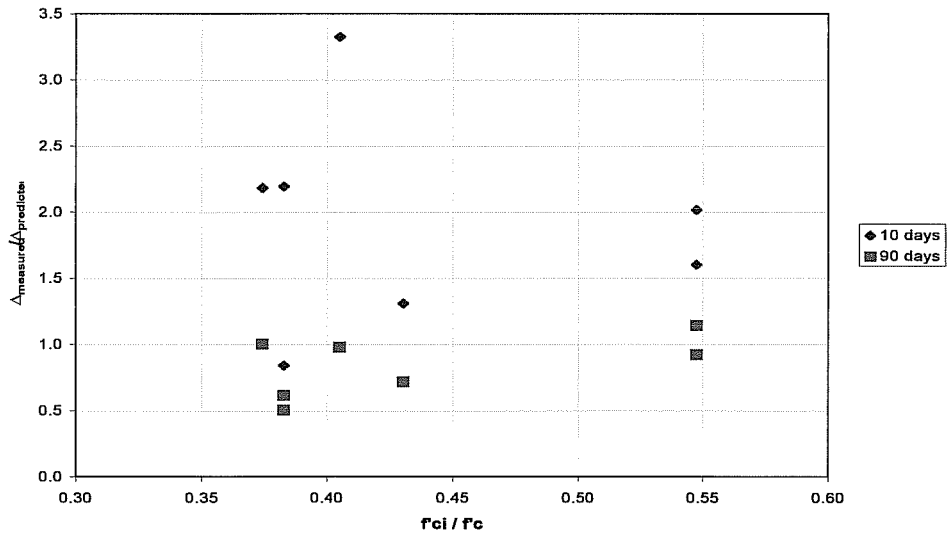***Figure D.1: Normalized camber change versus mix type (IT beams)***

Figure D.2: Normalized camber change versus f'_{ci}/f'_c (IT beams)
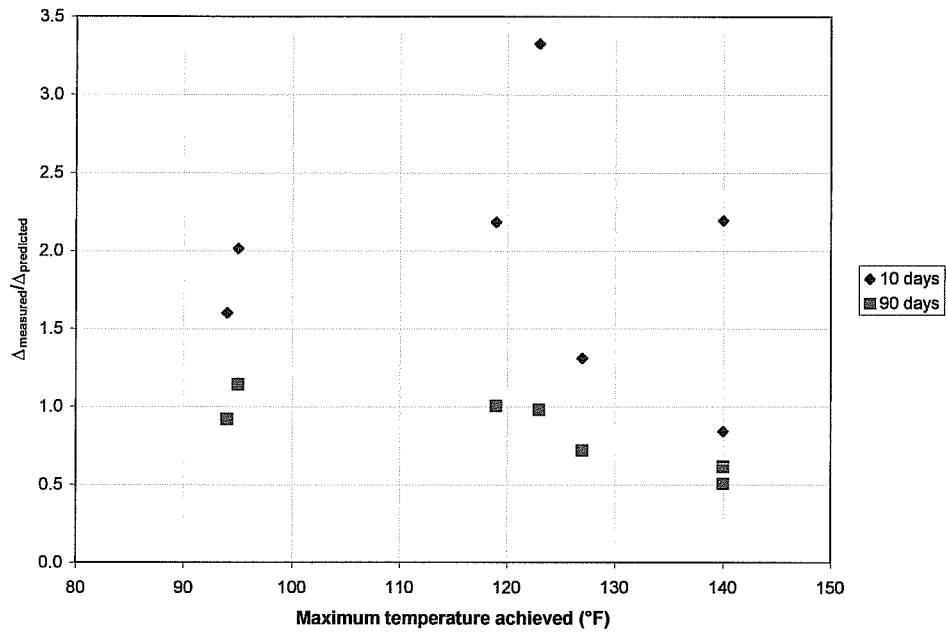
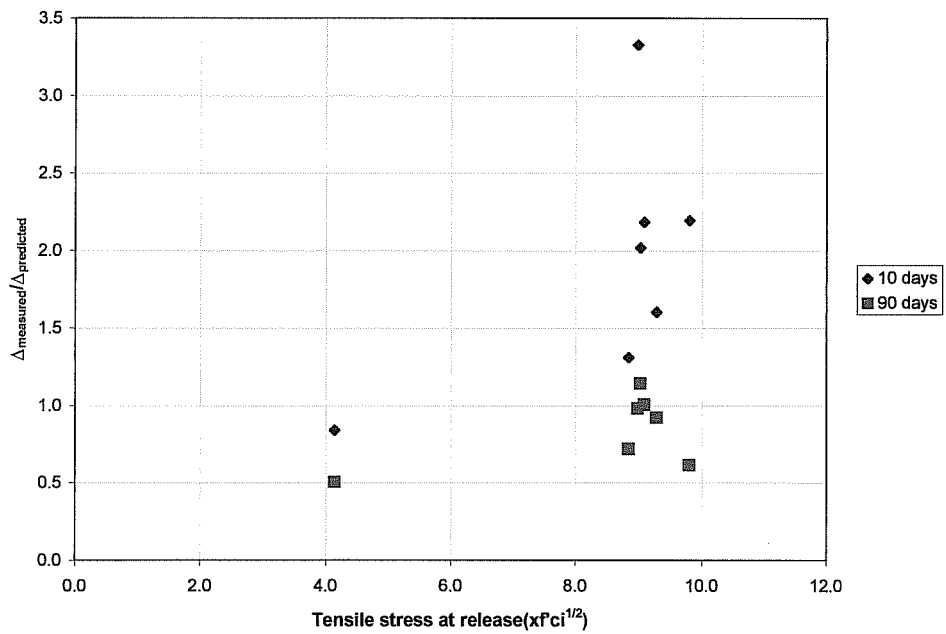*Figure D.3: Normalized camber change versus temperature (IT beams)*

Figure D.4: Normalized camber change versus tensile stress (IT beams)
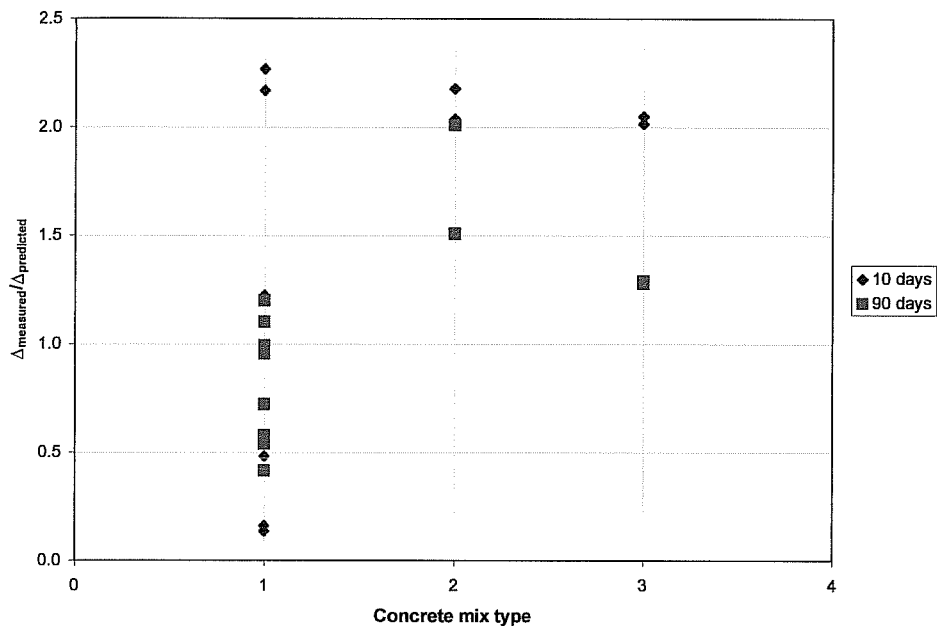
179

Figure D.5: Normalized camber change versus mix type (Rect. beams)
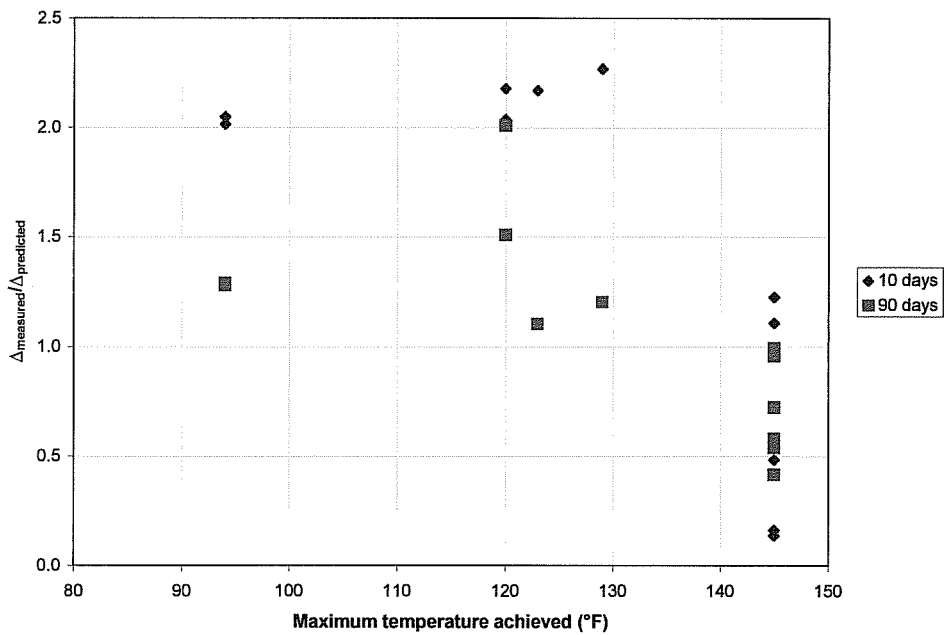
Figure D.6: Normalized camber change versus temperature (Rect. beams)

180

Figure D.7: Normalized camber change versus mix (Rect. Beams)

Figure D.8: Normalized long-term camber growth versus mix type (Rect. beams)

Figure D.9: Normalized camber change versus mix (Tee beams)

Figure D.10: Normalized camber change versus f'ci/f'c (Tee beams)

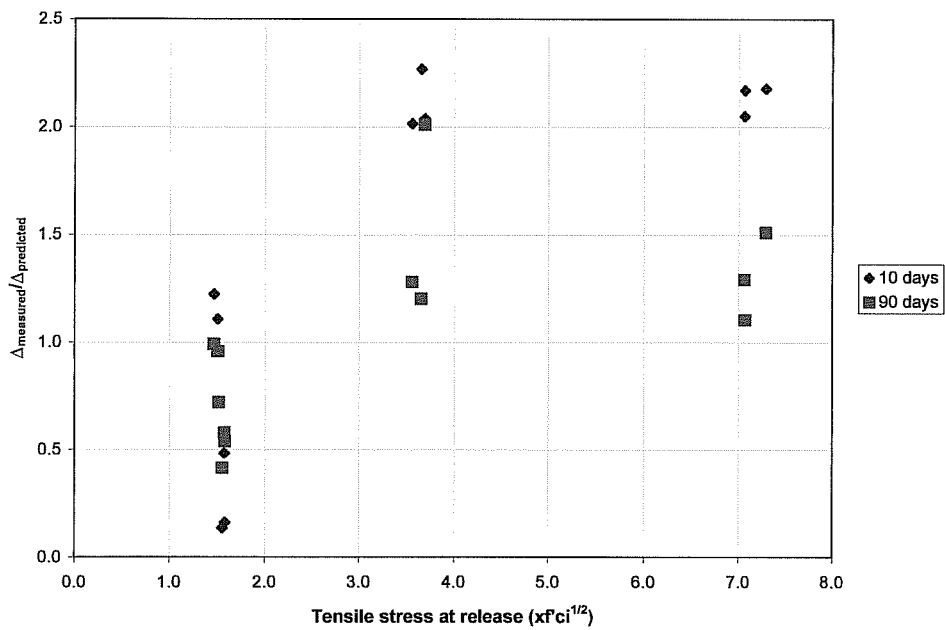*Figure D.11: Normalized camber change versus temperature (Tee beams)*
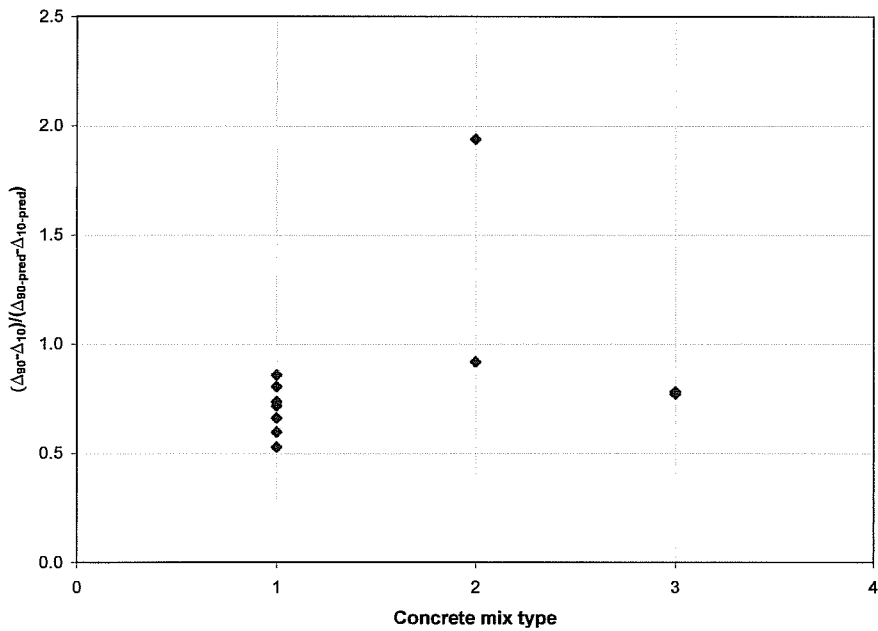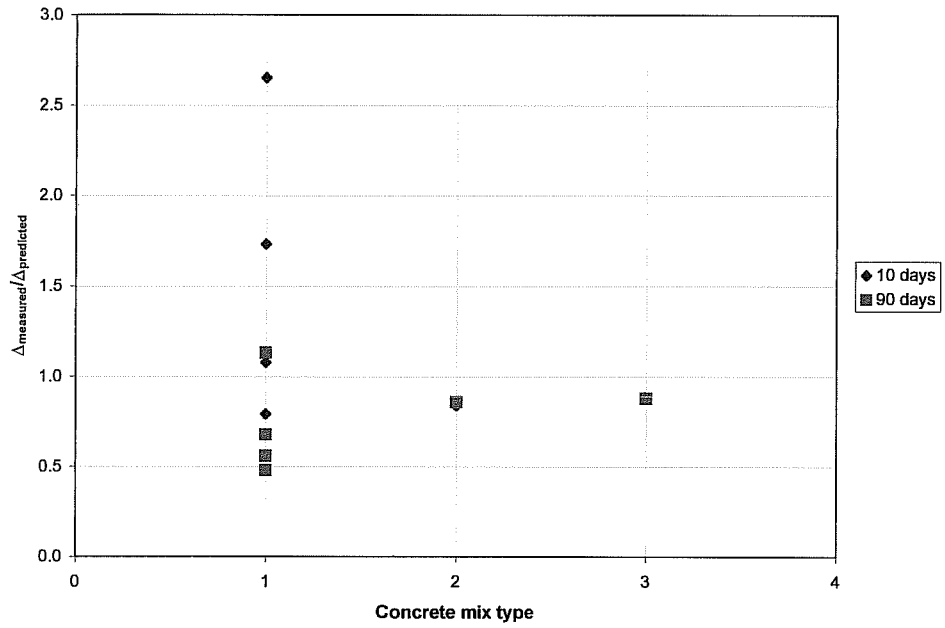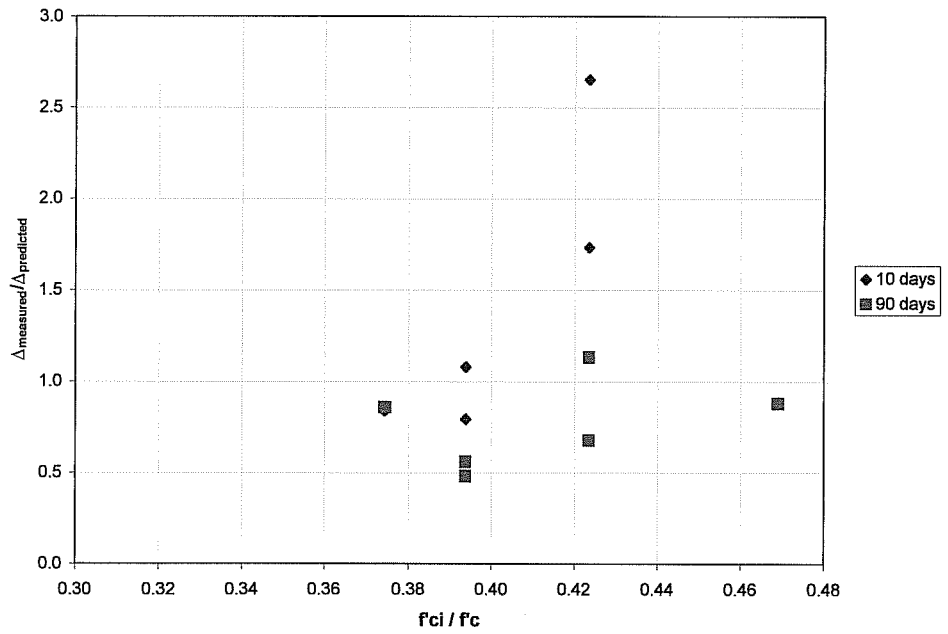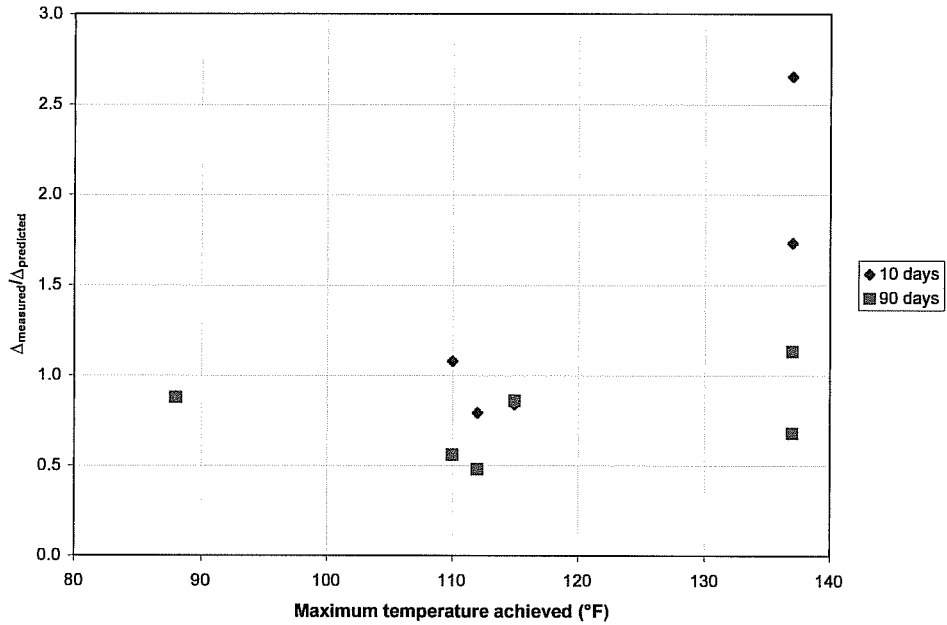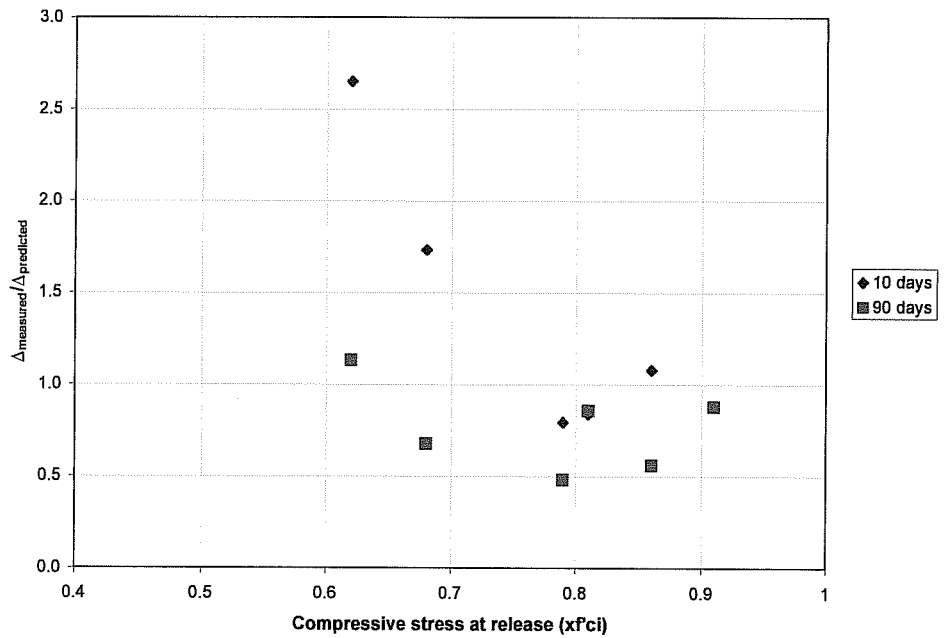

Figure D.12: Normalized camber change versus compressive stress (Tee beams)
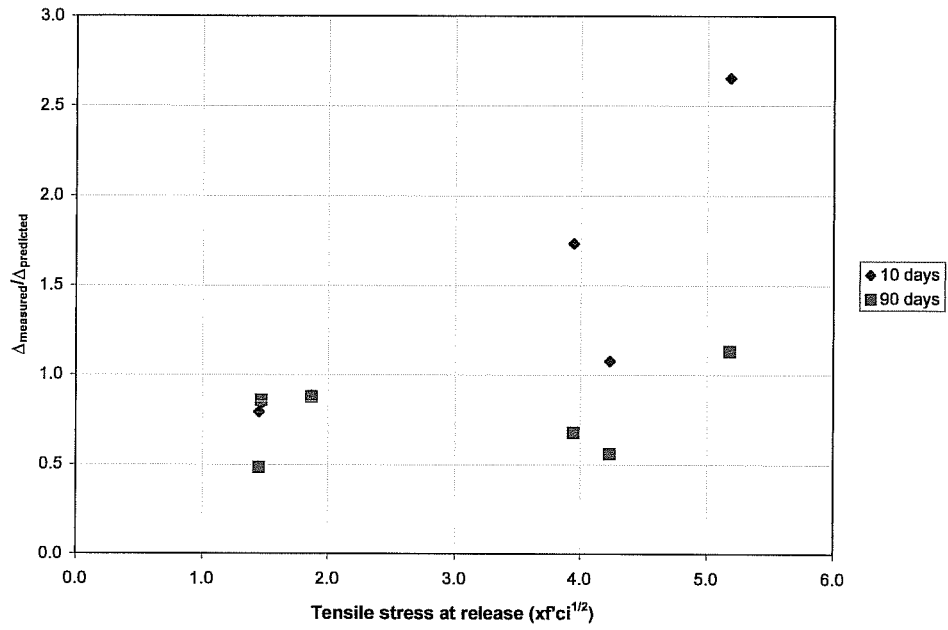
Figure D.13: Normalized camber change versus tensile stress (Tee beams)

GLOSSARY

a	depth of equivalent rectangular stress block
A_c	cross-section area of concrete
A_g	gross cross-section area
A_{ps}	total cross-section area of prestressing strand
A_s	area of tension reinforcement
A'_s	area of compression reinforcement
A_T, A_{trans}	transformed cross-section area of concrete
b	width of compression face of member
c	neutral axis depth
d	effective depth of section
d'	distance from extreme compression fiber to centroid of compression reinforcement
e	distance from section centroid to centroid of prestressed reinforcement
e_{pt}	distance from transformed section centroid to centroid of prestressed reinforcement
E_{ps}, E_p	modulus of elasticity of prestressed reinforcement
ES	elastic shortening loss
E_s	modulus of elasticity of nonprestressed reinforcement
E_c	modulus of elasticity of concrete
$E_{c,eff}$	effective modulus of elasticity of concrete to account for creep deformation
E_{ci}	modulus of elasticity of concrete at prestress release
f_c, σ_c	Stress in concrete

185

f_{cir}	compressive stress in concrete at center of gravity of prestressed reinforcement immediately after transfer
f_{cm}	average 28-day concrete compressive strength for CEB-FIP expression for estimating E_c
f_{ck}	characteristic compressive strength of a 6 by 12-inch cylinder
f'_c	28-day compressive strength of concrete
f'_{ci}	compressive strength of concrete at prestress transfer
f_p	stress in prestressed reinforcement
f_{pi}	stress in prestressed reinforcement immediately before transfer
f_{po}	effective prestress after transfer
f_{py}	yield strength of prestressing reinforcement
f_{pu}	ultimate tensile strength of prestressing steel
f_r	modulus of rupture of concrete
f_s	stress in tension reinforcement
f'_s	stress in compression reinforcement
h	overall height of the cross section
I_G	gross cross-sectional moment of inertia
I_T, I_{trans}	transformed cross-section moment of inertia
$E_{p,eff}$	effective modulus of elasticity of prestressing strand accounting for relaxation
E_{ps}	modulus of elasticity of prestressing strand
L, l	length of concrete member
M	applied moment
M_D, M_g, M_{sw}	moment due to self weight
M_n	nominal moment strength
N	applied axial load
n	modular ratio

P_i	initial prestress force immediately before transfer
P_n	nominal axial load strength
P_o	effective prestress force immediately after prestress transfer
T	temperature
$v(t, t_i)$	creep coefficient
w	distributed load
w_c	unit weight of concrete
y_b	distance from gross section centroid to extreme bottom fiber
y_{bt}	distance from transformed section centroid to extreme bottom fiber
y_{b-c}	distance from centroid of the net concrete area to extreme bottom fiber
y_{b-ps}	distance from centroid of prestressing steel to extreme bottom fiber
y_t	distance from gross section centroid to extreme top fiber
y_{tT}	distance from transformed section centroid to extreme top fiber
α_β	correction factor for type of aggregate taken as 1.2 for basalt/dense limestone, 1.0 for quartizitic, 0.9 for limestone, and 0.7 for sandstone
$\Delta_{initial}$	initial camber
Δ_{10}	difference between measured 10-day camber and initial camber
Δ_{90}	difference between measured 90-day camber and initial camber
$\Delta\varepsilon_p$	strain difference between prestressed reinforcement and surrounding concrete
ε_c	total strain in concrete
ε_{cf}	strain in concrete due to stress
ε_{co}	strain in concrete due to shrinkage plus thermal effects
$\varepsilon_o, \varepsilon'_c$	strain at peak stress for nonlinear concrete stress-strain models
ε_{cen}	strain in concrete at centroid of transformed cross section

ε_{cu}	ultimate concrete strain
ε_s	strain in tension reinforcement
ε_{sh}	shrinkage concrete strain
ε_{sf}	strain in nonprestressed reinforcement due to stress
ε_{so}	strain in nonprestressed reinforcement due to thermal effects
ε'_s	compression reinforcement strain
ε_p	total strain in prestressed reinforcement
ε_{po}	strain in prestressed reinforcement due to thermal effects
ε_{pf}	strain in prestressed reinforcement due to stress
ϕ	curvature
ϕ	strength reduction factor
σ_{top}	stress at top of section
σ_{bot}	stress at bottom of section

BIBLIOGRAPHY

1. AASHTO, *Standard Specifications for Highway Bridges*, 16th Edition, American Association of State Highway and Transportation Officials, Washington, D.C., 1996.

2. AASHTO, *LRFD Bridge Specifications*, 2nd Edition, American Association of State Highway and Transportation Officials, Washington, D.C., 1998.

3. ACI Committee 209, *Prediction of Creep, Shrinkage, and Temperature Effects in Concrete Structures (ACI 209R-92)*, American Concrete Institute, Detroit Michigan, 1992.

4. ACI Committee 318, *Building Code Requirements for Reinforced Concrete*, American Concrete Institute, Detroit, MI, 1963.

5. ACI Committee 318, *Building Code Requirements for Reinforced Concrete (ACI 318-02)*, American Concrete Institute, Detroit, Michigan, 2002.

6. ACI-ASCE Joint Committee 323, *Tentative Recommendations for Prestressed Concrete*, Journal of the American Concrete Institute, Detroit, January 1958. Vol. 29, No 7, p. 545-578.

7. AISC, ASD Manual of Steel Construction, Ninth Edition, American Institute of Steel Construction, Chicago, IL, 1989.

8. AISC, LRFD Manual of Steel Construction, Third Edition, American Institute of Steel Construction, Chicago, IL, 2001.

9. Baalbaki W., Aitcin P., and Ballivy G., *On Predicting Modulus of Elasticity in High-Strength Concrete*, ACI Materials Journal, V.89, No.5, September-October, 1992.

10. Baalbaki W., Benmokrane B., Chaallal O., and Aitcin P. *Influence of Coarse Aggregate on Elastic Properties of High-Performance Concrete*, ACI Materials Journal, V.88, No.5, September-October, 1991.

11. Bureau of Public Roads, *Criteria for Prestressed Concrete Bridges*, U.S. Department of Commerce, 1954.

12. Collins M., and Mitchell D., *Prestressed Concrete Structures*, Response Publications, Ontario, Canada, 1997.

13. Collins, M.P. and Mitchell, D., *Response (Version 1.0) for Prestressed Concrete Structures*, Department of Civil Engineering, University of Toronto, 1990.

14. Committee 501-Standard Building Code, *Proposed Revisions of Building Regulations for Reinforced Concrete*, Journal of the American Concrete Institute, Vol. 36, Detroit, MI, 1940, p. 237-260.

15. Computers and Structures Inc., *SAP2000*, Berkeley, CA 1998.

16. Hawkins, N.M., "Impact of Research on Prestressed Concrete Specimens." ACI SP-72, American Concrete Institute, Detroit, 1981. p. 163-176.

17. Huo, X., Savage, J.M., and Tadros, M. K., *Re-examination of Service Load Limit Compressive Stress in Prestressed Concrete Members*, ACI Structural Journal, V. 92, No.2, March-April 1995, p. 199-210.

18. Huo, Xiaoming, and Tadros, Maher, Ph.D., *Allowable Compressive Strength of Concrete at Prestress Release*, PCI Journal, January-February 1997, p. 95-99.

19. Iravani, S., *Mechanical Properties of High-Performance Concrete*, ACI Materials Journal, V.93, No.5, September-October 1996.

20. Kerekes, Frank and Reid, Harold B., *Fifty Years of Development in Building Code Requirements for Reinforced Concrete*, Journal of the American Concrete Institute, Vol. 25, No.6, Detroit, MI, February, 1954. p. 441-470.

21. Khan A., Cook W., Mitchell, D. *Early Age Compressive Stress-Strain Properties of Low, Medium, and High-Strength Concretes,* ACI Materials Journal, V.92, No.6, November-December 1995.

22. Khan A., Cook W., Mitchell, D. *Tensile Strength of Low, Medium, and High-Strength Concrete at Early Ages,* ACI Materials Journal, V.93, No.5, September-October 1996.

23. Lin, T. Y., *Tentative Recommendations for Prestressed Concrete,* Journal of the American Concrete Institute, Detroit, MI, Part 2 September 1958, p.1232-1233.

24. Maples, W. A., Wilde, R.E. *Fifty Years of the American Concrete Institute,* Journal of the American Concrete Institute, V. 25, No. 6, Feb. 1954.

25. Mesbah H.A., Lachemi M., Aitcin P., *Determination of Elastic Properties of High-Performance Concrete at Early Ages,* ACI Materials Journal, V.99, No.1, January-February 2002.

26. Mokhtarzadeh, A. and French, C., *Mechanical Properties of High-Strength Concrete with Consideration for Precast Applications,* ACI Materials Journal, V.97, No.2, March- April 2000.

27. Mokhtarzadeh, A. and French, C., *Time-Dependent Properties of High-Strength Concrete with Consideration for Precast Applications,* ACI Materials Journal, V.97, No.3, May- June 2000.

28. Noppakunwijai P., Tadros, M.K., Ma, Z., and Mast, R.F., *Strength Design of Pretensioned Flexural Concrete Members at Prestress Transfer,* PCI Journal, January-February 2001, p. 34-52.

29. OHBDC, *Ontario Highway Bridge Design Code,* 2nd Edition, Ontario Ministry of Transportation and Communications, Toronto, 1983, 357pp.

30. Pang, J. P., *Allowable Compressive Stresses for Prestressed Concrete.* PCI Research Report, 1996.

31. Patton, B., Private Conversation, May 2002.

32. PCI Technical Activities Council and PCI Committee on Building Code, *PCI Standard Design Practice*, PCI JOURNAL, V. 41, No. 4, July-August 1996, p. 31-43.

33. PCI, *PCI Design Handbook*, Fifth Edition, Precast/Prestressed Concrete Institute, Chicago, IL, 1999.

34. Peterson, J.L., *History and Development of Precast Concrete in the United States*, Journal of the American Concrete Institute, V. 25, No. 6, Feb. 1954.

35. Rogers, S., *Allowable Design Release Stresses for Pretensioned Concrete Beams – Preliminary Results*, Thesis, The University of Texas at Austin, 2002.

36. Russell, B., *Design Guidelines for Transfer, Development and Debonding of Large Diameter Seven Wire Strands in Pretensioned Concrete Girders*, Dissertation, The University of Texas at Austin, 1992.

37. Siess, C. P., Private Communication with Michael E. Kreger, 2000.

38. Siess, C. P., *Research, Building Codes and Engineering Practice*, Journal of the American Concrete Institute, Vol. 56, No. 11, May 1960, p. 1105-1122.

VITA

Alfredo Jesús Castro Morales was born in San José, Costa Rica, on October 19, 1975, the son of Ricardo Castro and Agnes Morales. After graduating from Saint Francis College, San José, Costa Rica, in 1992, he attended the University of Costa Rica (UCR) where he earned, in 1998, a Bachelor of Science in Civil Engineering degree. While still an undergraduate student, he worked as an engineering assistant at RAE Ingenieros S.A. Shortly before graduating from the UCR, he started working for EDICA Ltda. as a field engineer in the expansion and remodeling of the Juan Santamaría International Airport in Costa Rica. Upon completion of this project, he entered the Graduate School at The University of Texas at Austin in Spring 2001. After six months of graduate study, he began working as a research assistant in a project supervised by Dr. Michael E. Kreger. His research focused on determining the highest possible allowable concrete stresses than can be applied to pretensioned concrete beams at prestress force transfer. He received the degree of Master of Science in Civil Engineering in August 2003. He has been married to María Trejos Jinesta since July 2000.

Permanent address: P.O. Box 1349-2050
                     San José, Costa Rica

This thesis was typed by Alfredo Castro.